# Neurotoxicity of biodiesel exhaust particles *in vitro* and *in ovo* using PC12 cells and the chicken embryo model

Kristin Marie Dahlgren


Master Thesis in Toxicology

Department of Biosciences
Faculty of Mathematics and Natural Sciences

UNIVERSITY OF OSLO

September 2020

2020

Neurotoxicity of diesel exhaust particles *in vitro* and *in ovo* using PC12 cells and the chicken embryo model.

Kristin Marie Dahlgren

http://www.duo.uio.no/

Print: Reprosentralen, Universitetet i Oslo

This project was carried out as a collaboration between the University of Oslo and the Norwegian Institute of Public Health.


# Acknowledgements

The presented thesis was carried at out the Department of Biosciences at the University of Oslo (UiO) in collaboration with the Norwegian Institute of Public Health (NIPH). It was supervised by Senior scientist Oddvar Myhre (NIPH), Professor Ragnhild Elisabeth Paulsen (UiO) and the internal advisor was Professor Ketil Hylland (UiO). The cell culture work was done in the Department of Pharmaceutical Biosciences, School of Pharmacy (UiO), and the gene expression analysis was done in the lab of the Department for Molecular Biology at NIPH. This work was part of a project supported by funding from the Polish-Norwegian Research Cooperation Program [Pol-Nor/201040/72/2013, the Fuelhealth project].

I would like to thank my incredibly positive and supportive thesis supervisors, Ragnhild Elisabeth Paulsen and Oddvar Myhre for all of your valuable input and generous time spent guiding me. I learned so much from our meetings and I always left them feeling motivated and encouraged. You are both wonderfully inspiring mentors!

A shout out to all the ZEB crew, with special thanks to Beata for all her support during my project and for sharing her office, coffee, and hilarious insights with me; to Mussie for his patience and expertise in advising me on my experiments; Ajay for his collaboration in the lab, his moral support and friendship; Nils for helping me with everything lab and thesis related and for answering a million questions without ever seeming annoyed; Ala, for all of your kind words and help with my thesis during the final weeks.

I am grateful to Tonje and Anna for assisting me at Folkehelseinstitutet, I really enjoyed my short time there and learned a lot from both of you. Thank you also to Johan for your valuable insights and for sharing your expertise. Thank you to Kasia, who was always willing to advise me, all the way from Poland.

I am also grateful to Adam Robertson for allowing me to store the cerebella samples at ShareLab while the university was closed due to the COVID-19 pandemic. This allowed me to complete my gene expression studies!

Thanks to my “biology chicks” – Ricci, Clare, Viv, Mariana for your friendship and continued encouragement throughout our studies together. It would not have been the same without you!

Finally, I am eternally grateful to my loving family for all of their support, both near and far. The completion of this thesis would not have been possible without the support of the best partner in crime, Thomas. Thank you for taking over bedtime routine with our baby girl so I could work. Also, for supplying me with snacks and caffeine when I needed it most, and for always helping me put things into perspective. Last but certainly not least, thanks to my little Valentina. From the moment I found out of your existence, it has been the most beautiful (and the most challenging) time of my life. The thought of making you proud one day fueled all my late-night work sessions. It was worth it, and more.

# Abstract

Traffic-related air pollution (TRAP) is a major contributor to global air pollution. A growing number of studies have reported adverse effects on the central nervous system (CNS) linked to exposure to diesel exhaust emissions (DEE), the dominant component of TRAP. Furthermore, *in vitro* studies using neuronal cell models, *in vivo* studies using animal models, as well as human epidemiological studies have all found associations between particulate matter (PM), a major component of TRAP, and the onset of neurodegenerative diseases, developmental neurotoxicity (DNT) and neurodevelopmental disorders (NDDs). Oxidative stress and neuroinflammation are thought to be an important mechanism of action for TRAP-induced neurotoxicity. As biofuels have emerged as a sustainable alternative to fossil fuel-derived petroleum fuel, it is imperative to investigate if these represent a safe alternative with regards to human health. The aim of this study was therefore to investigate the neurotoxic effects of diesel exhaust particles (DEP) using PC12 cells and cultured cerebellar granule neurons (CGNs) as *in vitro* models. The chicken embryo model was used as an *in ovo* model, for injection of DEP, pyrene and benzo[a])pyrene (B[a]P) (two polycyclic hydrocarbons (PAHs) present in TRAP) followed by gene expression analysis. DEP from three different diesel blends were investigated: B7, containing 7% 1$^{st}$ generation (1G) biodiesel made from rapeseed methyl ester, B20, containing 20% generation 1G biodiesel made from rapeseed methyl ester, and SHB20, containing 7% 1G biodiesel made from rapeseed methyl ester and 13% 2$^{nd}$ generation (2G) biodiesel made from hydrogenated vegetable oil. The different end points measured *in vitro* were: cell viability, cell death, intracellular glutathione (GSH) levels, calcium ($Ca^{2+)}$ influx response. *In ovo* exposure of chicken embryo to DEP and PAHs was followed by qPCR analysis. B7 consistently showed cytotoxic effects, whereas B20 had conflicting results and SHB20 showed the least amount of negative effects. We analyzed gene expression of six genes related to oxidative stress and one gene related to xenobiotic metabolism after *in ovo* exposure to DEP, pyrene and B[a]P. None of the genes tested showed a statistically significant difference in expression, compared to the controls. Overall, our results show that the effects of DEP exposure on neurotoxicity were marginal, suggesting that biodiesel fuel may be a suitable alternative to conventional petroleum diesel fuel.

# Abbreviations

| | |
|---|---|
| AD | Alzheimer's disease |
| ADHD | Attention deficit hyperactivity disorder |
| AhR | Aryl hydrocarbon receptor |
| ANOVA | Analysis of variance |
| ARNT | AhR nuclear translocator |
| ASD | Autism spectrum disorder |
| B7 | Petrol diesel containing 7% 1$^{st}$ generation biodiesel |
| B20 | Petrol diesel containing 20% 1$^{st}$ generation biodiesel |
| B(a)P | Benzo[a]pyrene |
| BBB | Blood brain barrier |
| cAMP | Cyclic AMP |
| cDNA | Complementary DNA |
| $CH_4$ | Methane |
| CGNs | Cerebellar granule neurons |
| CNS | Central nervous system |
| CO | Carbon monoxide |
| $CO_2$ | Carbon dioxide |
| Cq | Quantification cycle |

| | |
|---|---|
| DEE | Diesel engine emissions |
| DEPs | Diesel exhaust particles |
| $dH_2O$ | Distilled water |
| DMEM | Dulbeccos Modified Eagles Medium |
| DMSO | Dimethyl sulfoxide |
| dNTPs | Deoxyribonucleotides |
| EU | European Union |
| FAME | Fatty acid methyl ester |
| GHG | Greenhouse gases |
| GPCR | G Protein-Coupled Receptors |
| GPX | Glutathione peroxidase |
| GSH | Glutathione |
| GSR | Glutathione reductase |
| HC | Hydrocarbons |
| $H_2O_2$ | Hydrogen peroxide |
| HVO | Hydrogenated vegetable oil |
| IF | Inorganic fraction |
| mRNA | Messenger ribonucleic acid |
| MTT | 3-(4,5-dimethylthiozol-2-yl)2,5-diphenyltetrazolium bromide |
| $N_2$ | Nitrogen |
| NDDs | Neurodevelopmental disorders |

| | |
|---|---|
| NGF | Nerve growth factor |
| NIPH | National Institute of Public Health |
| NMDAR | N-methyl-D-aspartate receptor |
| $NO_x$ | Nitrogen oxides |
| $O_2^-$ | Superoxide |
| $OH^-$ | Hydroxyl radical |
| PAHs | Polycyclic Aromatic Hydrocarbons |
| PBS | Phosphate-buffered saline |
| PC12 | Pheochromocytoma cells |
| PD | Parkinson's disease |
| PLL | Poly-L-lysine |
| PM | Particulate matter |
| $PM_{2.5}$ | Fine particulate matter (<2.5 μm) |
| qPCR | Quantitative real-time PCR |
| Rnase | Ribonuclease |
| ROS | Reactive oxygen species |
| RT | Reverse transcriptase |
| RT-PCR | Reverse transcription PCR |
| SEM | Standard error of the mean |
| SHB20 | Petrol diesel containing 7% 1st generation biodiesel and 13% 2nd generation biodiesel (SHB = Synthetic Hydrocarbon Biofuel) |

| | |
|---|---|
| SOD | Superoxide dismutase |
| SOF | Soluble organic fraction |
| TRAP | Traffic related air pollution |
| UFP | Ultrafine particulate matter (<1000 nm) |
| VOC | Volatile organic compound |

# Table of contents

Acknowledgements……V

Abstract……VI

Abbreviations……VII

1 Introduction……1

1.1 Air pollution……1

1.2 Background on biodiesel……2

1.3 Diesel exhaust particles……3

1.4 Neurotoxicity of traffic-related air pollution……6

1.4.1 Entry into the central nervous system……7

1.4.2 Generation of ROS and Oxidative Stress……8

1.4.3 Disturbances in cell signaling……10

1.4.4 Regulation of gene expression……11

1.5 Neurodevelopmental toxicity……11

1.5.1 Cerebellum……12

1.6 Model systems……14

1.6.1 PC12 cells……14

1.6.2 Chicken embryo model……14

1.7 The aim of the study……17

2. Materials and methods……18

2.1 Diesel exhaust particles……18

2.1.1 DEP exposure solutions……18

2.2 In vitro study……19

2.2.1 PC12 cell culture……19

2.2.2 Plating PC12 cells……20

2.2.3 MTT assay……20

2.2.4 Trypan Blue assay……21

2.2.5 Glutathione measurement……23

2.2.6 Hoechst staining……24

2.2.7 Calcium influx……24

2.3 Chicken embryo model……25

2.3.1 In ovo exposure of chicken embryos……26

2.3.2 Harvesting of the cerebella……28

2.3.3 Homogenization of the cerebella……28

2.3.4 Chicken neuronal cell culture……29

2.4 Gene expression analysis……30

2.4.1 Isolation of total RNA from cerebella……32

2.4.2 cDNA synthesis……32

2.4.5 Gene expression analysis……32

2.5 Statistical analysis……33

3 Results……34

3.1 PC12 cells……33

3.1.1 Cell viability as measured by MTT……33

3.1.2 Cell viability as measured by Trypan Blue exclusion assay……35

3.1.3 Intracellular glutathione measurement……37

3.1.4 Calcium-influx measurement……38

3.2 Chicken granule neurons……40

3.2.1 Cell viability as measured by MTT……40

3.2.2 Cell viability as measured by Trypan Blue exclusion assay……..……41

3.2.3 Intracellular glutathione measurement……..……..43

3.2.4 Calcium influx measurement……...……44

3.3 Chicken embryo cerebellar gene expression……...……49

4. Discussion……..……...53

4.1 Cell viability……..……...53

4.1.1 PC12 cells.…….……..53

4.1.2 Cerebellar granule neurons…….…….55

4.2 Intracellular glutathione levels…….……...56

4.2.1 PC12 cells……56

4.2.2 Cerebellar granule neurons……..57

4.3 Calcium influx……58

4.3.1 PC12 cells……58

4.3.2 Cerebellar granule neurons……..60

4.4 Gene expression by qPCR……..62

4.5 In ovo exposure……...63

4.5.1 Gene expression by qPCR……...63

5 Conclusion……..…...66

6 Further perspectives…….…..68

References……69

Appendices……86

# 1 Introduction

## 1.1 Air pollution

Fossil fuels such as oil and natural gas have been the primary source of energy used worldwide over the past century, due to their abundance, high energy value and low cost (1). The greenhouse gases (GHG) released upon their combustion include carbon dioxide ($CO_2$), methane ($CH_4$) and nitrous oxide ($N_2O$), all of which have been attributed to global warming and climate change. Furthermore, these GHG have been shown to dramatically increase air pollution, a major risk factor for human health (2). Air pollution is a complex mixture of gases, solid and liquid particles suspended in the air (particulate matter (PM)), trace metals, and adsorbed organic compounds. According to the World Health Organization, air pollution was estimated to have caused over four million premature deaths in 2016, in addition to leading to higher rates of cancer, heart disease, stroke, and respiratory diseases (3). In recent years, traffic-related air pollution (TRAP) exposure has been associated with diseases of the central nervous system (CNS), including Alzheimer's disease (AD) and Parkinson's disease (PD), as well as various neurodevelopmental disorders (NDDs) such as Autism spectrum disorder (ASD) and Attention-deficit hyperactivity disorder (ADHD) (4) (5). Air pollution has thus become an international public health concern, especially as the global population increases and brings with it a shift from rural to urban living. The United Nations estimated that 55% of the global population was living in urban areas in 2018, with this number projected to increase to 68% by 2050 (6). This urbanization is accompanied by an increased demand for transportation, and a corresponding increase in levels of TRAP, where diesel exhaust emissions (DEE) emitted from motor vehicles are a major contributor (7). Within the European Union (EU), road transportation has accounted for more than 70% of all GHG emissions within the transport sector, in addition to being the main source of air pollution in urbanized areas (8). Therefore, as part of its 2020 climate and energy strategy, the EU decided in 2009 to increase the use of renewable fuels in the transport sector to 10% over the course of the following decade (9). As a result of this, 99% of all conventional diesel sold in the EU in 2014, contained up to 7% biodiesel (10). While the implementation of biodiesel fuels may help to decrease the level of GHG emissions, it is imperative that these renewable fuels do not

pose a public health risk themselves. The potential impact that the increased use of biodiesel may have on the toxicity of DEE is currently unclear. Consequently, knowledge on the effects of biodiesel exhaust on both local air quality and human health is limited. Identification of this knowledge gap should therefore help to direct research towards the missing data.

## 1.2 Background on biodiesel

Biofuels have emerged as a more carbon-neutral fuel alternative, with global production increasing steadily over the past two decades (11). One variety, biodiesel, is produced from feedstocks like vegetable oils or animal fats, as opposed to fossil energy, and therefore represents a renewable and biodegradable option. The main benefit of biodiesel is that, when sustainably manufactured, it may be described as carbon neutral. In other words, biodiesel emits no net output of $CO_2$ since the crops that are grown absorb the same amount of $CO_2$ that is released when the fuel is combusted. This is a key factor, as $CO_2$ is the main GHG driving climate change, as well as a major contributor to air pollution. Biodiesel is categorized based on the source from which the fuel is derived. 1st generation (1G) biodiesel is produced directly from food crops such as sugar, animal fats, and vegetable oil consisting of long-chain fatty acid esters (FAME). 2nd generation (2G) biodiesel, known as advanced biodiesel, is derived from non-food crops such as waste from animal fats or cooking oils. While most studies indicate that 1G biodiesel shows a net benefit in terms of GHG emissions reduction, they also highlight several potential drawbacks (12) . The feedstock for 1G biodiesel must be grown, and thus directly competes with land used for food production, while also burdening the food chain. This may contribute to higher food prices and have a negative impact on biodiversity due to deforestation and other indirect land use effects. The production of 2G biodiesel on the other hand, does not directly compete with land used for food production and therefore does not threaten the food chain. 2G biodiesel is indeed regarded as a sustainable response to the drawbacks of 1G biodiesel and its implementation has therefore been promoted by the EU (13) .

## 1.3 Diesel exhaust particles

Vehicles equipped with diesel engines are extensively used worldwide, both in public and private transportation as well as in commercial transport and industrial machinery. DEE are thus pervasive in both urban and rural settings. These consist of a complex mixture of several hundred compounds, present in both particulate and gaseous form. The exact composition of emissions depends on several factors such as engine type and fuel source, but the main components include nitrogen ($N_2$), $CO_2$, and water vapor (14). While pollutants account for only about 1% of total emissions, these include several compounds known to exert harmful environmental and health effects, including carbon monoxide (CO), hydrocarbons (HC), nitrogen oxides ($NO_x$), and PM (15). Of these pollutants, PM has been shown to have the most negative impact on health (16). Diesel exhaust particles (DEP) are the main PM emitted, and have been associated with the majority of the negative effects exerted by DEE (17). DEP consist of a carbon core with a mixture of adsorbed compounds which can be divided into three main components: soot, a soluble organic fraction (SOF), and inorganic fraction (IF) (18). Soot accounts for more than 50% of the weight of emitted DEP and is involved in key mechanisms of pathology such as oxidative stress, DNA methylation, aryl hydrocarbon receptor activation and reactive oxygen species (ROS)-mediated DNA damage (19). SOF consists of hydrocarbons, including polycyclic aromatic hydrocarbons (PAHs), many of which have toxic, mutagenic and/or carcinogenic properties, while IF is made up of trace metals (figure 1.1).The toxicity of DEP is thus influenced by its elemental composition, as well as by its physicochemical properties such as size, shape, and surface properties (20).

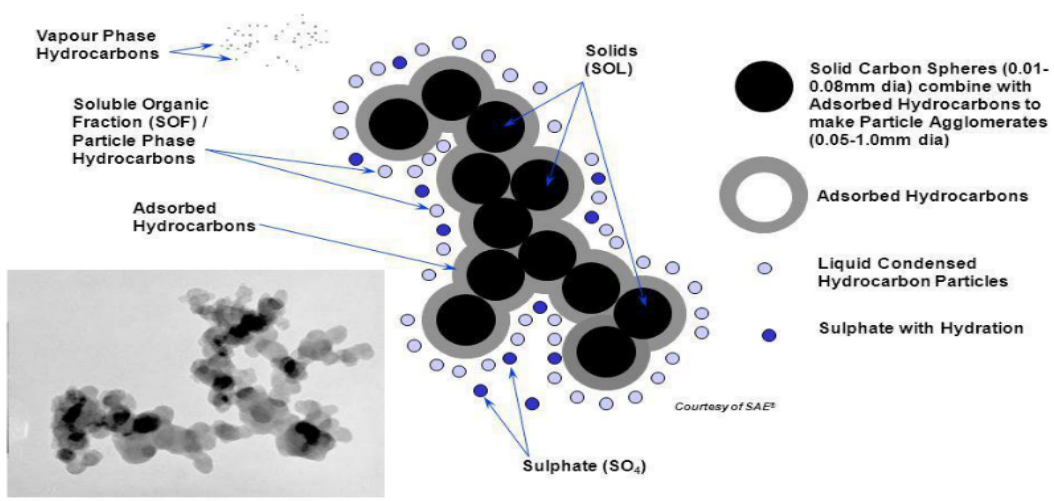


Figure 1.1 Schematic of diesel exhaust particles showing the spherical shape solid carbon core and adsorbed organic compounds. The inset shows a transmission electron microscopy (TEM) image of diesel exhaust particles, highlighting their propensity to form aggregates. Image from (21).

PM, including DEP, is often classified according to its aerodynamic diameter, since this governs the transport and removal of the particles from the air, dictates their deposition within the respiratory system, and is associated with the particles' source and chemical composition (22). Experimental investigations have shown DEP to be spherical shaped with size fractions including coarse particles ($PM_{10}$) <10 µm, fine particles ($PM_{2.5}$) <2.5 µm, and ultrafine particles ($PM_{0.1}$) <0.1 µm (23). Toxicity is generally inversely related to particle size, due to a larger surface-to-mass ratio, which enables adsorption of different compounds, both organic and inorganic, from the combustion process as well as those found in the ambient air (24). In addition, smaller particles tend to penetrate deeper and thus deposit more efficiently in the airways (figure 1.2).

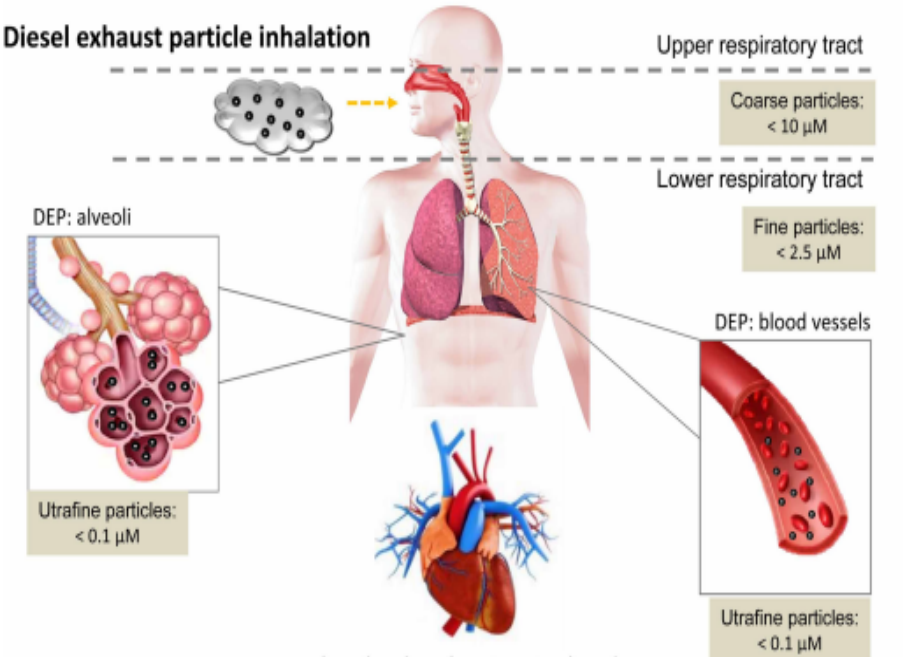


Figure 1.2 Deposition of PM in the human body via inhalation. Coarse particles ($PM_{10}$) deposit mostly in the upper respiratory tract. Fine particles ($PM_{2.5}$) may deposit in the lower respiratory tract. Very fine particles ($PM_1$) may reach the alveoli of the lungs. Ultrafine particles ($PM_{0.1}$) partially penetrate the body through the alveolar-capillary membrane, which separates air from the blood stream (85).

The respiratory tract is the dominant route of exposure for airborne pollutants as well as the site of initiation for ensuing systemic responses, including the CNS response (25). Although evidence is still emerging, $PM_{10}$ or larger have been shown to get trapped in the upper airways, while $PM_{2.5}$ and smaller may deposit throughout the respiratory tract, reaching the alveoli of the lungs. $PM_{0.1}$ may enter the systemic circulation by penetrating the alveolar-capillary membrane which separates the air from the bloodstream (26). Their ability to cross this membrane is a consequence of their size, chemical composition, and their propensity to form aggregates (25). Although animal studies have demonstrated the translocation of $PM_{0.1}$ across this barrier, it has been more challenging to demonstrate the same mechanism in humans (27). The effects of $PM_{0.1}$ have indeed not been investigated to the same extent as $PM_{2.5}$ and $PM_{10}$, however studies consistently show that the size of these particles is negatively correlated with their adverse impact on health (28). The potency of DEP as environmental toxicants depends also on the structure-function relationships of the human respiratory tract and how its defense mechanisms – such as mucociliary clearance and macrophage phagocytosis – are bypassed by PM (29). Additionally, a "Trojan-horse effect"

has been posited whereby DEP carrying adsorbed compounds of potentially high toxicity on their surface, such as PAHs, allow semi-volatile and non-volatile compounds to reach fluids and cellular compartments they could not otherwise reach (30). PAHs are ubiquitous environmentally persistent organic compounds formed from both anthropogenic and non-anthropogenic sources. This group of several hundred chemically related compounds are highly lipid soluble and are rapidly distributed in a wide variety of tissues, although they have various structures and varied toxicity (31). Motor vehicle emissions, including DEE, accounts for around 46–90% of the mass of individual PAHs in ambient air particles in urban areas (32).

## 1.4 Neurotoxicity of traffic-related air pollution

While there is extensive literature on the detrimental effects of air pollution on the cardiovascular and respiratory systems, the CNS has relatively recently, within the last decade, emerged as an important target (2). Nevertheless, human epidemiological studies, *in vitro* studies and experimental studies in animals have all linked TRAP with detrimental effects on the brain (33). Moreover, these effects are seen across the entire age spectrum of the population, with adverse outcomes reported in children's cognitive, behavioral and psychomotor development, as well as cognitive disturbances in the elderly, leading to higher risks of dementia and its related disorders (34) (35)(36). In fact, epidemiological and observational studies have suggested that chronic exposure to airborne pollutants such as TRAP, may contribute to neurodegenerative disease processes already from early childhood (37) (38) (39). Studies have also reported associations between TRAP exposure and certain neurodevelopmental psychological deficits including IQ loss, learning disabilities, developmental delay, ASD, and ADHD (40) (41) (42). Despite the growing number of studies highlighting these associations, identification of compounds in TRAP causing such effects, and the underlying mechanisms governing the onset of disease remain largely elusive (43). However, mounting evidence points to the generation of ROS, oxidative stress and inflammation as common mechanisms through which TRAP exposure causes damage (27). *In vitro* and *in vivo* animal studies have revealed these damages may lead to alterations in neuron morphology, synaptic toxicity, and neuronal cell death (44) (45) (46).

### 1.4.1 Entry into the central nervous system

The blood brain barrier (BBB) is the main line of defense from toxicants, acting as a chemical and physical barrier between the brain circulation and the systemic circulation. It is made up of multiple cell types, metabolizing enzymes, and transporter proteins, and is usually impermeable to lipid-insoluble compounds due the tight junctions between the cells (30). However, regions where junctions are very thin, less developed, or damaged, are thought to provide an entry to toxicants (47). Through respiratory uptake, PM can enter the systemic circulation and be transported across the blood brain BBB by mechanisms which are not yet fully understood (figure 1.3). For lipid soluble compounds such PAHs and metal ions, this may occur via transmembrane diffusion (48). Studies conducted using animal models have shown that $PM_{0.1}$ can translocate from the nose via the olfactory nerve directly into the brain, bypassing the BBB. Furthermore, presence of these particles has been found in the striatum, frontal cortex, and cerebellum (49). Importantly, PM can induce CNS damage without crossing the BBB, by triggering widespread inflammation through the activation of cytokines (43). This proinflammatory stimulus to the CNS has been shown to increase the permeability of the BBB and is considered a risk factor for neurodegenerative disease (30). The strong predisposition of the CNS to damage caused by inflammatory stimuli is thought to be a consequence of its limited ability for cellular regeneration (50). Thus, an evolutionary strategy of protecting the CNS from toxic insults has been favored over evolving mechanisms to regenerate damaged tissue.

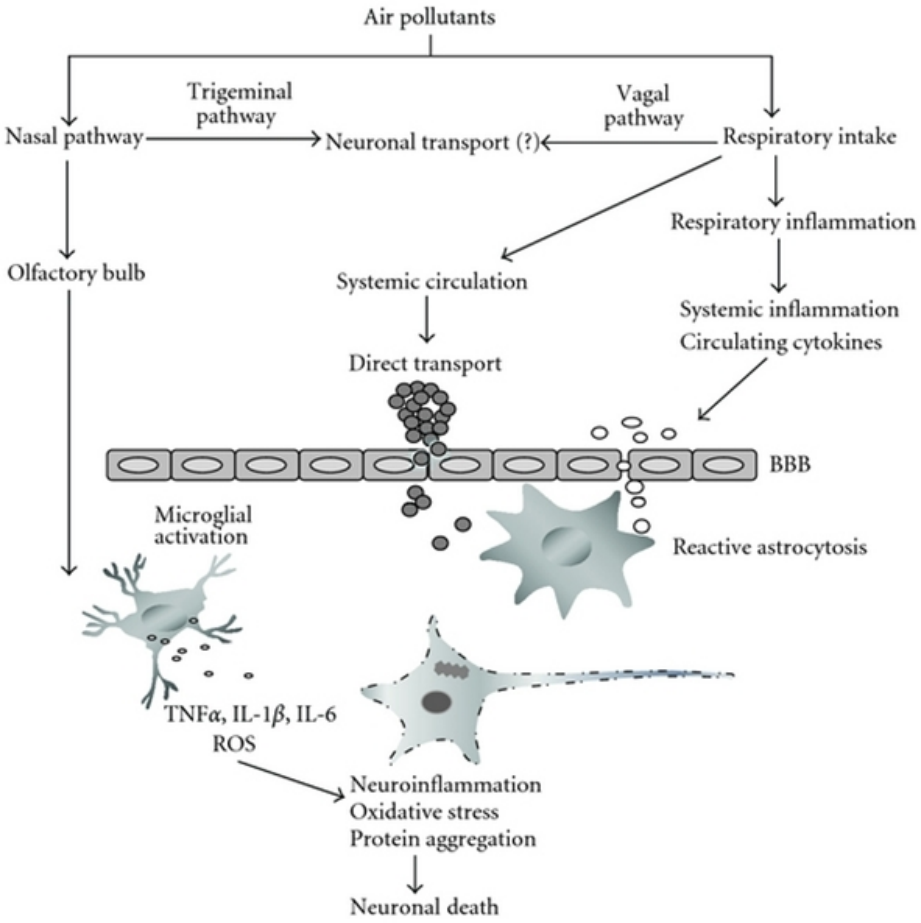


Figure 1.3 Entry of air pollutants into the CNS. Pollutants may cross the BBB directly or trigger the induction of proinflammatory cytokines such as tumor necrosis factor alpha (TNFα), interleukin-6 (IL-6), and interleukin-1beta (IL-1β). Activation of microglial cells generate reactive oxygen species (ROS). Via the nasal pathway, air pollutants travel through the olfactory bulb to reach the CNS directly, bypassing the blood brain barrier (BBB) (87).

## 1.4.2 Generation of ROS and oxidative Stress

Oxidative stress is caused by an imbalance between the production and the detoxification of reactive oxygen species (ROS) in the cell (51). ROS are a group of highly reactive molecules and free radicals derived from molecular oxygen, mostly formed as the by-products or intermediates of redox reactions. ROS may also arise in a cellular response to exogenous compounds such as pollution, radiation, or xenobiotics (52). In a normal functioning cell, ROS are involved in several vital processes, including acting as cellular signaling molecules (53). However, upon excessive production or insufficient detoxification, ROS are harmful to

cells since they can chemically modify lipids, proteins, and nucleic acids (16). These oxidative modifications may result in either direct or indirect ROS-mediated damage, leading to a state of oxidative stress. Studies have shown that cumulative oxidative stress plays a key role in the acceleration of the aging process and the development of neurodegenerative diseases, by mechanisms such as inducing cellular damage, impairment of the DNA repair system, and mitochondrial dysfunction (54). Detoxification of ROS is therefore of paramount importance, and a number of defense mechanisms have evolved to enable cells to handle the potential damaging effects. These include various antioxidant defense systems which include enzymes such as superoxide dismutase (SOD) and catalase, as well as non-enzymatic antioxidants such as glutathione, α-tocopherol (vitamin E) and ascorbic acid (vitamin C) (20). Glutathione is a major antioxidant involved in ROS detoxification, and of critical importance in the brain due to high oxidative metabolism. Glutathione exists in two forms: a thiol-reduced (GSH) form and a disulfide-oxidized (GSSG) form. Reactions with ROS molecules such as hydrogen peroxide ($H_2O_2$), oxidize GSH which generates GSSH, and in the process reduces the potentially harmful $H_2O_2$, generating two molecules of water ($H_2O$). GSSH is not able to perform antioxidant functions but may be converted back to GSH by participating in a redox reaction driven by NADPH-dependent glutathione reductase (figure 1.4). While this antioxidant system is efficient under normal conditions, it can be overwhelmed by an over accumulation of ROS. The ratio of GSSH to GSH serves as a dynamic indicator of the oxidative stress: in healthy cells, GSH accounts for over 90% of total glutathione (55).

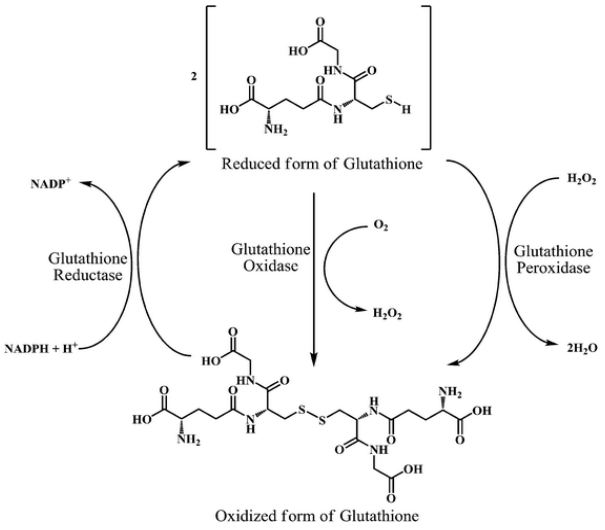


Figure 1.4 Interconversion of glutathione in its reduced form (GSH) and oxidized form (GSSG) by the action of glutathione oxidase, glutathione reductase, and glutathione peroxidase enzymes. Figure from (35).

The brain is more vulnerable to the effects of ROS than other organs and tissues in the body, due to several factors including its higher oxygen consumption, lower antioxidant activity, and high level of fatty acids, which are susceptible to oxidative modification (56). Furthermore, the increase in ROS that occurs during oxidative stress leads to altered intracellular signaling, which may lead to a dysregulation of the neuroinflammatory response (57). This response in turn, may further increase the state of oxidative stress, thereby creating a mutually reinforced cycle of inflammation and oxidative stress, two key pathologic factors of the onset and progression of neurodegenerative diseases (58).

### 1.4.3 Disturbances in cell signaling

It is widely acknowledged that intracellular signaling pathways are involved in the PM-induced inflammatory response (59). Moreover, exposure to PM has been shown to activate cellular signaling networks including membrane receptors and transcription factors that regulate stress responses (60). Calcium ($Ca^{2+}$) is an important signaling molecule, modulating a wide range of cellular physiological functions including cell death, metabolism, gene expression, and neuronal functioning (61). Neurotoxic agents may influence intracellular $Ca^{2+}$ levels by directly or indirectly disrupting its mechanisms of homeostasis (62). The N-methyl-D-aspartate receptor (NMDAR) has attracted much attention, in part due to its established role in the onset of excitotoxicity, a detrimental process which leads to neuronal injury and cell death (63) . NDMAR is highly permeable to $Ca^{2+}$ and overstimulation of this receptor leads to excessive intracellular $Ca^{2+}$ influx, which overloads mitochondria, leading to dysfunction and a subsequent decrease in ATP synthesis (63). In addition, excessive intracellular $Ca^{2+}$ induces the generation of ROS, as well as protein kinase cascades both of which further regulate antioxidant enzymes against oxidative injury. Excitotoxicity has been associated with the neuronal injury common to many neurodegenerative disorders (64).

Ambient PM has also been shown to activate the aryl hydrocarbon receptor (AhR), whose exogenous ligands are mainly environmental organic pollutants, including PAHs present in DEP (65). AhR acts as both a cytosolic receptor protein as well as a transcription factor. Upon ligand binding, it translocates into the nucleus and forms a heterodimer with AhR nuclear translocator (ARNT) (66). This heterodimer is a transcription factor, which induces the cytochrome P450 monooxygenases CYP1A1/B1, key xenobiotic-metabolizing enzymes.

Indeed, CYP1-expression has been shown to increase in response to low concentrations of DEP (20). Increased CYP1-levels may in turn contribute to increased formation of ROS and electrophilic metabolites from PAHs. AhR ligand neurotoxicity occurs via non-genomic pathways, such as through disturbed NMDAR neurotransmission and generation of ROS (66). AhR thus plays an important role as mediator of an adaptive response to xenobiotics.

### 1.4.4 Regulation of gene expression

Modulation of gene expression is an essential function of the adaptability and survival of an organism to external stressors, which thereby plays a critical role in the activation of toxicity pathways (67). A cell's response to a toxic insult may be examined at a molecular level by analyzing the gene expression response of the genes thought to be involved in the pathways. Two of the main processes thought to be involved in the biological response to PM—oxidative stress and inflammation—are known to be under genetic regulation (68). Although these processes are controlled by many genes, the up- or downregulation of biomarkers may give an indication of the mechanisms involved in the toxicity. For example, to protect against the damaging effects of accumulating ROS, an upregulation of the genes involved in antioxidant defense systems such as glutathione peroxidase 1 and 2 (Gpx1 and Gpx2) may be induced, indicating the need for an increase in antioxidant enzymes. Regulation of gene expression is however a complex, multistep process. Oxidative stress is indeed known to modulate a variety of biological processes by coupling cell surface signaling into changes in gene expression, suggesting multiple pathways are involved (69).

## 1.5 Neurodevelopmental toxicity

The development of the nervous system occurs gradually, continuing well after birth in both animals and humans. Environmental toxicant exposure during development may permanently change the brain's structure, physiology, and metabolism, leading to diseases in adult life (70). This is influenced in part by periods of developmental vulnerability that occur *in utero* until early childhood (71). During these sensitive developmental stages, exposures to toxicants may cause serious brain injury at levels of exposure that would have little or no

adverse effect on an adult. This is thought to be caused by the dependence of the nervous system on the emergence of critical processes such as proliferation, migration, differentiation, synaptogenesis, myelination, and apoptosis, as well as the immaturity of metabolic pathways and development of vital organ systems (72). In addition, before the BBB is fully developed, the CNS does not have a protective transport barrier, which may result in the accumulation of compounds in the brain in greater quantities than in adults. Research conducted on exposure to PAHs *in utero* at current environmental levels, showed that high levels of PAHs were inversely associated with IQ scores five years later (73). These findings highlight the fact that toxins may be neurotoxic years after exposure, as well as the fact that the placenta does not act as an impenetrable barrier against all toxic substances. Furthermore, an extensive amount of evidence has linked exposure to environmental toxicants such as those found in DEP, including PM, PAHs, and $NO_2$, with a multitude of NDDs, such as ASD and ADHD, the prevalence of which are increasing at alarming rates (74) (75) . While the root causes of the increase are not fully understood, it is thought to result from a complex mechanism of genetic and environmental factors that change brain development. Nonetheless, genetic factors seem to account for no more than 40% of all cases of NDDs, therefore environmental exposures are assumed to play a substantial role in the mechanism of disease (76). Many epidemiological studies of neurodevelopmental toxicity are complicated by the exposure to more than one neurotoxicant at a time, i.e. mixed exposures. Due to the variable composition of environmental exposure, any single compound will most likely not be representative of all exposure conditions. Therefore, precision in this type of exposure assessment is challenging.

### 1.5.1 Cerebellum

The cerebellum is a structure located at the back of the brain, underlying the occipital and temporal lobes of the cerebral cortex, and is involved in sensory-motor processing and cognitive functions. Damage to the cerebellum early in life has been linked to poorer outcomes than damage in adulthood, suggesting it is particularly important during development. Moreover, cerebellar dysfunction is known to play a critical role in NDDs. This is particularly well-documented in ASD, ADHD, and developmental dyslexia, where structural and functional neuroimaging studies have demonstrated differences in cerebellar physiology (77).

Despite comprising only about one-tenth of the brain's volume, the cerebellum is extremely neuron-rich, containing at least half of the total number of neurons in the brain. Its relatively simple structure makes it a suitable model for the study of neurotoxic effects (figure 1.5). The cerebellar cortex consists of a simple three-layered structure: the molecular layer, the Purkinje cell layer, and the granular cell layer. The Purkinje cells and the granule cells seem to be the most important targets in the cerebellum for toxic substances (57). Studies show that toxins acting through free radical production and excitotoxicity, as well as a deficiency of antioxidants may all play important roles in the explaining this increased sensitivity towards neurotoxins (57). The Purkinje cells are among the largest neurons in the brain and easily identified in a single layer. The granule neurons by contrast, are the smallest neurons in the vertebrate brain, however they are also the most abundant, accounting for roughly 80% of all neurons in the human brain (78). The granule cells undergo all stages of neuronal development in a limited time frame, which may be isolated in culture, and used for studies. Due to its relatively simple structure, it being the target for several toxic compounds, as well as the possibility to isolate cerebellar granule cells in culture, the cerebellum thus serves as a befitting structure for neurotoxicity testing.

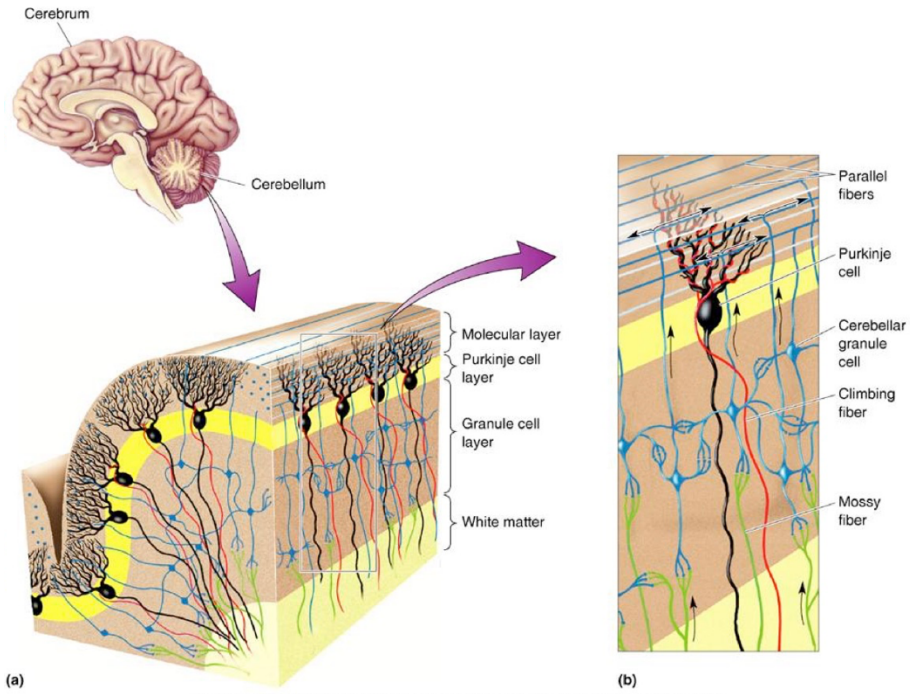


Figure 1.5 The basic structure of the cerebellar cortex. Figure from (79).

## 1.6 Model systems

### 1.6.1 PC12 Cells

The PC12 cell line is an established clonal cell line widely used as a neuronal model system in neurobiological research (80). PC12 cells originate from an adrenal medullary tumor in rats, called a pheochromocytoma. These cells may be cultured indefinitely, and under normal conditions they resemble adrenal chromaffin cells in morphology, physiology, and biochemistry (43). As these cells have an embryological origin however, they may also be differentiated into a neuronal phenotype in the presence of a neurotrophic factor called nerve growth factor (NGF). This differentiation causes cell division to stop and long neurites to grow and extend from the cells, which then become electrically excitable and begin to resemble mature sympathetic neurons, both morphologically and functionally (81). PC12 cells are able to synthesize, store and release the neurotransmitters dopamine, norepinephrine, and acetylcholine, and also contain important cell signaling channels such as sodium ($Na^+$), potassium ($K^+$) and $Ca^{2+}$, as well as G Protein-Coupled Receptors (GPCRs) (82). Thus, PC12 cells are very well-suited for studying chemical disruptions of neuronal differentiation, cell signaling and other closely related processes. In addition, the relative homogeneity of PC12 cell cultures, ease of culture, and the extensive amount of background knowledge available on its proliferation and differentiation, have made this cell line an excellent alternative to cultured neurons for studies on neuronal development and function (83). Indeed, PC12 cells have been extensively used in studies of neurodegenerative disorders such as AD, neurodevelopmental disorders such as ADHD, as well as screening for developmental neurotoxicity, thus providing a large amount of information on their physiology and biological composition (84).

### 1.6.2 Chicken embryo model

The chicken embryo (*Gallus gallus*) has a long history as a model system in developmental biology, with major contributions made to the fields of immunology, genetics, and cancer biology, to name a few (85). More recently it has been adopted as an in vivo model for neurobiological research, due to its many advantages: fertilized eggs are inexpensive, easily obtained and housed in the lab, convenient size for manipulation and visualization, and have

rapid development. The chicken genome, which has fewer genes than some of the other model organisms, has already been sequenced, providing an additional molecular resource. Moreover, as the eggs are laid by different hens, genetic variation is introduced into the experiment. Most importantly, however, the development of chicken embryos is comparable to the human embryo at the molecular, cellular, and anatomical levels (86). As seen in Figure 1.6, the entire spectrum of developmental stages occurs in just 21 days, allowing for timely collection of data.

Lastly, the use of this model presents ethical advantages by contributing to the principles of the 3Rs (Replacement, Reduction and Refinement) which provide a framework for performing more humane animal research (87). As chicken eggs are nutritionally self-sufficient and develop outside of the hen, the hens are completely excluded from the experiments, and the sacrifice of pregnant animals is avoided. Thus, there is a reduction in the number of animals involved, as well as a refinement of the experiment. Furthermore, by ordering the exact amount of eggs needed for each experiment, any potential unnecessary use of eggs is reduced. Finally, the harvest of cerebellar granule neurons (CGNs) represents a partial replacement, as the embryos are not used in a procedure that causes suffering prior to the harvest.

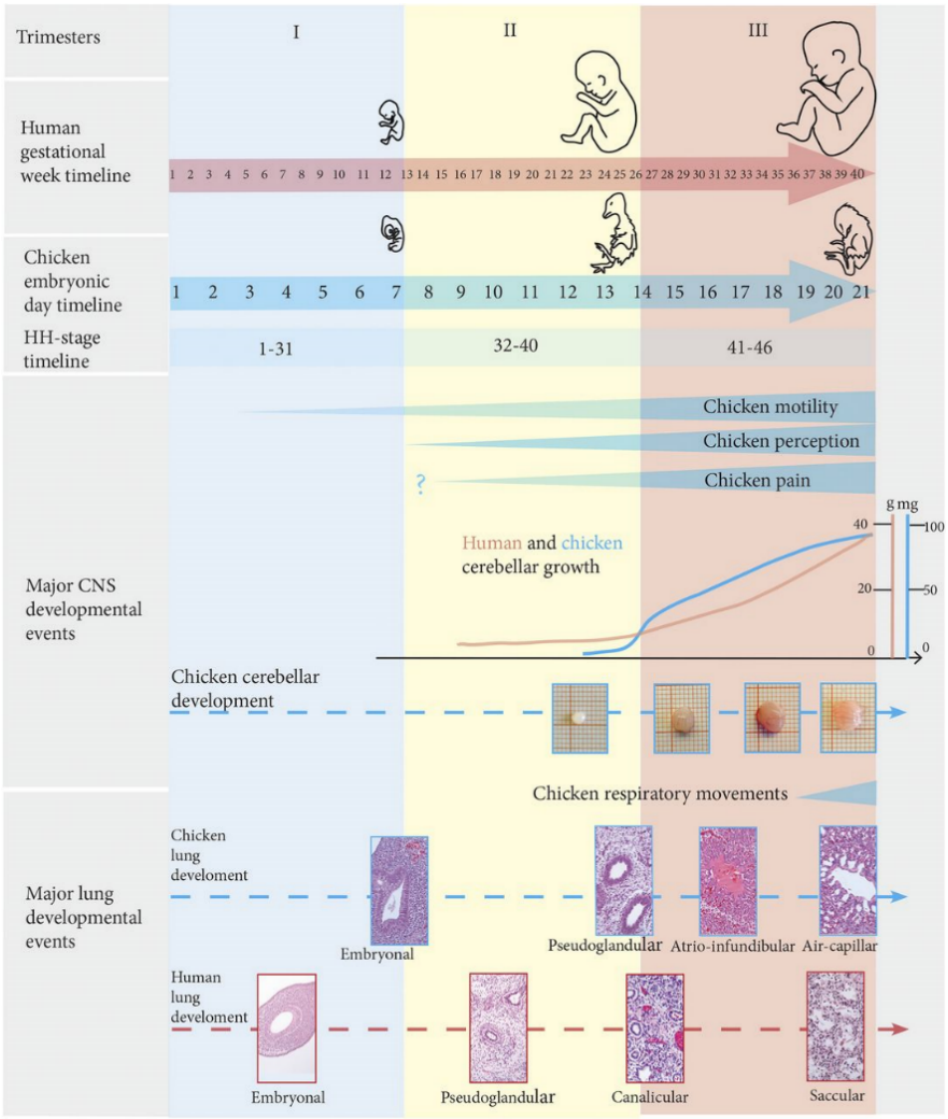


Figure 1.6 Developmental events during the embryonic and fetal period in humans and chickens. The cerebellum histology of the chicken embryo at embryonic day 16 (E16) correlates most closely to human birth. Figure obtained from (86).

## 1.7 The aims of the study

Biodiesel has received considerable attention in recent years as an alternative fuel that is able to replace petroleum diesel in many engines. Recent studies, however, show that exhaust emissions from the combustion of biodiesel fuels contain physical and chemical characteristics that have the potential to negatively impact on both the environment as well as human health (88) (89). Moreover, these characteristics have been shown to vary significantly, depending on several factors such as the feedstock and the blend ratio of biodiesel to petroleum diesel in the fuel mix (90). As the implementation of biodiesel fuel is projected to increase over the next decade, it is therefore of paramount importance to comprehensively assess the potential negative impacts of biodiesel fuel emissions on air quality and human health (91).

Thus, the aim of this study was to test and compare the effects of DEP of emissions from different diesel blends: B7, petroleum diesel containing 7% 1G biodiesel; B20, petroleum diesel containing 20% 1G biodiesel; and SHB20, petroleum diesel containing 7% 1G and 13% 2G biodiesel. In addition, the effects of the PAHs pyrene and B(a)P, which are important constituents of TRAP, were investigated.

The research was centered around three overarching questions:

1. Will exposure to DEP lead to decreased cell viability and induce neurotoxicity in PC12 cell cultures and in CGN cells?

2. Will exposure to DEP lead to disturbed calcium signaling and AhR dysregulation in PC12 cell cultures and in CGN cells?

3. Will the exposure to DEP lead to changes in gene expression related to oxidative stress, and inflammation pathways in the chicken embryo?

# 2 Materials & Methods

## 2.1 Diesel exhaust particles

DEP from a Euro 5-classified diesel engine were collected by NIPH, in collaboration with Warsaw University of Life Sciences. The diesel engine ran on three blends of petroleum diesel: B7, which contained 7% 1st generation biodiesel made from rapeseed methyl ester; B20, which contained 20% 1st generation biodiesel made from rapeseed methyl ester; and SHB20, which contained 7% 1st generation biodiesel made from rapeseed methyl ester and 13% 2nd generation biodiesel, made from hydrogenated vegetable oil (HVO). The DEP were dissolved in distilled water ($dH_2O$) to a final concentration of 2 mg/ml. They were then sonicated using the Sonic Vibra Cell ultrasonic liquid processor (Sonics & material, Inc., Newtown, USA) for 10 minutes using an energy of $3 \times 10^9$ J that was provided in pulses of 30 seconds on / 10 seconds off, at an amplitude of 60%. The DEP solutions were aliquoted into 1.5 ml Eppendorf tubes and the stocks were stored at -20°C.

### 2.1.1 DEP exposure solutions

The aliquoted DEP stocks were thawed and then vortexed thoroughly to resuspend the particles which had settled at the bottom of the Eppendorf tubes. The DEP solutions were then diluted in MQ-water such that the volume of DEP added to the experimental medium would be the same for each concentration (i.e. the ratio of DEP to medium would remain constant). For each of the DEP concentrations, 50 µL of the particles were added to 950 µl of medium, to make 1 ml of exposure. This was then multiplied as needed, for larger volumes. In total three different concentrations were used throughout this study: 2 / 10 / 50 µg /ml.

## 2.2 *In vitro* study

### 2.2.1 PC12 cell culture

A PC12 cell line culture was cultivated in a T75 cell culture flask (ThermoFisher, Waltham, USA) in an incubator set to 37°C and 5% $CO_2$. In order to keep the cell culture alive and expanding, the cells were passaged in a laminar air flow (LAF) bench two times per week when the cells had reached about 80% confluency; this was checked by visual inspection under a light microscope (Figure 2.1). It was important to ensure that the cells never reached 100% confluency as this would affect the homogeneity of our subculture. Since PC12 cells are adherent, the first step in passaging was to dislodge the cells from the surface of the culture flask. This was done by replacing the PC12 media (Table 2.1) with new PC12 media which had been warmed to 37°C in a water bath, and subsequently hitting the sides of the flask to loosen the adherent cells. The media containing the cells was then triturated using a sterile glass Pasteur pipette in order to break up any clumps of aggregated cells. Once no more cell clumps were visible under the microscope, 1.5 ml of this single-cell suspension was added to a new flask containing 20 ml of PC12 media, and the same was done with the original flask. The passage number and date were noted on the flasks and they were returned to the incubator. The passaged cells were either maintained in the incubator for further growth or plated for experiments. The entirety of the cell culture work was conducted using sterile technique in the cell lab (See Appendix B for a detailed protocol).

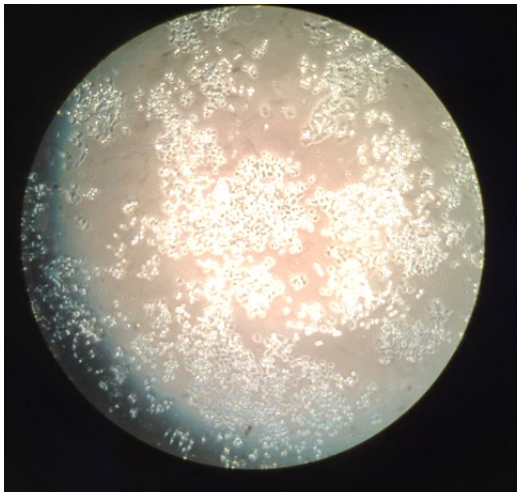

**Figure 2.1** PC12 cells, checked for confluency under a light microscope.

**Table 2.1 PC12 medium**

| Reagent | Final concentration in medium | Quantity |
|---|---|---|
| Dulbecco's Modified Eagle Medium (DMEM) | -- | 500 ml |
| Fetal Bovine Serum (FBS) | 10% | 50 ml |
| Horse serum (HS) | 5% | 25 ml |
| Pyruvate (P) | 1% | 5 ml |
| Pen-strep (PS) | 1% | 5 ml |
| L-Glutamine (G) | 2% | 10 ml |

### 2.2.2 Plating PC12 cells

In order to obtain a plating cell density of $7x10^4$ cells/ml, a cell count of the suspension was measured after passaging. This was done by placing 20 µl of the cell suspension onto a Neubauer Haemocytometer (VWR International LLC, Randor, USA) and counting three separate gridded square fields using a light microscope. The average of the three fields was used as the estimated cell density. The following equation was then used to calculate the volume of cell suspension required for plating:

$$Volume\ in\ \mu L = \frac{10 * 10^4\ cells/ml * 1000\ \mu L\ media}{Calculated\ Average *\ 10^4\ cells/ml} = \frac{10^4}{Calculated\ Average}\mu L$$

**Table 2.2 Plating of PC12 Cells**

| Experiment | Type of plate | Volume of medium | Cell density/ml |
|---|---|---|---|
| MTT assay | Transparent 96-well cell culture plate Nunc$^{TM}$ | 1 ml | 7 x $10^4$ |
| Trypan blue exclusion counting assay | Small petri dishes (35 mm) | 1 ml | 7 x $10^4$ |
| Glutathione / Hoechst staining | Black 96-well plate | 1 ml | 7 x $10^4$ |
| Calcium-influx assay | Black glass bottom 96-well plate | 1 ml | 7 x $10^4$ |

## 2.2.3 MTT Assay

The MTT assay is a widely used colorimetric assay which measures the cell viability of a given population of cells. MTT, (3-(4,5-dimethylthiazol-2-yl)-2,5-diphenyltetrazolium bromide, is a yellow tetrazolium salt that—upon dissolution into an aqueous medium—carries a positive charge, and thus readily enters viable cells via the plasma membrane potential (10). Inside the cell, mitochondrial NAD(P)H-dependent enzymes reduce MTT to a purple water-insoluble formazan compound. The MTT assay thus measures cell viability by proxy of metabolism, since only viable, metabolically active cells are able to convert MTT into formazan.

PC12 cells were plated in a 96-well plate at the cell density described by Table 2.4, and incubated for 24 hours. The following day B7, B20 and SHB20 exposure solutions were prepared as described in section 2.1.1. The medium was then removed from the wells which would contain the treatment/exposure and the exposure solutions were added as (n = 8). A column containing untreated cells with only fresh medium was used as a blank, and a column of untreated cells with MTT were used controls (n = 8 in both cases). The cells were exposed for 24, 48 and 72 hours, respectively.

The MTT solution was prepared before each use. Due to its toxicity, extra care was taken when handling MTT (laboratory mask and protective eye wear were used in addition to lab coat and gloves). MTT (5 mg) (ThermoFisher Scientific, Waltham, USA) was weighed and dissolved in an Eppendorf tube with 1 ml of phosphate-buffered saline solution, PBS. (Table 2.5). 10 µl of the MTT solution was then added to each well, except the blank column, and the plate was incubated for 3 hours. Lastly, the contents of all the wells were replaced with 100 µl of dimethyl sulfoxide, DMSO (Sigma-Aldrich, St. Louis, USA). The formazan was solubilized in DMSO (figure 2.2), and after 30 minutes incubation, the absorbance of the solution was measured in the CLARIOstar® plate reader (BMG Labtech, Germany) at 570 nm. See Appendix B for a detailed protocol.

**Table 2.3 PBS**

| **Reagent** | **Final concentration in solution** |
|---|---|
| NaCl | 138 mM |
| KCl | 2.7 mM |
| $KH_2HPO_4$ | 2 mM |
| $Na_2HPO_4$ x 2 $H_2O$ | 10 mM |
| MQ water | ad 4000 ml |

The pH of the solution was adjusted to 7.4 and the solution was subsequently autoclaved and stored at 4°C.

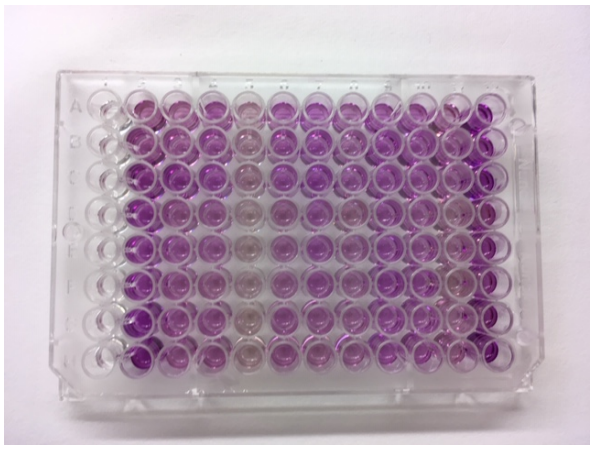

**Figure 2.2.** MTT plate upon addition of DMSO

### 2.2.4 Trypan Blue Assay

The functional nature of the MTT assay comes with limitations, namely not being possible to distinguish between cell death and reduced metabolic cellular activity. Therefore, the Trypan Blue exclusion counting assay was also performed alongside the MTT assay. Four 1 ml dishes for each DEP were plated in duplicate, as follows in Table 2.6:

**Table 2.4 Trypan Blue plating**

| | **Dish** | | | |
|---|---|---|---|---|
| **DEP** | **1** | **2** | **3** | **4** |
| B7 | Control (untreated cells) | 5 µl/ml | 10 µl/ml | 50 µl/ml |
| B20 | Control (untreated cells) | 5 µl/ml | 10 µl/ml | 50 µl/ml |
| SHB20 | Control (untreated cells) | 5 µl/ml | 10 µl/ml | 50 µl/ml |

Cells were plated alongside the MTT plates, as described in Table 2.4, and incubated for 24/48/72 hours respectively, at 37°C and 5% $CO_2$. The following day, exposure solutions

were made and added to the plates according to section 2.1.1. After 24/48/72 hours of exposure, a 1:1 volume solution of 1.8% NaCl and trypan blue stain was made and 250 µl was added to each dish and they were incubated for 30 minutes. The contents of the dishes were then removed, and the number of blue cells versus unstained cells were counted under a light microscope. 100 cells were counted in each dish. (See Appendix B for a detailed protocol).

### 2.2.5 Glutathione Measurement

Cells were seeded in black 96-well plates (Thermo Scientific, Roskilde, Denmark), as indicated in Table 2.4 and incubated for 24 hours. Exposure solutions were made according to section 2.1.1 and added to all the wells except the blank and control columns. After 24 hours of exposure, 40 uM of monochlorobimane (mBCl) (Sigma-Aldrich, St. Louis, USA) was diluted in 10 ml medium and this was added to all of the wells except for the mBCl control column. The plate was incubated for 30 minutes, and N-buffer was prepared (table 2.7) during this time. After the incubation, the medium was removed, washed and replaced with the N-buffer. The fluorescence was recorded using the CLARIOstar® plate reader at excitation and emission wavelengths of 380 nm (15 nm bandwidths) and 478 nm (21 nm bandwidths), respectively. (See Appendix B for a detailed protocol)

### 2.2.6 Hoechst staining

Hoechst dye was used to normalize glutathione measurements to the cell density. Since Hoechst binds to DNA it can give a more accurate value than glutathione measurements alone. This was done immediately after glutathione measurement by replacing the contents of the wells with 0,4ug/ml Hoechst 33342 dissolved in N-buffer and the plate was incubated in a dark drawer for 1 minute. The contents of the wells were then replaced with 100 µl of N-buffer and the plate was read at excitation and emission wavelengths of 350 nm (22 nm bandwidths) and 461 nm (36 nm bandwidths), respectively.

### 2.2.7 Calcium influx

PC12 cells were seeded as described in Table 2.4 using Corning® CellBIND® 96-well Flat Clear Bottom Black Polystyrene Microplates precoated with poly-L-lysine and incubated for 24 hours. The medium was then replaced with serum-free medium (PC12 medium which contained no horse serum) with NGF added at a concentration of 2.5 ul/ml. The plate was then incubated for 48 hours, after which time 55 µl of medium from each well—except the first column which was used as the blank—was removed using a multi-pipettor and placed in a reagent reservoir. Next, 50 µl of Fura-2 was added to the reservoir and mixed well using the multi-pipettor. 45 µl of the Fura-2 solution was then added back to each well (except the first column), and the plate was then incubated for 20 minutes. Next, the media was removed from every well and replaced with 100 µl Wash Buffer, and then repeated once more so as to wash the cells. The plate was then incubated for 12 minutes in a dark drawer. The baseline $Ca^{2+}$ level in the cells was then immediately measured in the CLARIOstar® Plate reader. The wash buffer was then removed from the wells and 100 µl of N-buffer with DEP exposure treatment was added to the wells except the control columns. The response was measured in the plate reader immediately after exposure and 15, 30, 45, 60 and 75 minutes after exposure. (See detailed protocol in Appendix B).

**Table 2.7 Calcium-influx Solutions**

| Solution | Reagent | Final concentration | Volume |
|---|---|---|---|
| N-buffer | NaCl 5M | 140 mM | 1.12 mL |
| | KCl 1M | 3.5 mM | 140 µL |
| | Tris-HCl 1M pH 7 | 15 mM | 600 µL |
| | $Na_2HPO_4$ x $NaH_2PO_4$ 0.1 M pH 7.4 | 1.2 mM | 480 µL |

| | | | |
|---|---|---|---|
| | Glucose 1 M | 5 mM | 200 µL |
| | $CaCl_2$ 1M | 2 mM | 80 µL |
| | MQ-water | - | ad 40 mL |
| **Solution** | **Reagent** | **Volume** | |
| Wash buffer | N-buffer | 10 mL | |
| | $MgSO_4$ 1 M | 10 µL | |
| Stimulating buffer | N-buffer | 4 mL | |
| | NMDA 0.1 M | 20 µL | |
| | Glycine 0.1 M | 10 µL | |
| All of the solutions were made the same day of the experiment | | | |

## 2.3 Chicken embryo model

Fertilized chicken eggs (*Gallus gallus*) were obtained from Nortura Samvirkekylling (Våler, Norway) and were assigned a number and registered in a logbook upon delivery. The eggs were placed in an incubator (Ova Easy Advance II series ®) in racks which were pre-programed to tilt mechanically, so as to mimic the brooding of a hen. This was considered embryonic day 0 (E0). The incubator was set to 37 °C and 45% humidity. The eggs were obtained with the national project permission with FOTS-id:13896 and experiments were in line with the EU directive 2010/63/EU on the protection of animals used for scientific purposes.

### 2.3.1 *In ovo* exposure of chicken embryos

On embryonic day 13 (E13), the eggs were removed from the incubator and randomly assigned to groups, and then labeled according to their group. The average weight of the eggs was taken, and from this the volume of the exposure solutions to be injected was calculated as 10 µl exposure/10 g egg. DEP solutions were made as described in Table 2.4. Next, the viability of the eggs was checked by using a LED light to transilluminate the eggs, while the room was kept dark. The viability of the eggs was determined as described in Table 2.8. The embryos that were either dead or unfertilized were registered in the logbook and discarded. As the eggs were checked for viability, an injection site was marked with a pencil. A site was chosen that avoided major visible blood vessels but was reasonably close to one. The injection site was wiped with 70% isopropyl alcohol swabs (Alkotip®) and a small superficial hole about 0,4mm was made by carefully puncturing the shell with a disinfected needle. The non-injected control group was not punctured, as they did not receive any injection. The exposure solutions were then injected into the eggs via the punctured hole using a sterile syringe (30G). The eggs were returned to the incubator until day embryonic day 17 (E17).

**Table 2.8 Determination of embryo viability**

| |
|---|
| **Viable Embryos:** Well-defined blood vessels present, spontaneous movements in response to the light and/or movement of the egg. |
| **Early deaths:** A small dark area and deteriorating blood vessels appear as a dark ring around the egg. |
| **Late Deaths:** Blood vessels might still appear intact, but there is an absence of spontaneous movement. |
| **Infertile eggs:** The egg is clear (no embryo). |

**Table 2.9 Exposure of chicken embryos**

| Exposure of chicken embryos | Final concentration in the egg |
|---|---|
| Pyrene | 1 uM |
| Benzo(a)pyrene | 1uM |
| DSMO control | 0,001% |
| B7 | 50 ug/egg |
| B20 | 50 ug/egg |
| SHB20 | 50 ug/egg |
| Saline Control | |
| Non-injected control | -- |

## 2.3.2 Harvesting of the cerebella

On E17, the chicken embryos were sacrificed, four days before normal hatching (E21). The eggs were removed from the incubator and submerged in crushed ice for 7 minutes so as to anesthetize the embryos before the cerebellar isolation. The eggs were cracked in a sterile petri dish (14 cm) and the embryos (Figure 2.4) were decapitated using a sterile scalpel. The cerebella were then extracted using scissors to make a T-cut through the skin and meninges and tweezers and a spatula were used for the extraction. The cerebella were then carefully cleaned of extraneous tissues and immediately transferred to pre-labeled cryotubes which were placed in liquid nitrogen (-196 °C) until the end of the harvest. Once all of the cerebella had been harvested, the cryotubes were stored in the freezer at -80 °C until homogenization the following day.

**Figure 2.4.** Chicken embryo at E17, just before decapitation

### 2.3.3 Homogenization of the cerebella

The isolated cerebella were individually weighed and then transferred to an Eppendorf tube for homogenization. The solutions used (Table 2.10) were made earlier the same day. Next, 120 µL of TE-buffer with protease inhibitors was added to the brain tissue in the Eppendorf tube and homogenized using the Pellet pestle®. Then, 70 µL of the homogenate was removed and placed in a new Eppendorf tube for qPCR analysis and frozen until RNA isolation. Afterwards, 80 µL of TE-buffer with protease inhibitors was then added to the remaining homogenate and was homogenized once more using the pestle. Next, 150 µL of TE with 4% SDS was added to the homogenate and it was homogenized using a sterile needle (1 ml) and syringe (21G). The homogenate was then boiled for 5 minutes at 95°C using a heat block. Lastly, a 1:20 dilution was made by adding 10 µL of the homogenate to 190 µL of the TE-stock solution into a new Eppendorf tube. All of the samples were stored at -20°C.

| **Table 2.10 Cerebellar Homogenization Solutions** | | |
|---|---|---|
| Solution | Reagent | Quantity |

| | | |
|---|---|---|
| Tris-EDTA (TE)-buffer | EDTA 0.5M | 0.1 mL |
| | Tris pH 8.0 | 0.5 mL |
| | MQ | 49.4 mL |
| TE-buffer with 4% SDS | 20 % SDS | 5 mL |
| | TE-stock | 15 mL |
| TE-buffer med protease inhibitors | Leupeptin 5 mg/ml | 8 µL |
| | PMSF 100 mM | 24 µL |
| | Pepstatin A 1 mg/ml | 40 µL |
| | $Na_3VO_4$ 10 mM | 80 µL |
| | TE-Stock | 4 mL |

### 2.3.4 Chicken neuronal cell culture

Cerebellar granular neurons (CGNs) were harvested from chicken embryos to obtain a primary neuronal cell culture. Since CGNs do not adhere well to culture plates, the plates were first coated with poly-L-lysine (PLL). This polymer has a positive charge that interacts with the negative charge of the cells and this ionic interaction allows for better cell adhesion. The harvest was performed on Monday, and the plates were coated the Friday before. A 0.5 mg/ml solution of PLL was prepared by dissolving 5 mg of poly-L-lysine in 10 ml of MQ-water. This solution was further diluted to a concentration of 0,01 mg/ml and 100 µl was

added to all the wells of 96-well glass-bottomed plate. After 45 minutes, the PLL solution was removed from the wells and the plates were left covered, in the LAF bench to dry over the weekend with the air flow at maximum speed.

On E17 the eggs were removed from the incubator and placed in crushed ice for 7 minutes so as to anesthetize the embryos before the cerebellar isolation, which was performed as previously described in section 2.3.2. The isolated cerebella were placed in a sterile petri dish containing (14 cm) containing solution 1. Once all cerebella had been isolated, solution 1 was removed from the petri dish and the cerebella were thoroughly cut into small pieces by using a sterile scalpel and cutting in two perpendicular directions. Next, 10 ml of solution 1 was added and this suspension was transferred to a 50 ml tube which was centrifuged at 1000 rpm for 1 minute. The supernatant was then removed and 8 ml of solution 2 was added and the entire cell suspension was pipetted up and down to disperse the pellet at the bottom of the tube that had formed from centrifugation. The suspension was then transferred to a trypsinizing flask and placed in a 37 °C water bath for 15 minutes. The caps were on loosely. The flask was periodically shaken during this time, so as to enhance the conversion of tissue to a cell suspension. The suspension was then transferred to a new 50 ml tube containing 15 ml of solution 4 and centrifuged at 1000 rpm for 2 minutes. The supernatant was removed and 3 ml of solution 3 was added, pipetting up and down using a sterile Pasteur pipette (Thermo Scientific, South Wales, UK). The suspension was then allowed to stand until lumps of tissue had settled. Then the top portion of the suspension containing single cells was transferred to a new sterile 50 ml tube containing 15 ml of solution 5. Then 2 ml of solution 3 was added to the tube still containing the sedimented tissue and incubated again. The supernatant was then transferred to the tube containing solution 5 until no clumps were visible, and then centrifuged at 900 rpm for 7 minutes. The supernatant was once again removed and 10 ml of cell culture medium with chicken serum and without KCl was added. The cell suspension was thoroughly mixed and finally 10 µL was removed for counting and diluted to 100 µL with the medium containing chicken serum and no KCl (10 times dilution).

## 2.4 Gene expression analysis

### 2.4.1 Isolation of total RNA from cerebella

RNA was isolated from the homogenized cerebella using RNeasy® Plus Mini Kit.

### 2.4.2 cDNA synthesis

To be able to use the qPCR assay, the mRNA must first be reversely transcribed into complementary DNA (cDNA) using a reverse transcriptase enzyme in a reverse transcription (RT)-reaction. This RT-reaction creates a representative population of cDNA from the original mRNA population. The cDNA can be used as a template for the real-time quantification in the qPCR assay

cDNA was made using the Applied Biosystems High-Capacity RNA-to-cDNA ™ Kit.

1. Make a cDNA pool with 5 µl of each sample which give a cDNA concentration of 50 ng/ µl.
2. 50 ul av cDNA pool plus 450 ul water
3. Make a 1:1 dilution of the cDNA pool (yields 5 ng/ul)
4. Make a dilution series where we dilute 1/5 so that we get 1/5; 1/25; 1/125; 1/625 which is the same as 5; 1; 0.2; 0.04; 0.008 ng/ul
5. Make mastermix for 4 different primers
6. Add the primers to the PCR plate, add 11 µl/well
7. Add 9 µl cDNA, seal the plate, centrifuge briefly
8. Run qPCR

## 2.5 Statistical analysis

Data were processed using Microsoft Excel version 2013 for macOS. The statistical analyses and graphical presentations were performed using GraphPad Prism 8.1 (Graph-Pad Software, La Jolla, CA, USA). DEP-treated groups were compared to those obtained from the control group. Statistical significance was determined using One Way analysis of variance (ANOVA) followed by Dunn's, Tukey's, or Dunnett's *post hoc* tests for normally distributed data. Data that were not normally distributed were testing using Kruskal-Wallis Dunn's *post hoc* test. Differences between two groups were tested using a t-test. In all tests, a p-value $< 0.05$ was considered a statistically significant difference and data are shown as means ± Standard error of the mean (SEM).

# 3 Results

## 3.1 PC12 Cells

### 3.1.1 Cell viability as measured by MTT

MTT assay was performed on PC12 cells exposed to B7, B20, and SHB20 at three different concentrations (2, 10, 50 µg/ml cell medium). The cells were then incubated for 24/48/72 hours, respectively. The plates were treated equally with the exception of the duration of the incubation.

After 24 hours of exposure, there was a dose-dependent reduction in viability which was significant for the cells exposed to the highest concentration of B7 (50 µg/ml) as well as SHB20 (Figure 3.1). In addition, B20 showed a significant decrease in cell viability for the intermediate concentration, 10 µg/ml. At 24 hours, the intermediate concentration of B20 (10 µg/ml) had a lower viability (that was significantly different than the control) than the highest concentration (50 µg/ml). The 48-hour exposure indicated similar results, in addition to B20 (50 µg/ml) having a significant decrease in cell viability compared to the control. At 72 hours of exposure, the overall tendency of decreasing viability remained similar, and all of the DEP at their highest concentration were significantly different from the control. Starting at the 48-hour time point, a dose-dependent response became evident (Figure 3.1 B, C), and the highest concentration of each DEP was significantly different from the control as of this time point as well.

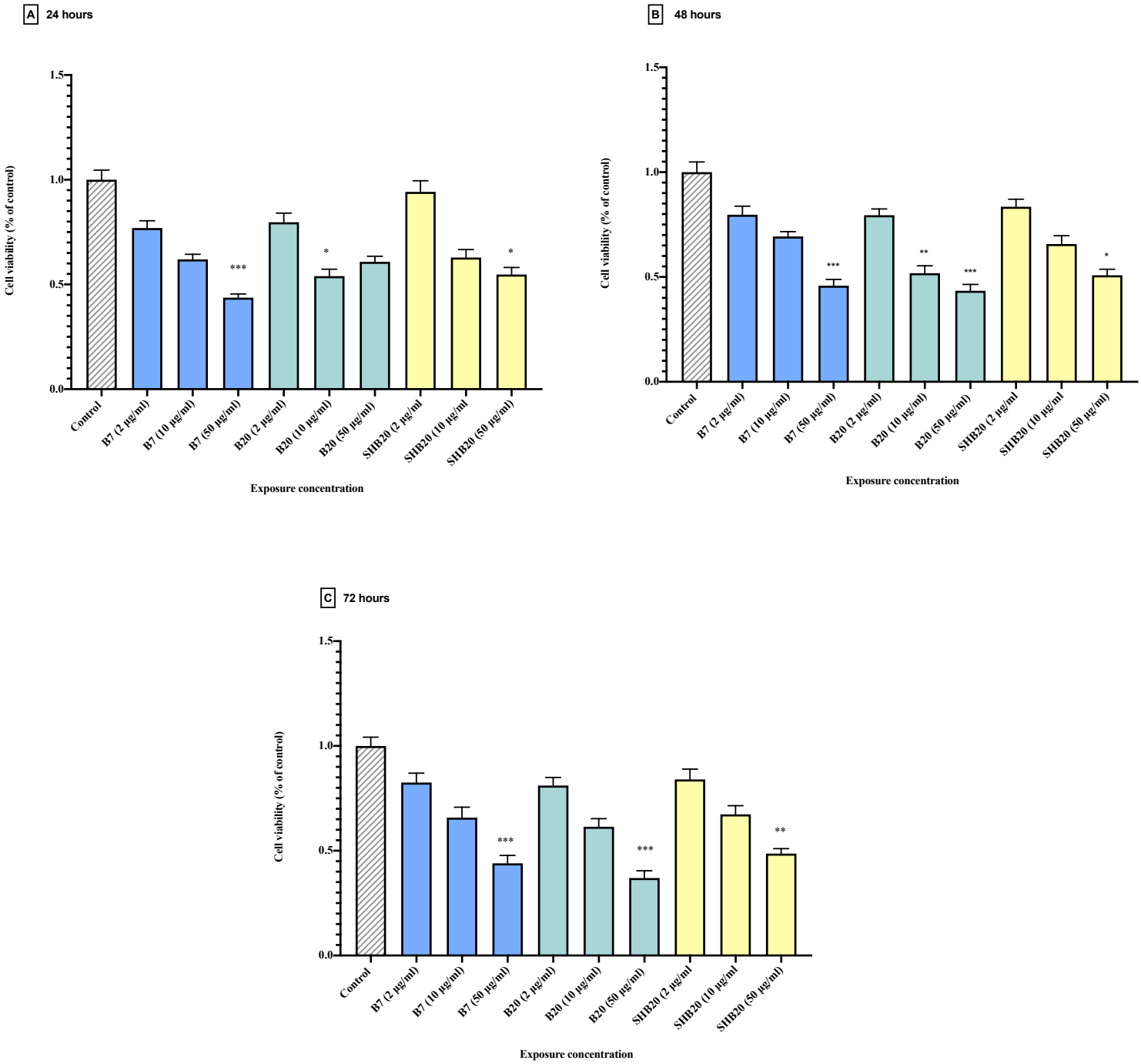


**Figure 3.1 Cell viability in PC12 cells as measured by MTT assay after exposure to DEP.** PC12 cells were seeded and 24 hours later exposed to B7, B20, SHB20 at three different concentrations (2, 10, 50 µg/ml). MTT assay was performed 24 hours after exposure **(A),** 48 hours after exposure **(B)** and 72 hours after exposure **(C).** The data are displayed as relative values normalized to the control (untreated cells) ± SEM. For each treatment n = 3. Significance is shown by: $p \leq 0.05$ (*), $p \leq 0.01$, $p \leq 0.001$ (***), compared to the control as analyzed by One Way ANOVA with Kruskal-Wallis *post hoc* test.

### 3.1.2 Cell viability as measured by trypan blue exclusion assay

Trypan blue staining was performed following the MTT assay, to investigate whether the decrease of PC12 cell viability was actually due to cell death, or if it alternatively was a reduction of metabolic cellular activity or change in cell proliferation. The PC12 cells were plated in parallel to the MTT plates and under the same conditions (same cell passage number, same exposures and incubation periods). While there was a general tendency that agreed with the MTT data – increase in cell death at higher concentrations of DEP— B7 (50 µg/ml) was the only one to have a statistically significant difference compared with the untreated control (Figure 3.2) Moreover, B7 had a very clear dose-dependent increase in cell death, which correlated with the same dose-dependent decrease in cell viability (Figure 3.1). The approximately 40% cell death at 24 hours and the increase to 50% cell death at 72 hours thus confirms the MTT data. This was not the case however, for B20 or SHB20, which did not follow as clear a trend for all exposure times. The lowest dose of SHB20 for example, was more lethal than the intermediate dose at 48 hours (18% and 12%, respectively), and slightly more lethal than the highest dose (about 18% and 15%, respectively). Likewise, the lowest dose of B20 was more lethal than the higher dose of 10 µg/ml, at 72 hours (about 20% and 25%, respectively).

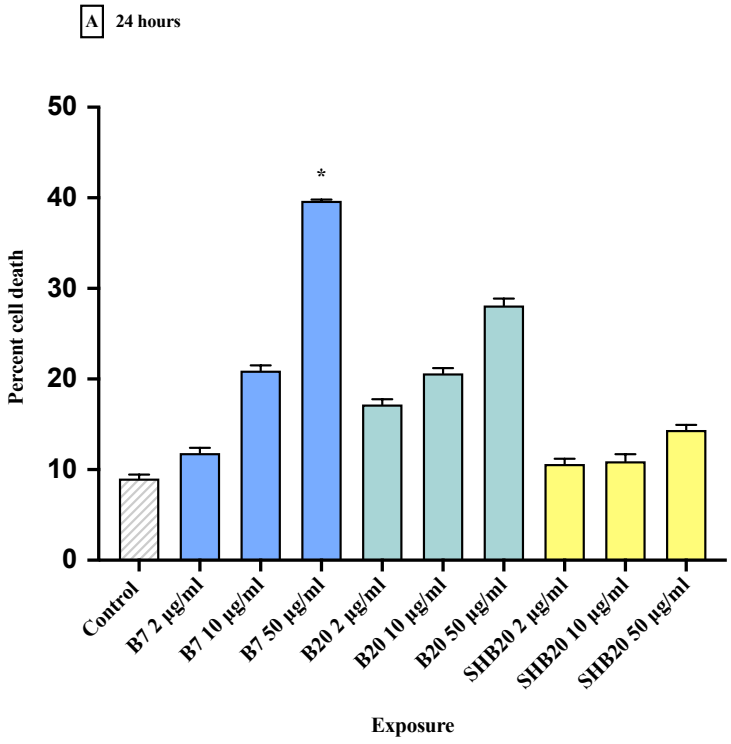

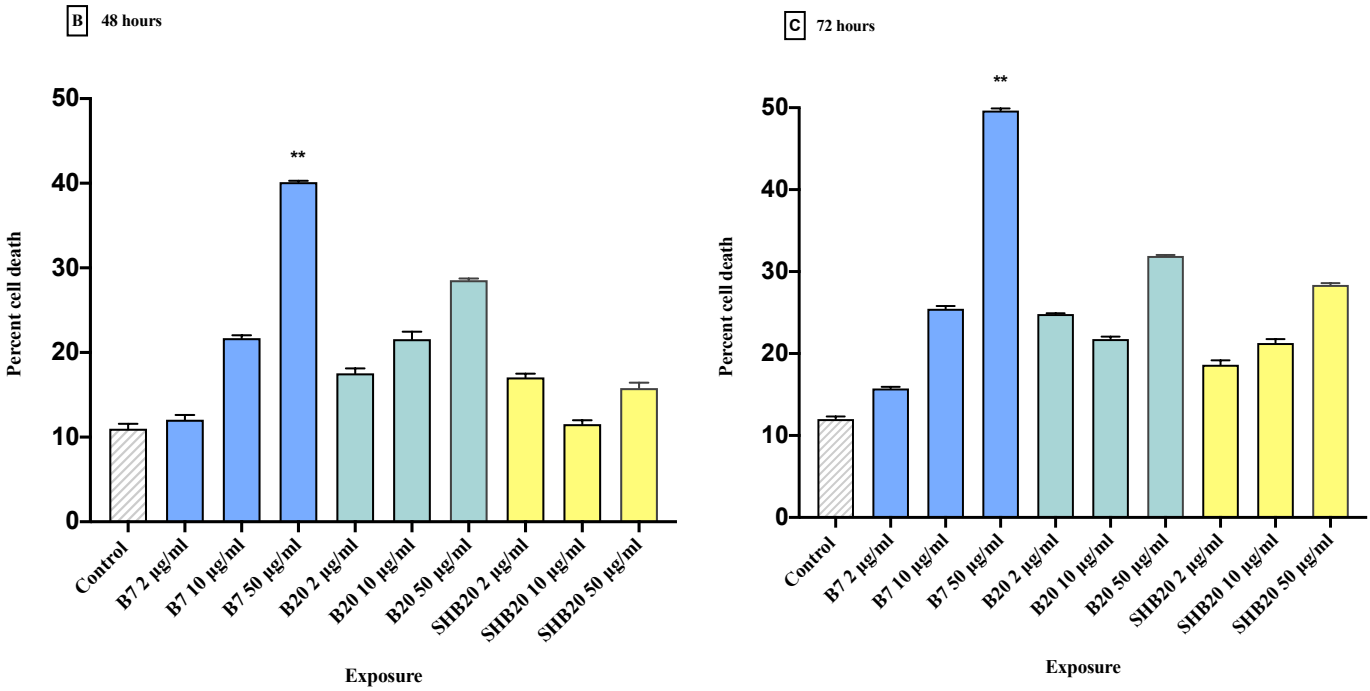


**Figure 3.2 PC12 cell death measured by Trypan blue exclusion assay.** Cells were seeded into small dishes and 24 hours later exposed to B7, B20, SHB20 at three different concentrations (2, 10, 50 µg/ml). The number of live versus dead cells were counted 24 hours after exposure **(A),** 48 hours after exposure **(B)** and 72 hours after exposure **(C).** The data are displayed as average values ± SEM. For each treatment n = 3. Significance is denoted as $p \leq 0.05$ (*), compared to the control as analyzed by One Way ANOVA, with Kruskal-Wallis post hoc test.

### 3.1.3 Intracellular glutathione measurement

Figure 3.3 shows the boxplot for the levels of glutathione measured 24 hours after exposure to B7, B20, and SHB20. There was an observable decreasing tendency with increasing doses of DEP. B7 at both 10 and 50 µg/ml had a statistically significant decrease in GSH levels compared to the control, as well as B20 at 10 µg/ml. This corresponded with the results from the 24-hour MTT assay in which B20 10 µg/ml had a significant decrease in cell viability, while the higher dose did not (Figure 3.1 A).

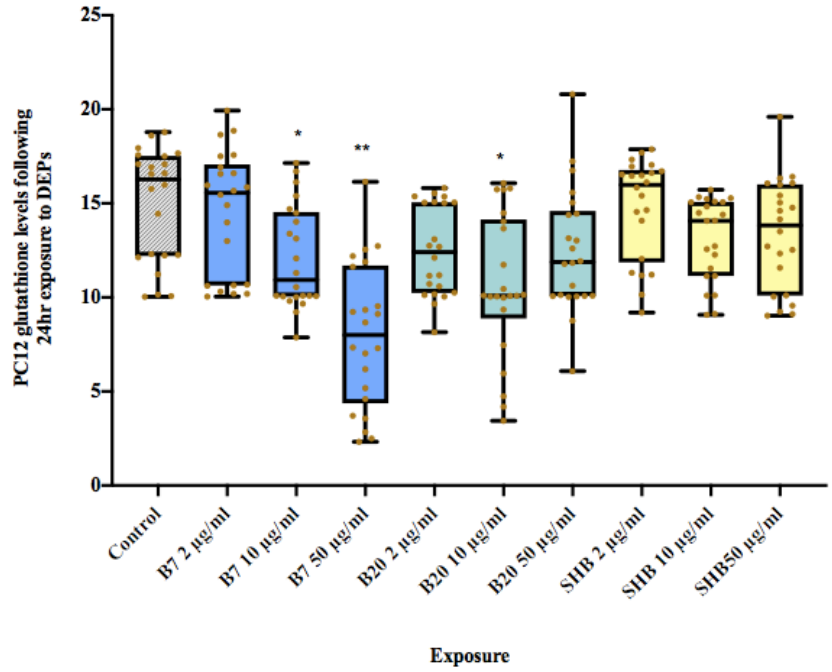


**Figure 3.3 Glutathione levels in PC12 cells measured by the mBCl fluorometric assay.** Cells were seeded and plated and 24 hours later exposed to B7, B20, SHB20 at three different concentrations (2, 10, 50 µg/ml). GSH was measured 24 hours after exposure, followed by staining with Hoechst 33342. The boxes represent the second and third quartiles. The horizontal lines represent the median. The whiskers represent the minimum to maximum value range, with all data points represented as yellow dots. The data are displayed as corrected against fluorescent intensity with Hoechst 3342. For each treatment n = 3. Significance is shown by: $p \leq 0.05$ (*), $p \leq 0.01$ (**), $p \leq 0.001$ (***) compared to the control (untreated cells). Analyzed by One Way ANOVA with Kruskal-Wallis post hoc test.

### 3.1.4 Calcium-influx measurement

PC12 cells were induced to differentiate in the presence of NGF 48 hours prior to exposure as described in section 2.2.7. Cells were plated alongside the $Ca^{2+}$ influx plate and visually inspected for morphological signs of differentiation, using a light microscope. As indicated in Figure 3.4A, the cells were first observed at 24 hours, in which the neurites began to grow and elongate outwards. At 48 hours (Figure 3.4 B), the neurites were observed to have elongated considerably, in addition to a higher quantity of cells growing neurites. It was also apparent that the PC12 cells had ceased dividing, as the plate was not at the same confluency level as the plate which was not treated with NGF.

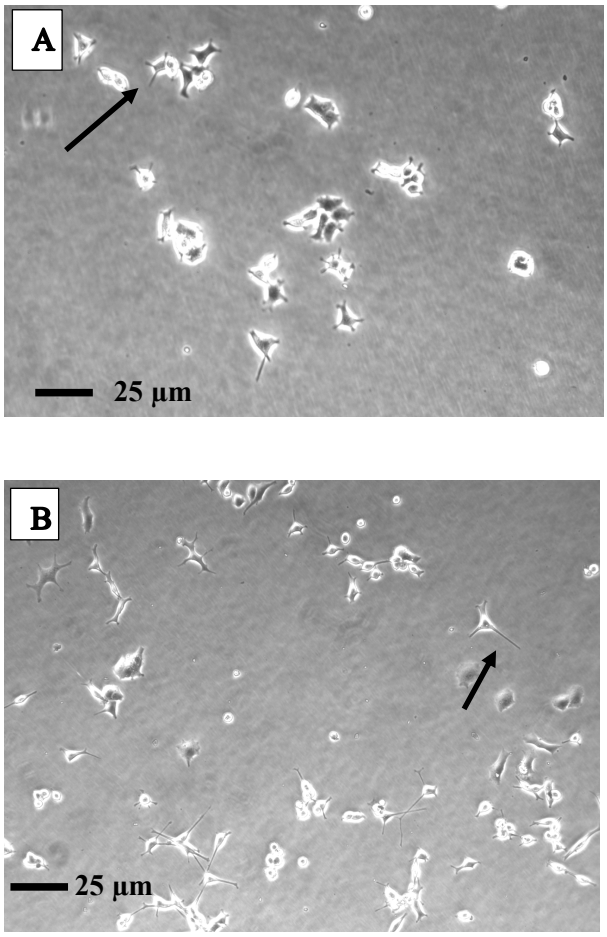


Figure 3.4 PC12 cells after incubation with NGF. PC12 cells observed: **(A)** 24 hours after incubation with NGF and **(B)** 48 hours after incubation. Arrows indicate neurite outgrowth.

PC12 cells were loaded with fura-2 fluorometric dye and baseline levels read before the DEP exposure treatments were added. The calcium response was measured immediately, then at 15, 30, 45, 60 and 75 minutes post-exposure (Figure 3.5). While there were no statistically significant changes, similar trends were observed as those seen with the MTT and GSH data. B7 had once again a positive correlation between the concentration of the exposure and the response: at all the time points, the level of calcium influx increased with increasing concentration of the DEP. SHB20 showed a similar response, although much more nuanced. B20 however, did not follow this trend, as it was the 10 µg/ml concentration that evoked the highest levels of calcium influx. This concentration was significant for B20 in the MTT assay at both the 24- and 48-hour time points, and for GSH levels at 24 hours as well.

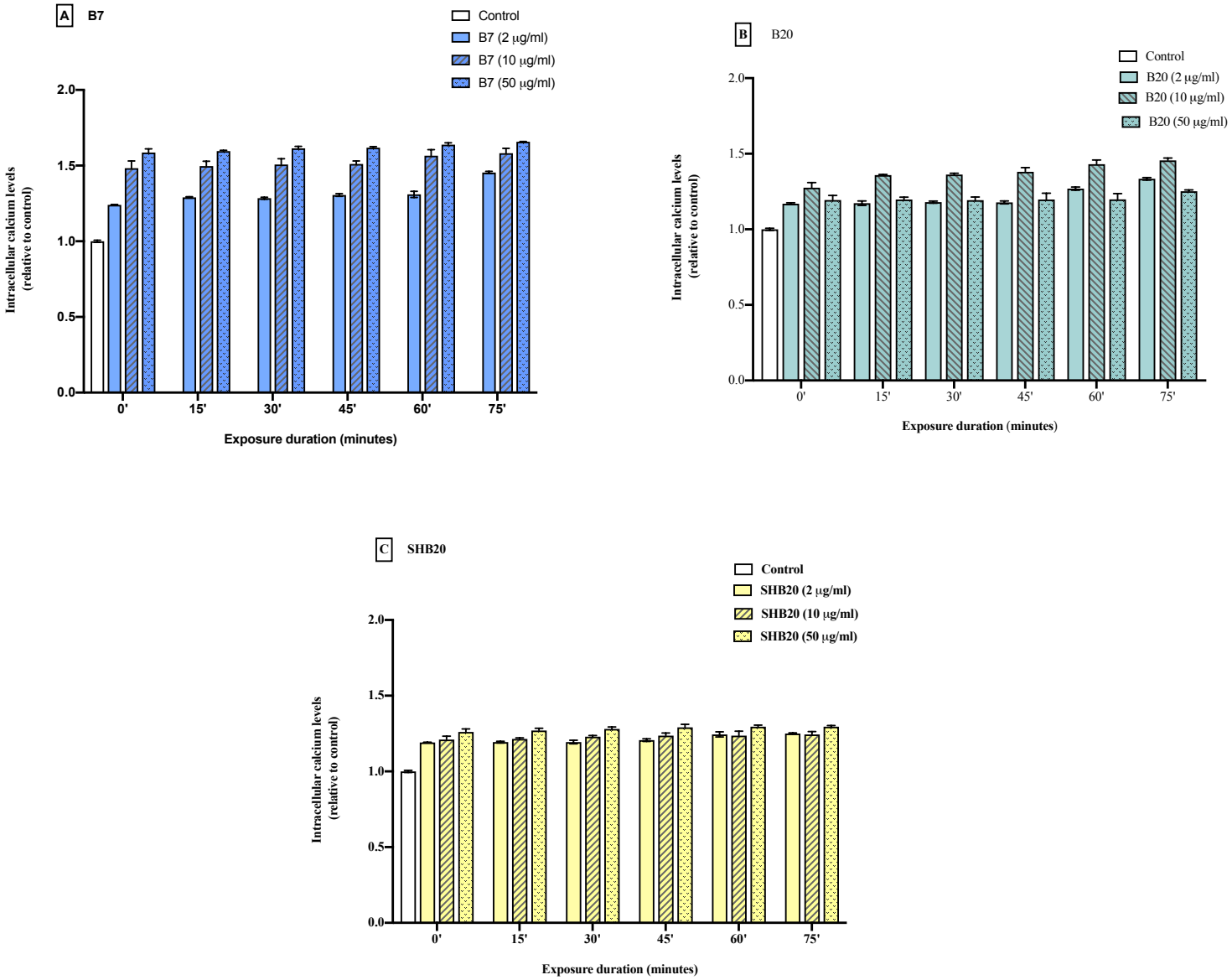


**Figure 3.5 Calcium influx measurement in PC12 cells as measured by Fura-2 after exposure to DEP.** PC12 cells were induced to differentiate in the presence of NGF and 24 hours later exposed to B7, B20, SHB20 at three different concentrations (2, 10, 50 μg/ml). Calcium influx was measured by use of Fura-2 assay at 0, 15, 30, 45, 60, and 75 minutes. **(A)** B7 exposure **(B)** B20 exposure **(C)** SHB20 exposure. The data are displayed as relative values normalized to the control (untreated cells) ± SEM. For each treatment n = 3. Data were analyzed using a One-Way ANOVA. Kruskal-Wallis was used as a post hoc test. No significant differences among exposures were found for any of the DEP.

## 3.2 Chicken granule neurons

### 3.2.1 Cell viability as measured by MTT

The MTT assay was performed to measure cell viability of the CGN cell culture. As with the PC12 cells, viability was measured at 24, 48, and 72 hours post exposure to DEP. At 24 hours, the viability of cells exposed to B7 50 µg/ml and B20 50 µg/ml were significantly lower than those of the control, and there was indication of a dose-dependent response which became evident at 72 hours. In addition, all the DEP at their highest concentrations were significant at 72 hours. The 48-hour exposure, however, differed from the pattern seen by the 24- and 72-hour time points, as the intermediate concentration (10 µg/ml) of all DEP appeared to have higher cellular viability than their lowest concentration (2 µg/ml). Moreover, at the 48-hour time point, only B7 at 50 µg/ml showed a significant decrease in viability.

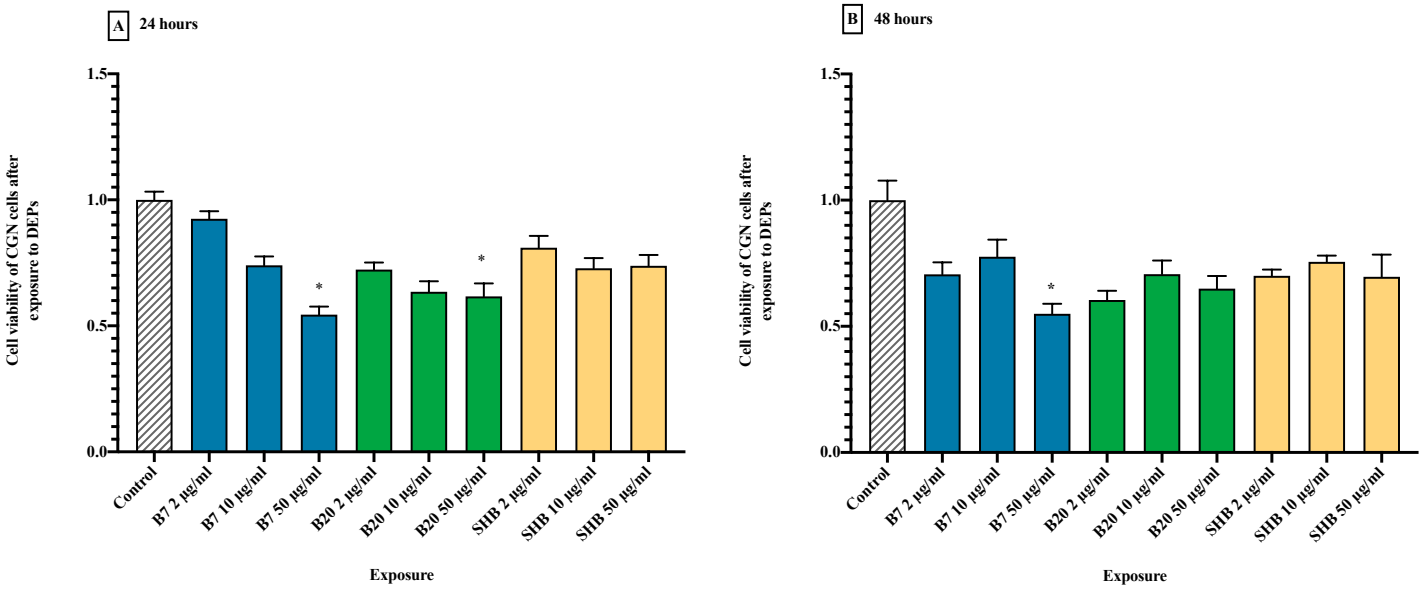

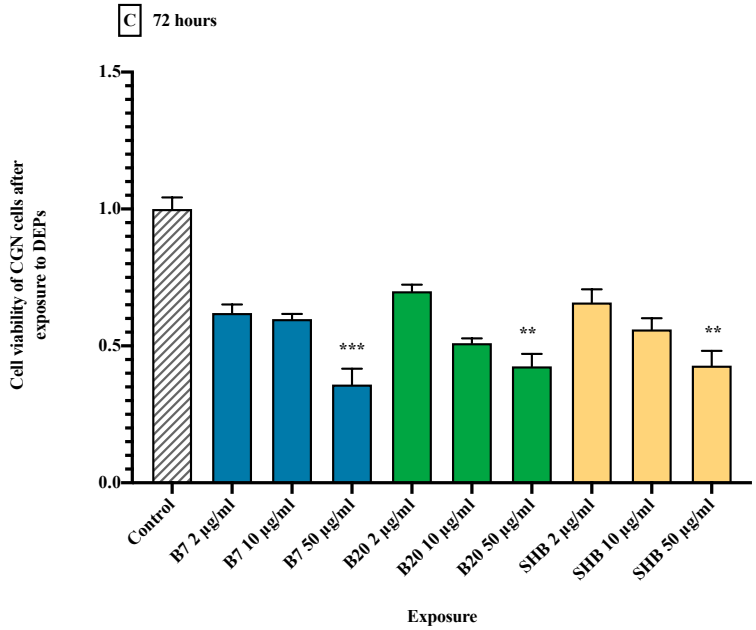


**Figure 3.6 Cell viability in CGN cells as measured by MTT assay after exposure to DEP.**

CGNs were seeded and 24 hours later exposed to B7, B20, SHB20 at three different concentrations (2, 10, 50 µg/ml). MTT assay was performed 24 hours after exposure **(A),** 48 hours after exposure **(B)** and 72 hours after exposure **(C).** The data are displayed as relative values normalized to the control (untreated cells) ± SEM. For each treatment n = 3. Significance is shown by: p≤ 0.05 (*), p≤ 0.01 (**), p≤ 0.001 (***), compared to the control as analyzed by One Way ANOVA with Kruskal-Wallis post hoc test.

## 3.2.2 Cell viability as measured by trypan blue exclusion assay

At 24 hours, an increase in cell death was not significant for any exposure. B7 50 µg/ml had the highest amount of cell death, about 25%. At 48 hours, it nearly doubled however, and was the only significant increase. At 72 hours exposure, the highest concentration of each DEP corresponded with the highest amount of cell death, and both B7 and B20 were significantly different from the untreated control at this time point. There was in general, a positive correlation between cell death and increasing exposure concentration for all DEP blends.

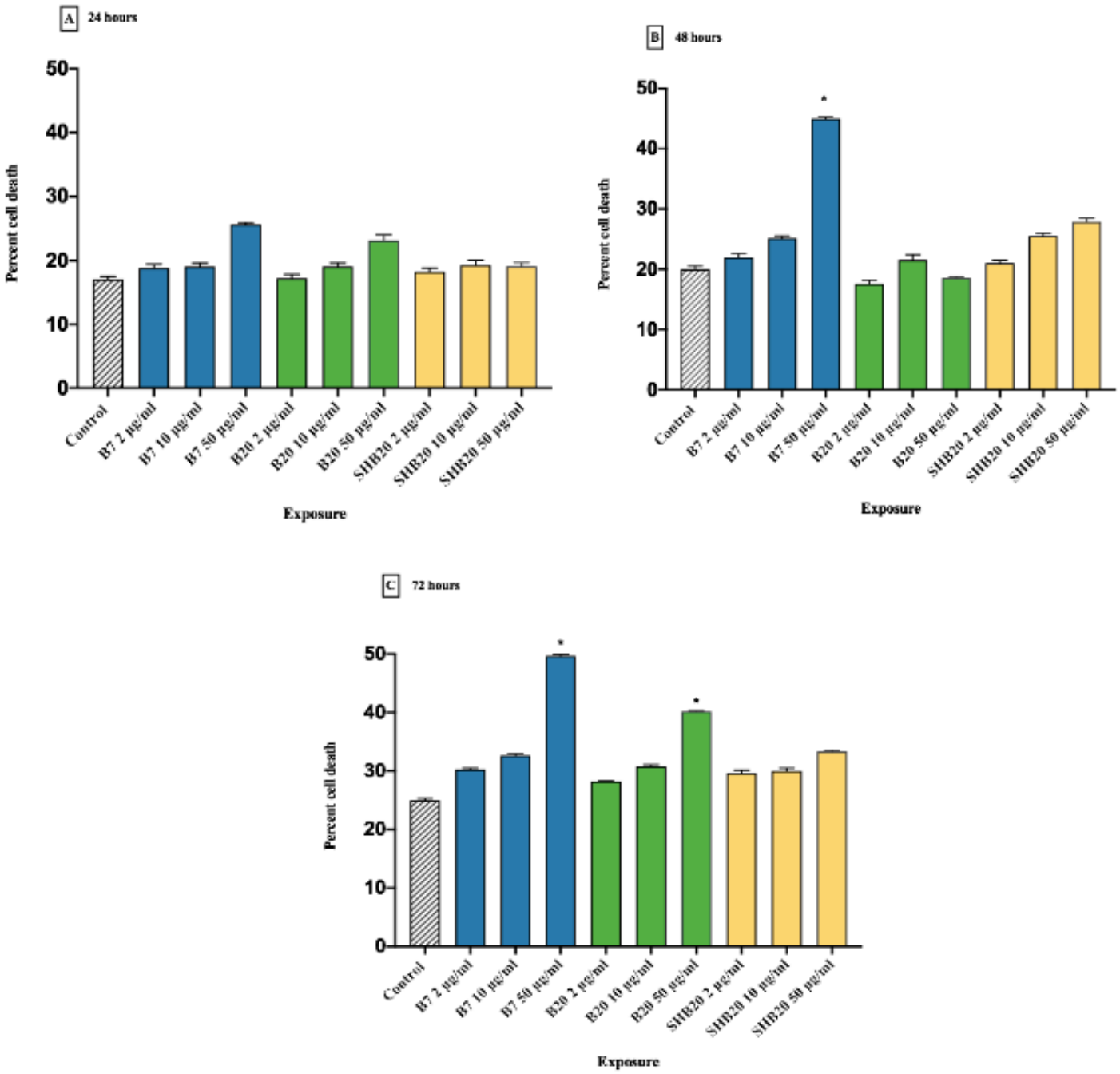


**Figure 3.7 CGN cell death measured by Trypan blue exclusion assay.** Cells were seeded into small dishes and 24 hours later exposed to B7, B20, SHB20 at three different concentrations (2, 10, 50 µg/ml). The number of live and dead cells were counted 24 hours after exposure **(A),** 48 hours after exposure **(B)** and 72 hours after exposure **(C).** The data are displayed as averages values ± SEM. For each treatment n = 3. Significance is denoted as $p \leq 0.05$ (*) compared to the control as analyzed by One-Way ANOVA, with Kruskal-Wallis post hoc test.

### 3.2.3 Intracellular glutathione measurement

Figure 3.8 indicates there was a decrease in the levels of GSH with increasing DEP concentration for every blend type. However, this effect was only significant for cells exposed to B7 and B20 at their highest concentrations, 50 µg/ml. This result was correlated with the decrease in cell viability seen at 24 hours (Figure 3.6A). Of the three DEP, cells exposed to SHB20 had the highest levels of GSH while those exposed to B7 had the lowest levels.

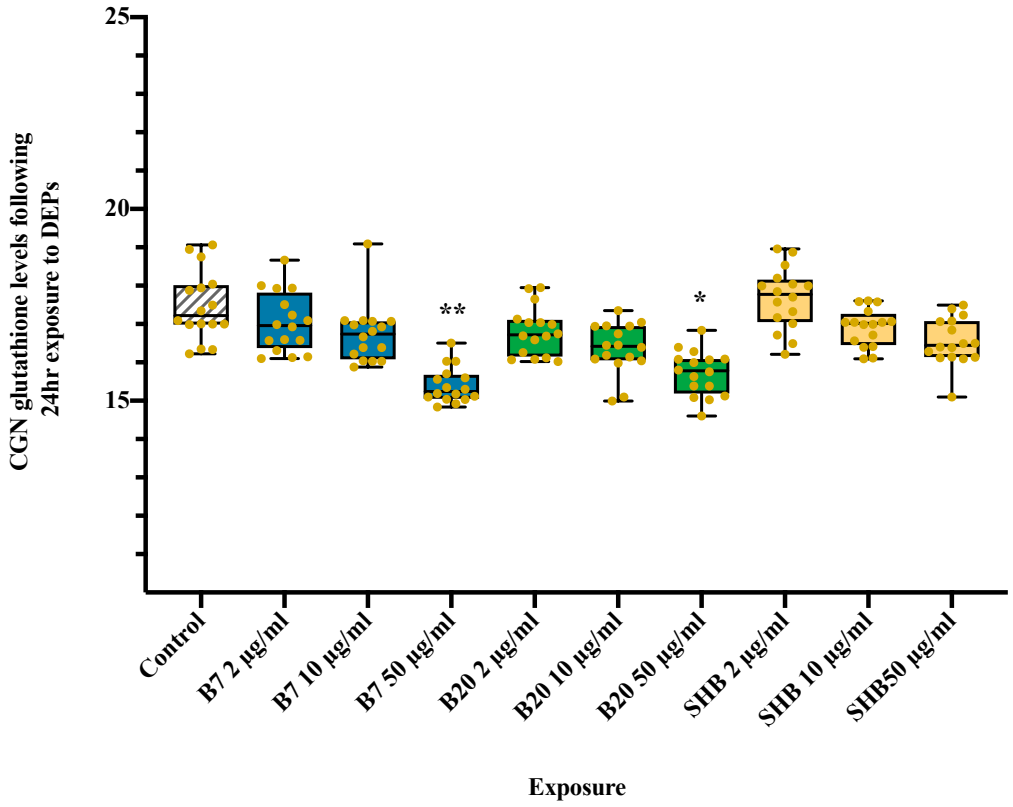


**Figure 3.8 Glutathione levels in CGN cells measured by the mBCl fluorometric assay.** Cells were seeded and plated and 24 hours later exposed to B7, B20, SHB20 at three different concentrations (2, 10, 50 µg/ml). GSH was measured 24 hours after exposure, followed by staining with Hoechst 33342. The boxes represent the second and third quartiles. The horizontal lines represent the median. The whiskers represent the minimum to maximum value range, with all data points represented as yellow dots. The data are displayed as corrected against fluorescent intensity with Hoechst 33342. For each treatment n = 3. Significance is shown by: $p \leq 0.05$ (*), $p \leq 0.01$ (**), compared to the control (untreated cells). Analyzed by One Way ANOVA, with Kruskal-Wallis post hoc test.

### 3.2.4 Calcium influx measurement

Direct measurement of calcium influx in CGN cells was done by the Fura-2 fluorometric assay. Calcium was measured both in the presence and the absence of $Mg^{2+}$. The reasoning for was this that extracellular $Mg^{2+}$ has the ability to block NMDAR, leading to a decrease of $Ca^{2+}$ permeability. It was therefore of interest to investigate whether its presence would show any significant difference in the calcium influx levels compared to an absence of extracellular $Mg^{2+}$. On the other hand, addition of NMDA leads to an increase of $Ca^{2+}$ permeability, by stimulating the NMDAR. To investigate this effect, NMDA was added to the cells before the 30-minute measurement. By comparing the graphs in Figure 3.9 A-F, the attenuation of calcium influx response by $Mg^{2+}$ is visible (A, C, E) compared to the response in its absence (B, D, F). This effect however, was not significantly different from the absence of $Mg^{2+}$, however. B7 2, 10, 50 were all significant at 24 minutes exposure in the absence of $Mg^{2+}$.

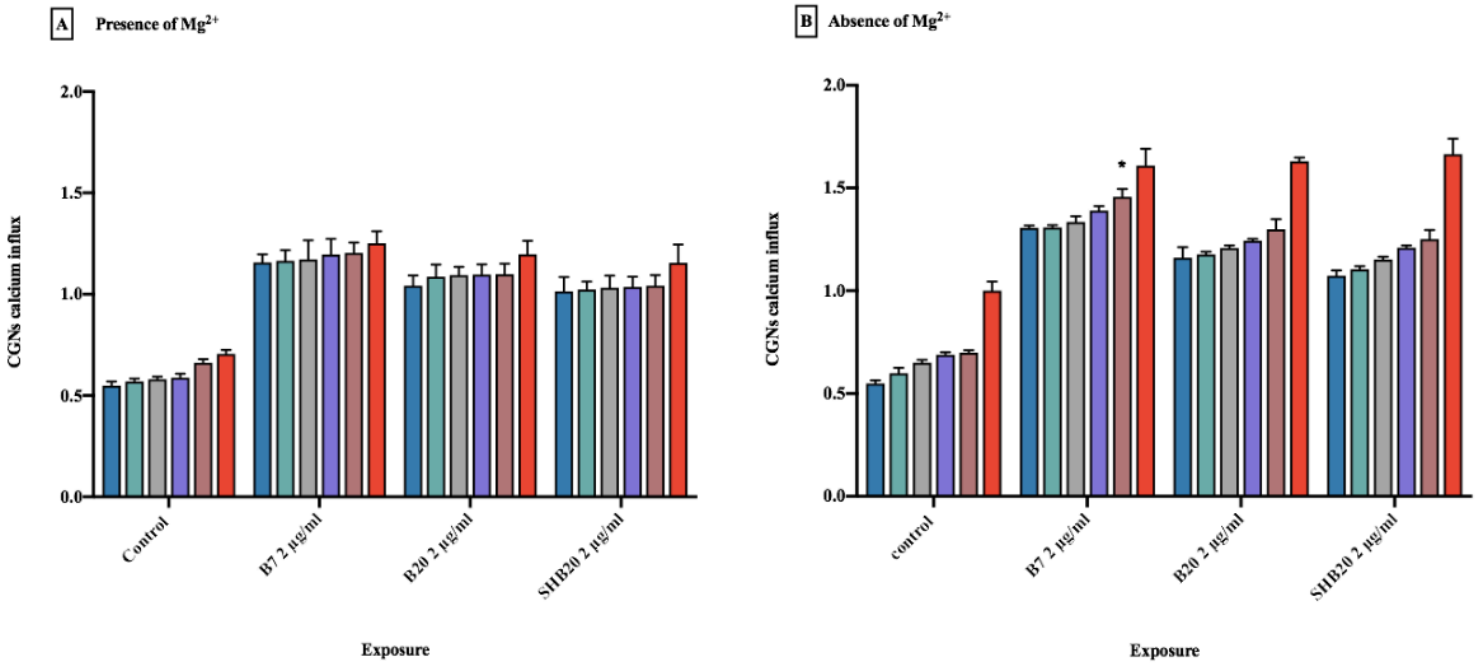

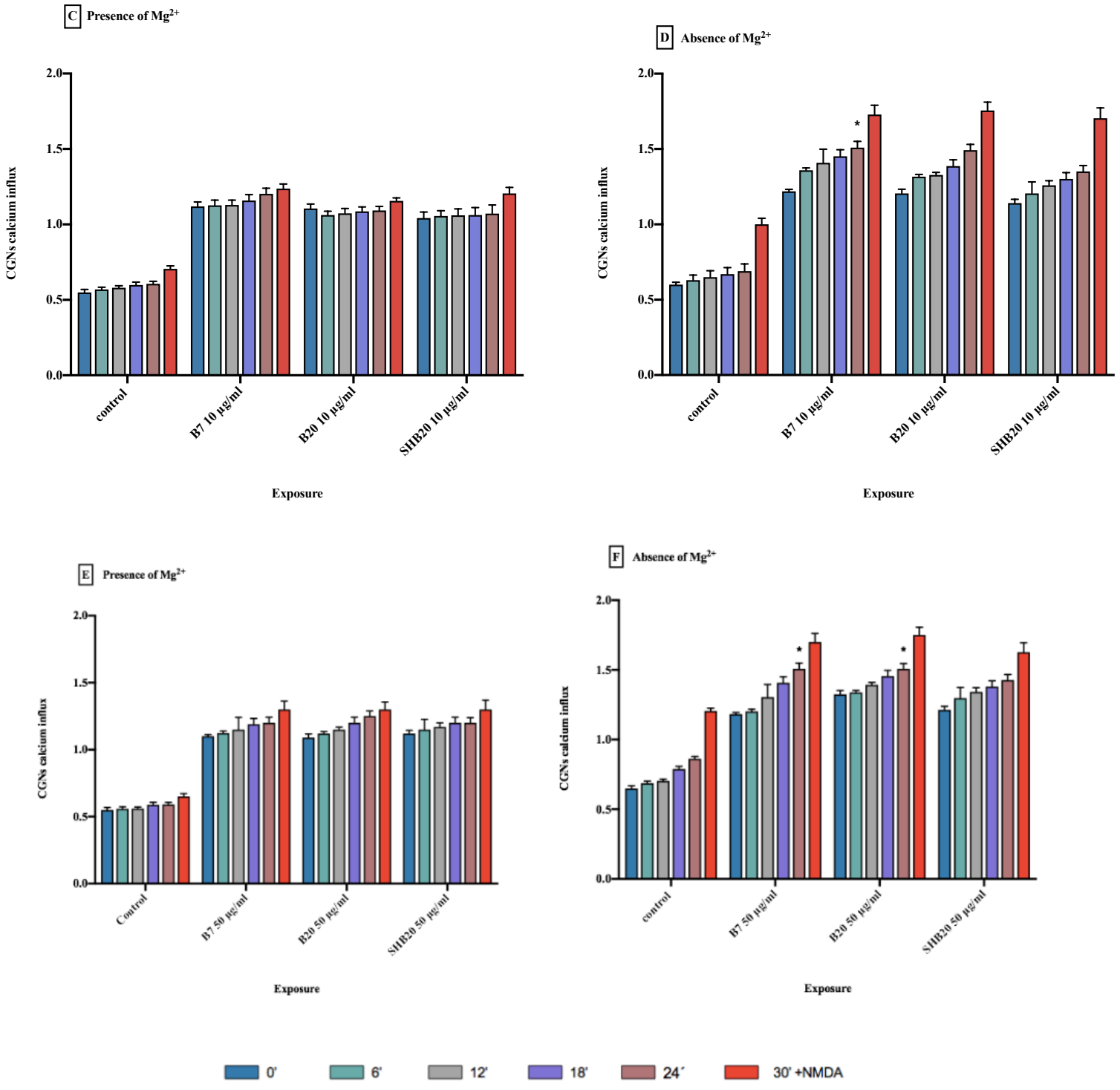


**Figure 3.9 Calcium influx measurement in CGN cells as measured by Fura-2 after exposure to DEP.** CGN cells were exposed to B7, B20, SHB20 at three different concentrations (2, 10, 50 µg/ml). Calcium influx was measured by use of Fura-2 assay at 0, 6, 12, 18, 24, and 30 minutes. NMDA was added immediately prior to the 30-minute measurement. **(A)** B7, B20, SHB 2µg/ml exposure in the presence of $Mg^{2+}$ **(B)** B7, B20, SHB 2µg/ml exposure in the absence of $Mg^{2+}$ **(C)** B7, B20, SHB 10 µg/ml exposure in the presence of $Mg^{2+}$ **(D)** B7, B20, SHB 10 µg/ml exposure in the absence of $Mg^{2+}$ **(E)** B7, B20, SHB 50 µg/ml exposure in the presence of $Mg^{2+}$ **(F)** B7, B20, SHB 50 µg/ml exposure in

the absence of $Mg^{2+}$. The data are displayed as average values ± SEM. For each treatment n = 3. Data were analyzed using a One-Way ANOVA. Kruskal-Wallis was used as a post hoc test. Significance is shown by $p \leq 0.05$ (*).

Pyrene and B(a)P are two known environmental toxins present in DEP, and it was of interest to compare the changes in intracellular $Ca^{2+}$ levels between these and the DEP. The cells that were exposed in the presence of $Mg^{2+}$ again showed a difference in $Ca^{2+}$ levels compared with the cells without the addition of extracellular $Mg^{2+}$. This effect was however not statistically significantly different versus controls in our analysis. Both pyrene and B(a)P showed significant changes in calcium influx at 24 and 30 mins for both concentrations in the absence of $Mg^{2+}$.

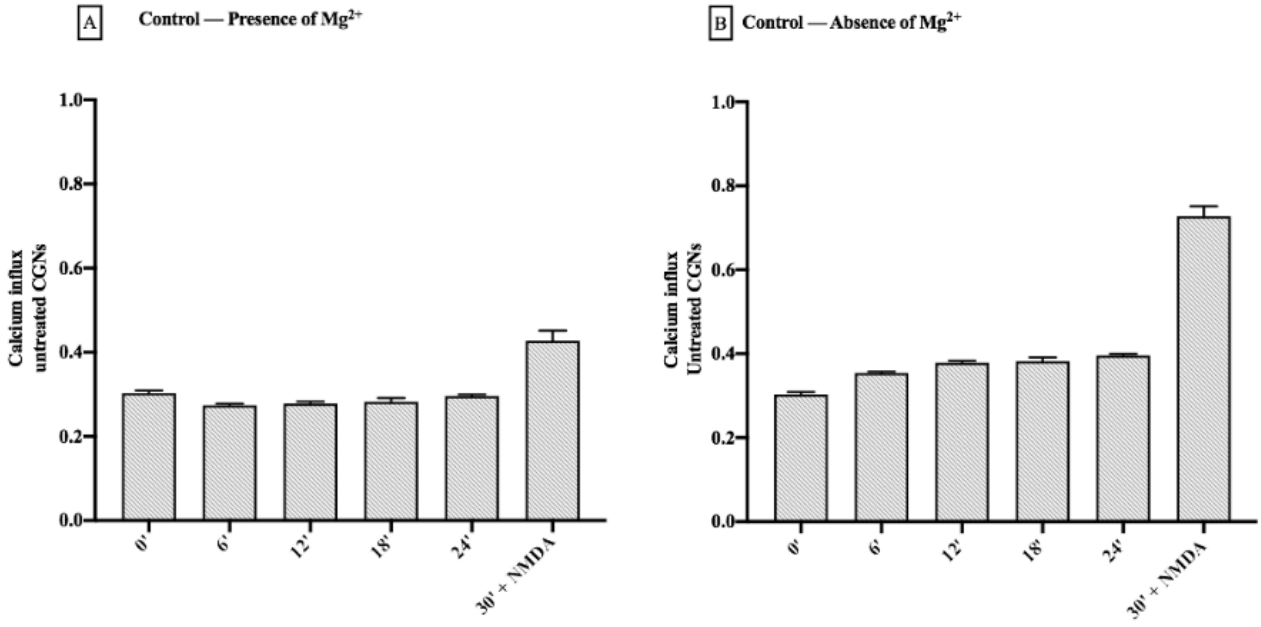

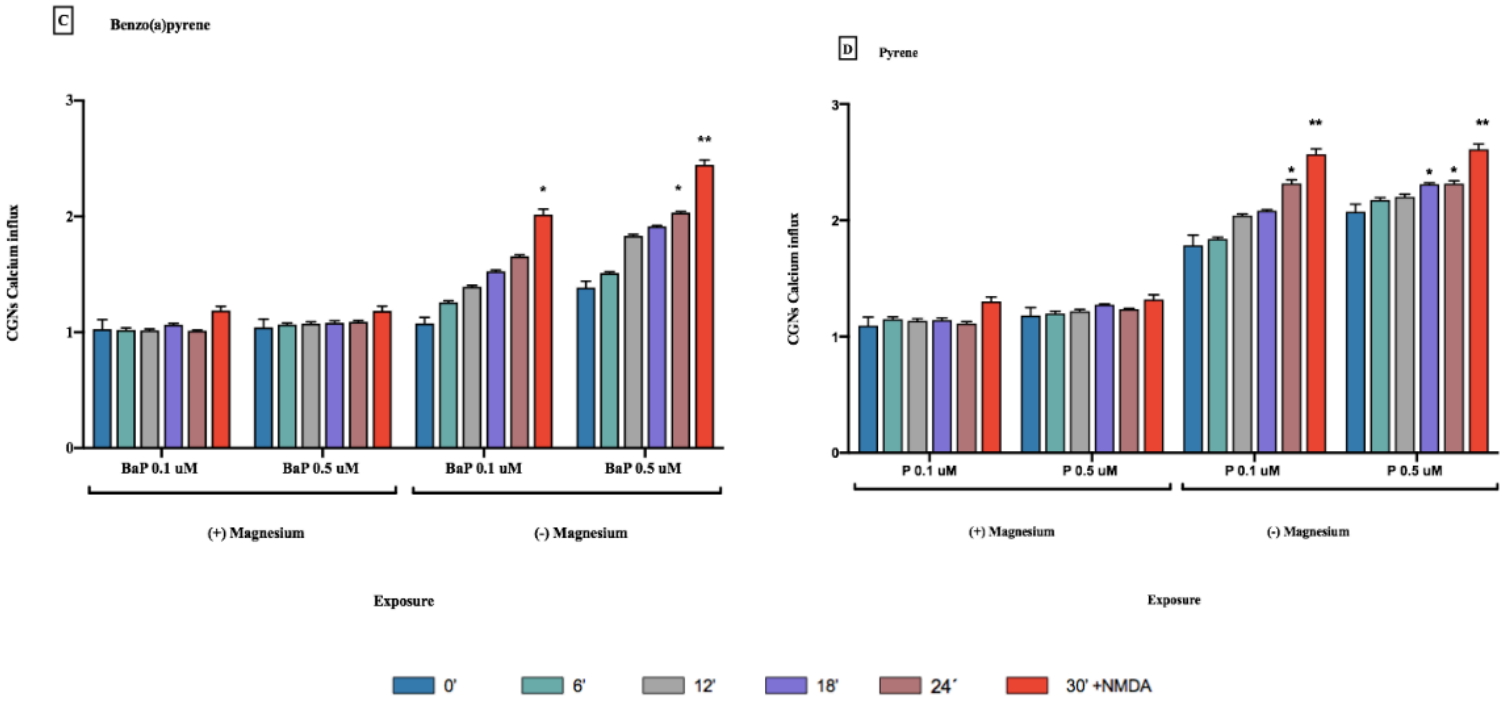


**Figure 3.10 Calcium influx measurement in CGN cells as measured by Fura-2 after exposure to PAHs.** CGN cells were exposed to pyrene and B(a)P at three different concentrations (2, 10, 50 µg/ml). Calcium influx was measured by use of Fura-2 assay at 0, 6, 12, 18, 24, and 30 minutes. NMDA was added to cells prior to 30-minute measurement. The data are displayed average values ± SEM. For each treatment n = 3. Data were analyzed using a One-Way ANOVA with Kruskal-Wallis was used as a post hoc test. Significance is shown by $p \leq 0.05$ (*), $p \leq 0.01$ (**), compared to the control (untreated cells).

To investigate the role of the AhR on the calcium influx response, the inhibitors GNF-351 and CH223191were added to the cells. These were diluted in DMSO, however a DMSO control was unfortunately not added to the plate. It was therefore not possible to detect the influence that DMSO itself had on the response. In addition, this experiment was performed one time (one biological replicate), with four technical replicates per treatment, therefore statistical analysis was not possible. The preliminary results however were surprising and we thought worth including. As seen from Figure 3.11, the addition of the inhibitors caused a sharp increase in the $Ca^{2+}$ response. In fact, when the inhibitors were tested alone (Figure 3.11 A) it was indicated that calcium influx was greatly increased by their presence alone. In addition to the increase in calcium influx, the cells that were exposed to GNF-351 and CH223191 did not respond to the addition of NMDA as did the cells without the inhibitors. At 30 minutes there was a sharp increase in the level of calcium influx for all of the cells exposed to the DEP, the cells exposed to the PAHs, as well as for the control (untreated cells).

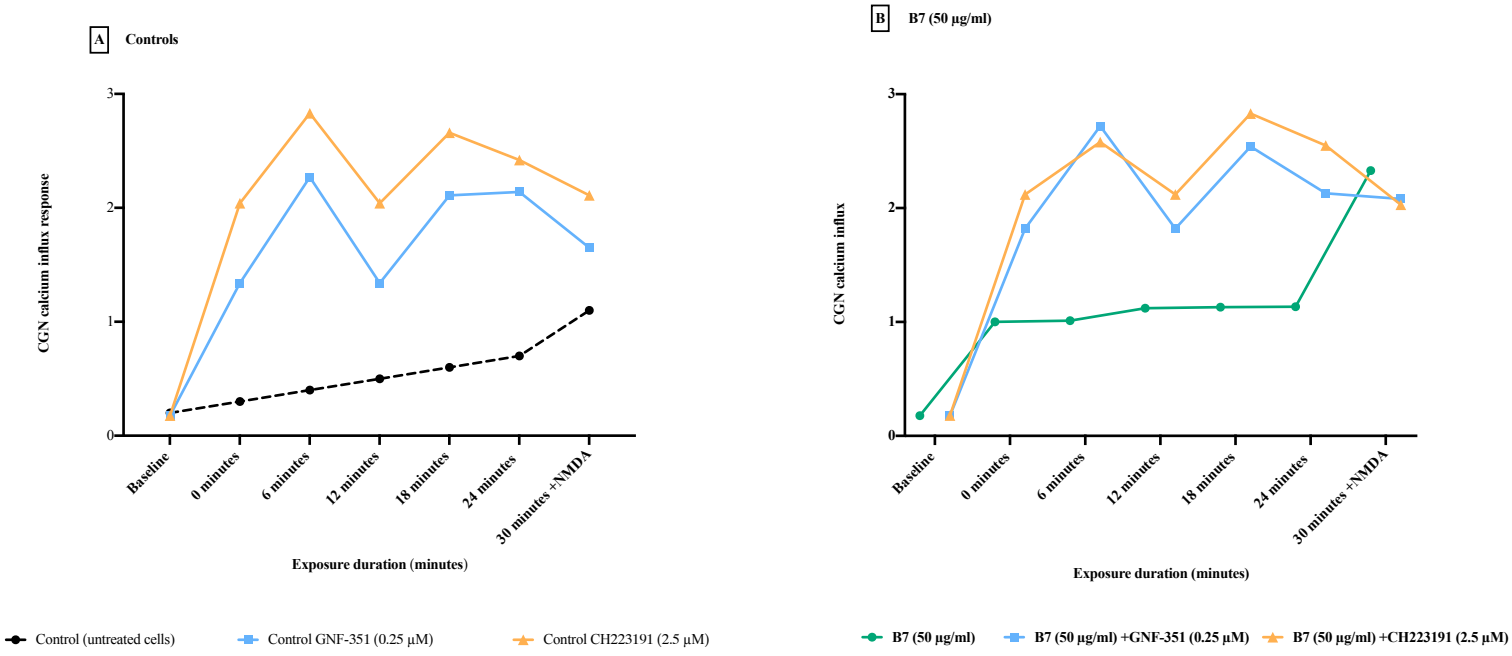
A Controls
CGN calcium influx response
Exposure duration (minutes)
Baseline
0 minutes
6 minutes
12 minutes
18 minutes
24 minutes
30 minutes +NMDA
Control (untreated cells)
Control GNF-351 (0.25 µM)
Control CH223191 (2.5 µM)
B B7 (50 µg/ml)
CGN calcium influx
Exposure duration (minutes)
B7 (50 µg/ml)
B7 (50 µg/ml) +GNF-351 (0.25 µM)
B7 (50 µg/ml) +CH223191 (2.5 µM)

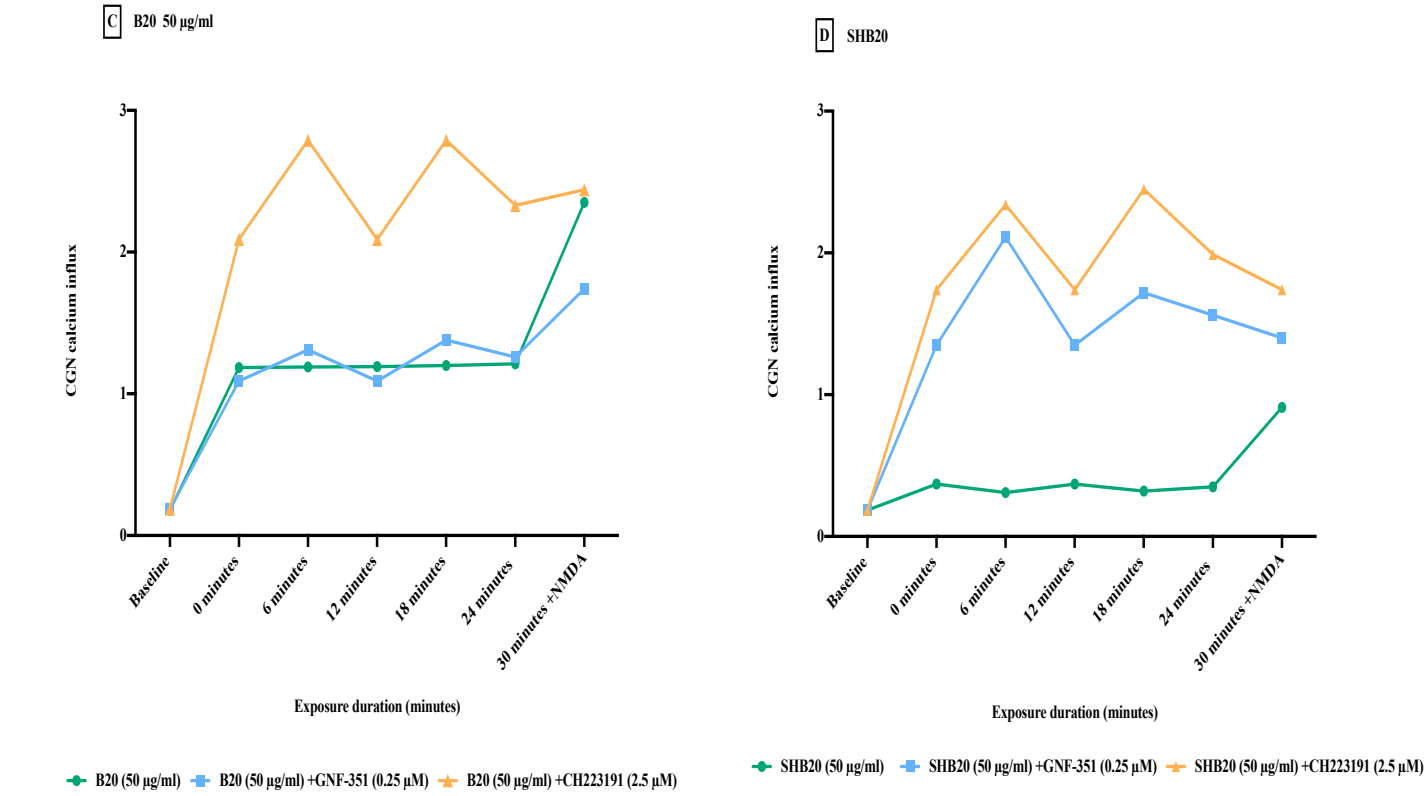
C B20 50 µg/ml
CGN calcium influx
Exposure duration (minutes)
Baseline
0 minutes
6 minutes
12 minutes
18 minutes
24 minutes
30 minutes +NMDA
B20 (50 µg/ml)
B20 (50 µg/ml) +GNF-351 (0.25 µM)
B20 (50 µg/ml) +CH223191 (2.5 µM)
D SHB20
CGN calcium influx
Exposure duration (minutes)
SHB20 (50 µg/ml)
SHB20 (50 µg/ml) +GNF-351 (0.25 µM)
SHB20 (50 µg/ml) +CH223191 (2.5 µM)

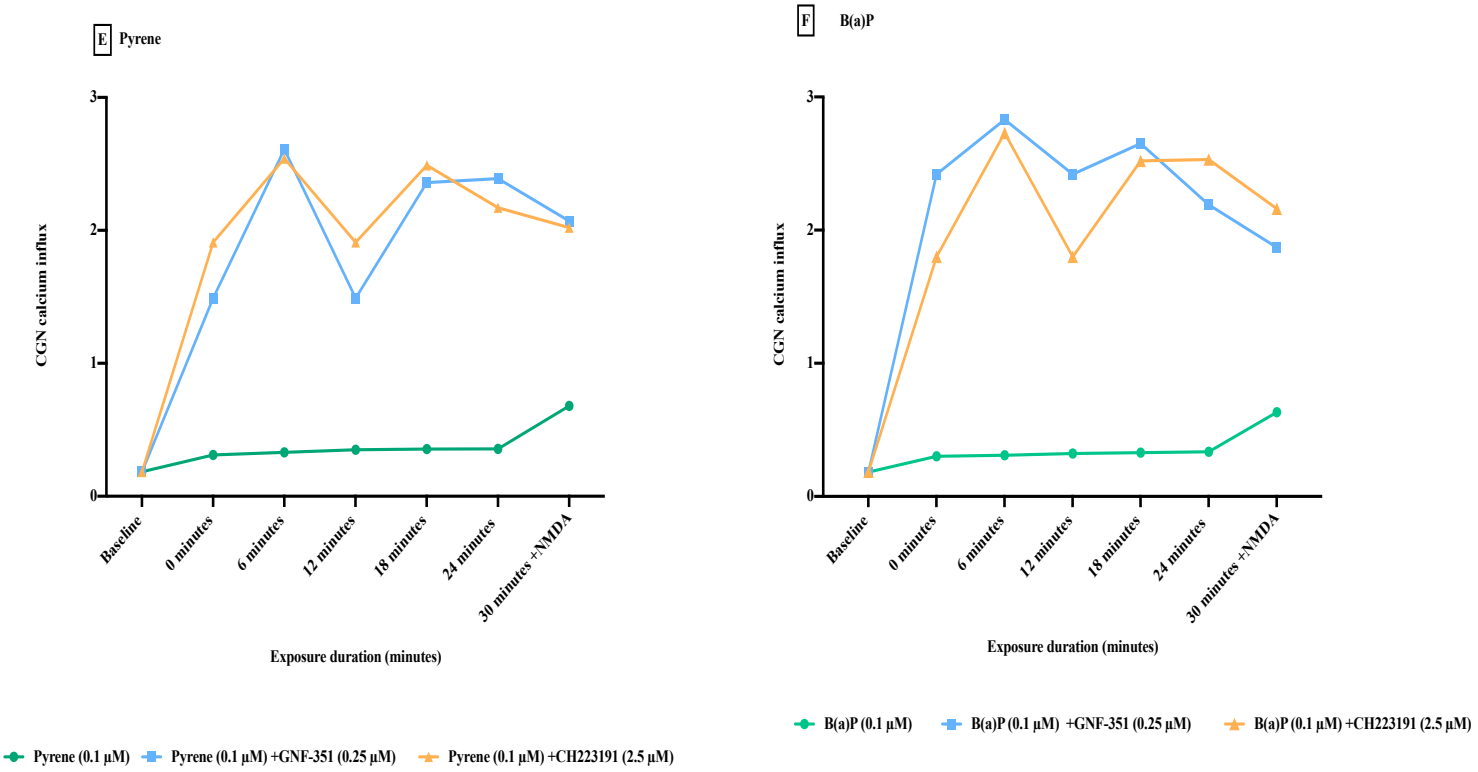


**Figure 3.11 Calcium influx measurement in CGN cells as measured by Fura-2 after exposure to DEP.** CGN cells were exposed to B7, B20, and SHB20 at 50 µg/ml alone and in the presence of the AhR inhibitors, GNF-351 and CH223191. Calcium influx was measured by use of Fura-2 assay at 0, 6, 12, 18, 24, and 30 minutes. NMDA was added to cells prior to 30-minute measurement. Statistical analysis was not possible due to n = 1 for each treatment.

## 3.3 Chicken embryo cerebellar gene expression

Chicken embryos were exposed *in ovo* on day E13 to B7, B20, SHB20 at 50 µg/ml, and pyrene and B(a)P at 1µM each. Controls were included for the dilutions both for the DEP (saline) and for the PAHs (DMSO) at the highest concentrations present in dilutions. No statistically significant differences in the expression of the selected genes (CYP1A1, Gpx1, Gpx2, Prdx1, GSR, and SOD1) were found between any of the exposures and the non-injection (untreated embryos) control. Saline control had the highest expression in CYP1A1.

SHB20 had the highest expression in Gpx1. The non-injection control had the highest expression in Gpx2. DMSO showed the largest change in expression in GSR, Prdx1, SOD 1. As gene expression analysis took place on E17, it is possible that an effect may have occurred after the injection on E13 but that was no longer present on E17.

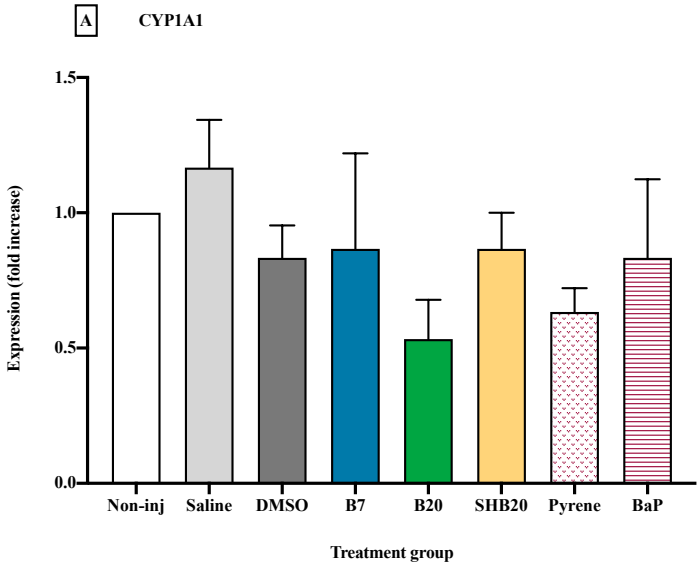


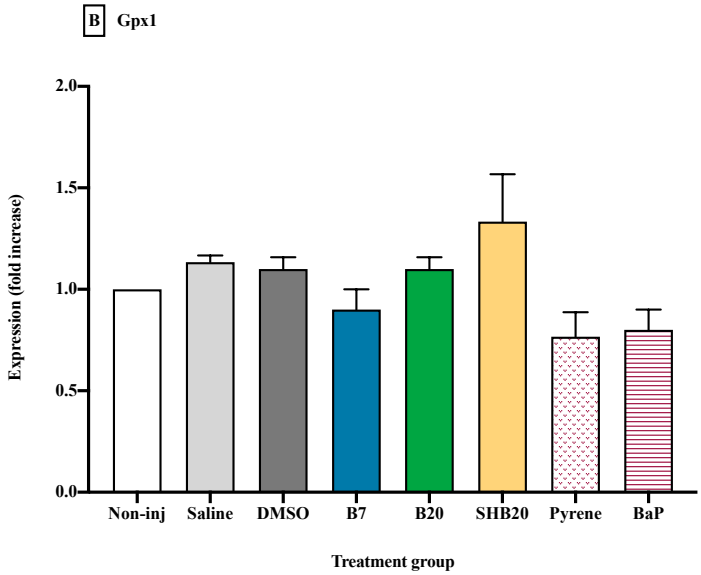


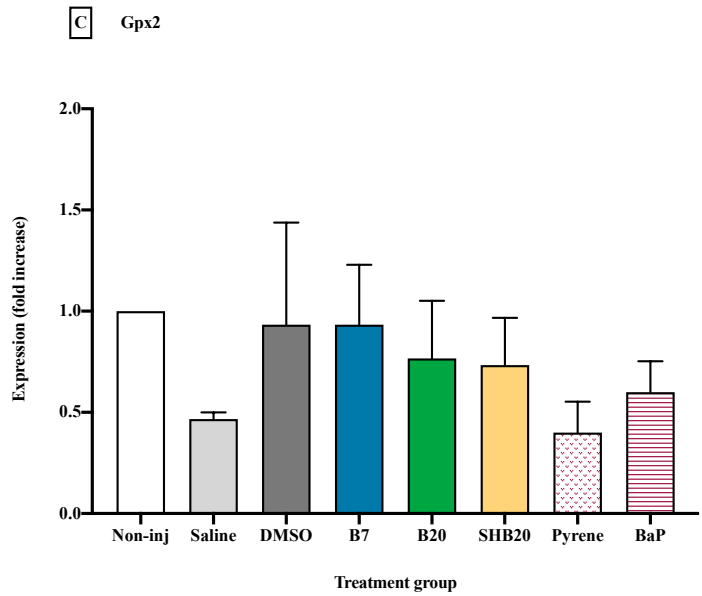


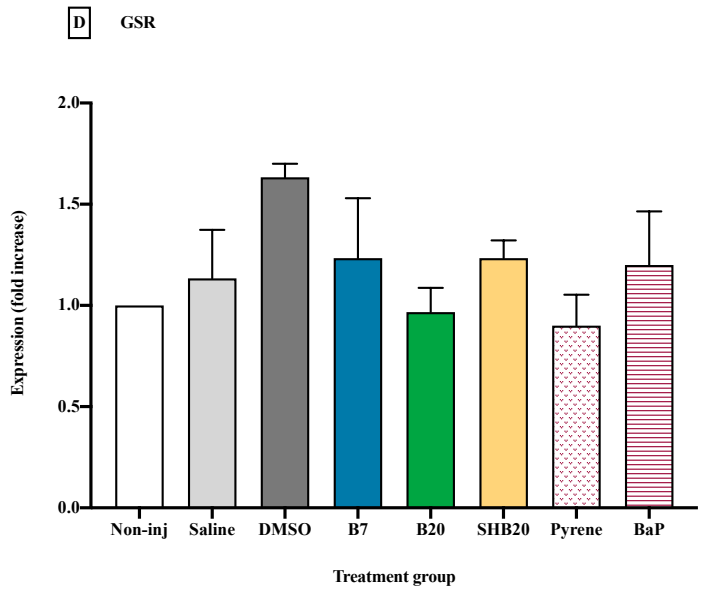

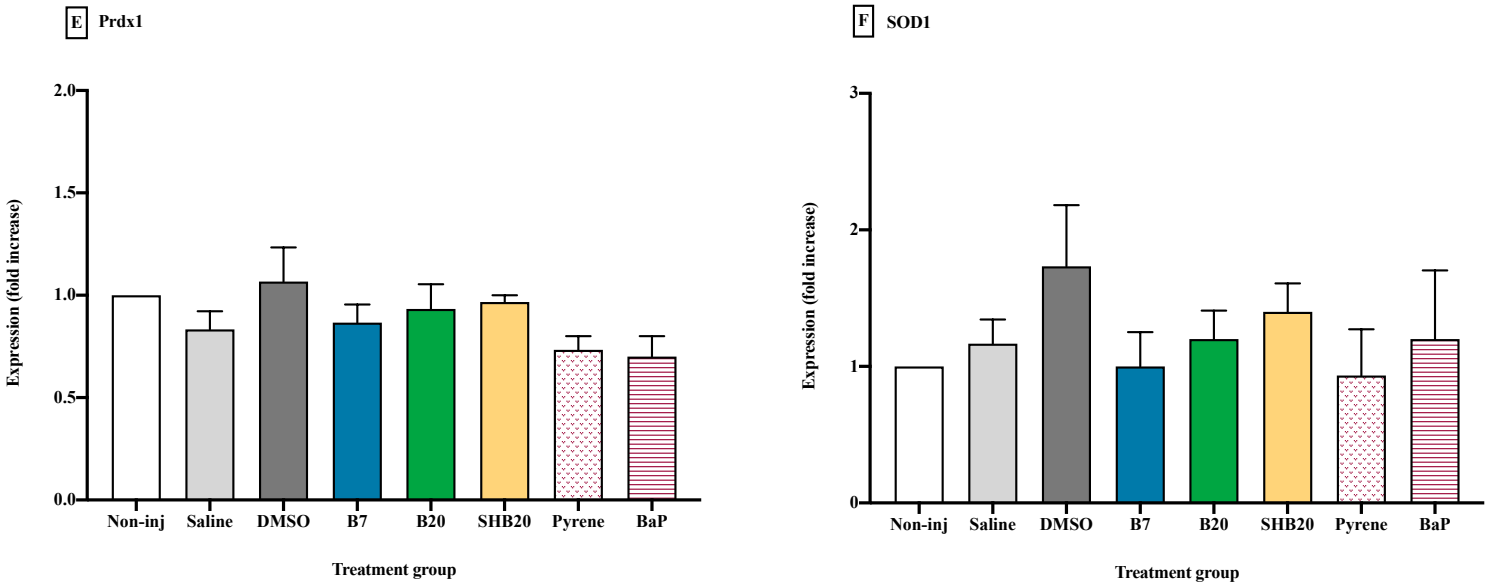


**Figure 3.12 Gene expression changes in chicken embryo cerebella exposed *in ovo* on E13 and analyzed on E17.**

Data were normalized to the non-injection control, and displayed as the average concentration ± SEM. n = 3 for each treatment. **A)** CYP1A1 gene **B)** Gpx1 gene **C)** Gpx2 gene **D)** GSR gene **E)** SOD1 gene. No statistically significant differences were found between any of the exposures and the non-injection controls. Data were analyzed using a One-Way ANOVA with Kruskal-Wallis was used as a post hoc test.

# 4 Discussion

The demand for biofuels continues to rise rapidly, driven in part by the blending mandates in the transportation sectors of the major global economies, in an attempt to reduce GHG and improve energy security (92) . However, the impact that biodiesel fuels may have on reducing the amount of toxic air pollutants is currently unclear. Our main aim with this study, therefore, was to test and compare the toxicity of DEP from B7, B20, and SHB20 biodiesel blends using cell cultures of PC12 cells and CGN cells as *in vitro* neuronal models, and the chicken embryo as an *in ovo* model. One of the limitations of using cell cultures for neurotoxicity testing is that they cannot completely resemble the central nervous system. It was therefore important to utilize more than one *in vitro* model and measure several different end points, in an attempt to approach proposed mechanisms of neurotoxicity seen in *in vivo*.

Our first objective was to investigate the effect of DEP on the viability of PC12 and CGN cell cultures, and on the induction of neurotoxic effects. We used different endpoints: cell viability, cell death, intracellular GSH levels, and $Ca^{2+}$ influx as different indicators of the health and the oxidative status of the cells. Our second objective was to determine whether exposure to DEP would lead to a disturbance in calcium signaling and AhR dysregulation in cell cultures of PC12 cells and CGN cells, as well as two PAHs known to be present in DEP, pyrene and B(a)P. We therefore measured $Ca^{2+}$ influx responses in the presence of AhR inhibitors. Finally, we used the chicken embryo model to investigate our third objective, whether DEP affect the expression of genes related to oxidative stress and inflammation using *in ovo* exposure followed by qPCR analysis.

## 4.1 Cell viability

### 4.1.1 PC12 cells

Our MTT results indicate that cells exposed to B20 50 μg/ml at 72-hour exposure showed the greatest level of cytotoxicity, via a reduction in cell viability of about 55%, while cells exposed to SHB20 at 2 μg/ml showed the least amount of cytotoxic effects, at every time point (24, 48, 72 hours). Furthermore, the results after the 24-hour exposure showed that cell viability was affected in both an intra- and an inter-group manner. In other words, the three concentrations within each DEP group (2, 10, 50 μg/ml) affected viability as well as did the three groups compared to each other (B7, B20, SHB20). It is also worth noting that cell viability was always lower for PC12 cells exposed to any of the DEP types compared to the control, irrespective of statistical significance. It appeared that B20 displayed the largest effect in cell viability (about 55% decrease at 72 hours), followed by B7 (reaching about 50% decrease in viability at 72 hours) and finally SHB20 (about 45% decrease at 72 hours). For the 48 and 72-hour exposures, therefore, the diesel blend containing 20% biodiesel from 1G biofuels was shown to be more cytotoxic than the diesel blend containing 7% biodiesel from 1G biofuels, as well as the diesel blend containing 20% biodiesel (13% 1G biofuel and 7% 2G biofuel). These results concur with several studies which have reported that the composition of the exhaust emissions – and thereby of the DEP emissions— does not change in a linear fashion with regards to the blending ratio (93) . Several factors have been identified that affect exhaust composition such as engine type, operating conditions, biodiesel feedstock blend, as well as percentage in the blended fuel (94). It should therefore not be expected for the toxicity of the different diesel blend types to follow a linear pattern.
Consequently, while we may compare the three types of diesel blends for any potential differences, it is also important to assess the toxicity of each DEP separately.

Cytotoxicity studies are a useful starting point for determining the potential toxicity of a compound. Exposure to a cytotoxic compound may result in variety of cell fates such as reduced cell viability and proliferation or the induction of cell death through the processes of necrosis or apoptosis (95). Since the MTT assay does not allow us to differentiate between dead cells and metabolically inactive cells, we used the trypan blue exclusion assay as a complementary test to demonstrate whether the results of the MTT assay could be explained

by cell death. From the 24-hour exposure, a clear dose-dependent response to cell death was visible for every DEP type, with increasing exposure concentrations leading to increased cell death (Figure 3.2 A). However, the exposure of B7 at 50 µg/ml was the only statistically significant difference in cell death versus the control for all time points. Comparing these results with the results from the MTT assay, (Figure 3.1) we can see that B7 (50 µg/ml) exposure led to an approximately 50 % decrease in cell viability, which corresponds to the approximately 50% cell death confirmed by trypan blue staining. Also at 24 hours, the exposure of B20 at 10 µg/ml and SHB20 at 50 µg/ml led to a statistically significant decrease in cell viability of about 45% compared to the control, yet their corresponding cell death was only about 20% and 15%, respectively. The same pattern may be observed for B20 and SHB20 at the 48- and 72-hour exposures, where the percentage of decrease in cell viability was much lower than the percentage of cell death. These results indicate that the decrease in cell viability could not be explained solely by cell death, and that another mechanism must be involved. It may therefore be concluded that only the decrease in cell viability by exposure to B7 was attributable to cell death. The stress exerted on the cells exposed to B20 and SHB20 was perhaps not severe enough to cause cell death, yet critical enough to impair cell viability. It would therefore be interesting to investigate whether the decrease in viability was transient and/or reversible, once the stress was removed. Cells may employ several mechanisms to alleviate the effects of oxidative stress, including the use of enzymatic and non-enzymatic antioxidants (96). Therefore, the addition of antioxidants such as vitamins C and E could further our understanding of the qualitative properties of the cytotoxic effects. Indeed, previous studies have shown the reversible effects of such antioxidants on neurotoxicity in PC12 cells (97). The activation of muscarinic receptors (mAChR) has also been shown to exert neuroprotection in PC12 cells, and agonists of mAChR are currently used in the treatment of neurodegenerative disease including AD (98). Further insight could thus be gained by treatment of PC12 cells with a muscarinic agonist prior to DEP exposure, to see whether cytotoxicity is dependent on mAChR activity. Additionally, it would be beneficial to examine the mode of cell death, e.g. apoptosis, necrosis, or autophagy, since these are triggered by responses to specific stimuli and activate distinct signaling pathways (99). This could be accomplished by morphological analysis or flow cytometry, for example, and the results could help further elucidate the underlying mechanisms that lead to DEP toxicity.

### 4.1.2 Cerebellar granule neurons

A similar negative trend was observed with CGNs as with PC12 cells, whereby increasing concentrations of DEP led to a decrease in cell viability (Figure 3.6). However, the exposure of B7 at 50 µg/ml was the most cytotoxic to CGNs, with a decrease in cell viability of 55% at 72 hours. B20, which was the most cytotoxic to PC12 cells, was only significantly different from the control at 24- and 72-hour exposures, at 50 µg/ml. SHB20 exerted the least cytotoxic effects, as was the case for the PC12 cells. Overall, the CGNs appeared to be less susceptible to the effects of all three DEP than the PC12 cells. Given that PC12 cells are a tumor-derived line, we had expected the neurons to be more vulnerable in comparison. However, this may be due to the differences in the serum present in the cell media. PC12 cells were plated in medium supplemented with 10% fetal bovine serum and 5% horse serum, whereas CGN cells were plated in medium supplemented with 7.5% chicken serum. The serums all contained nutrients, growth factors, vitamins, and proteins such as albumin, but perhaps the CGNs were able to bind to the proteins in the serum such as the albumin, which could have offered an additional protective role. In future experiments, it would be wise to control for these differences, for example by using serum-free media in both cell cultures. The percent of cell death was correspondingly much lower for the DEP exposures in CGNs compared to PC12 cells. The only significant differences in cell death compared to the control were at 48 and 72 hours by B7 (50 µg/ml) and by B20 (50 µg/ml) at 72 hours. For these time points, the approximately 50% cell death of cells exposed to B7 (50 µg/ml) corresponded with the 50% decrease in cell viability seen by MTT. However, from the 24-hour exposure we see that the highest concentration of B7 had a nearly 50% decrease in viability (Figure 3.6 A) but less than a 30% cell death (Figure 3.7 A), which was not considered significant. Moreover, cells exposed to SHB20 showed a 50% decrease in viability, at 72 hours, while only a 30% cell death for that time point. Thus, there was an effect exerted on these cells by the DEP which led to a decrease in cell viability, which was not entirely accountable by cell death. Because trypan blue staining cannot distinguish between dead cells and cells that are still alive but in the process of losing their cellular functions, it would be possible for lethally injured cells that have not yet lost their membrane integrity to be counted as live cells. As with the PC12 cells, it would be interesting to see if the cell viability were able to be regenerated, or if the damage were permanent. Metabolic assays such as MTT, rely on the efficiency of metabolic enzymes, so to account for the differences seen between the results of cell viability and cell death it would be useful to measure DNA content, since cellular DNA is

independent of metabolic changes (100). Hoechst 33343 is an intercalating dye used to stain double-stranded DNA (dsDNA) which can distinguish between healthy, apoptotic, or necrotic cells, by their nuclear condensation (101). Application of this dye would therefore shed light on the discrepancies seen between cell viability and cell death.

## 4.2 Intracellular glutathione levels

### 4.2.1 PC12 cells

GSH plays an essential role in a multitude of cellular processes, and imbalances in GSH homeostasis have been linked to disturbances in cell proliferation, differentiation, as well as triggering apoptosis and oxidative stress (55) . As the trypan blue exclusion assay did not confirm cell death for the entirety of the significant decrease in cell viability witnessed by the MTT assay, we reasoned that this decrease in metabolic activity may have been instead caused by reduced or impaired cell metabolic activity. Intracellular levels of GSH were therefore measured, where consumption and subsequent depletion were used as an indicator for oxidative stress. The cells exposed to B7 at 10 and 50 µg/ml and B20 at 10 µg/ml had statistically significant lower levels of GSH than the control (Figure 3.3). When comparing to the MTT data, we see that the latter two values correspond with the decrease in MTT seen at the same exposure time (Figure 3.1A). In addition, there was a visible dose-dependent response to B7 exposure, as seen previously with the MTT and trypan blue results. It may be hypothesized that B7 (10 and 50 µg/ml) and B20 (10 µg/ml) induced a state of oxidative stress which consumed antioxidant molecules of GSH, resulting in a significant decrease of its level within the cells. It has additionally been shown that glutathione-s-transferase (GST) may interfere with the MTT assay by leading to a non-enzymatic reduction of MTT (102). Therefore, the cells that had a lower level of GST (which catalyzes the GSH-dependent conjugation and redox reactions) had a corresponding lower potential to reduce MTT, which was reflected as a lower cell viability. SHB20 at 50 µg/ml on the other hand, had a significant decrease in cell viability at 24 hours, but the decrease in the GSH level was not considered significantly different from the control, nor was there a significant increase in cell death compared to the control. This indicates that although there was a negative effect on the cells ability to reduce MTT, we cannot confidently link this effect to oxidative stress or cell death, and it is more likely the interference involved other mechanisms. It would therefore be

of interest to test the effects of a known free-radical generating compound on the levels of GSH in our cell culture and compare these results with those of the DEP. Hydrogen peroxide ($H_2O_2$), for example, has been shown to induce oxidative stress and subsequent apoptosis in PC12 cells (103). This comparison could thus provide insight into the different mechanisms being triggered by exposure to $H_2O_2$ versus DEP, and whether there is any overlap, or if they are different mechanisms of toxicity altogether. Additionally, air pollution has emerged as a possible etiological factor in neurodegenerative diseases including AD (104). Finally, it would be useful to treat the exposed cells with a glutathione precursor, such as N-acetylcysteine which has been shown to protect against ROS-dependent cell death, thereby confirming whether the witnessed cell death was in fact due to a depletion of GSH (105).

### 4.2.2 Cerebellar granule neurons

As the trypan blue exclusion assay did not show any significant increase in cell death except for B7 and B20 at the highest dose, it was again reasoned that the decrease in cell viability of CGN cells may have been caused by a homeostatic imbalance leading to decreased cellular metabolic activity. GSH levels were measured as an indication of an oxidative state.

The cells exposed to B7 and B20 at 50 µg/ml had statistically significant lower levels of GSH compared with the control. This corresponds with the significant decrease in cell viability seen at 24 hours (figure 3.6A). Moreover, there was a clear dose-dependent response across all DEP, which also corresponds with decreases in cell viability and increases in cell death witnessed previously. The exposure of SHB20 at 2 µg/ml did not seem to exert any immediate observable negative effect on the cells, as these had the highest levels of GSH, which were comparable to the control. In addition, cell death was equal to that of the control as measured by trypan blue, and the cell viability was non-significantly reduced. The exposure of B7 (50 µg/ml) on the other hand, had the opposite tendency, displaying reduced cell viability, cell survival and GSH levels, all significantly different from the control. Thus, these DEP exerted different effects on the exposed cells. Of the three DEP, cells exposed to SHB20 had the highest levels of GSH while those exposed to B7 had the lowest levels, an indication that this antioxidant was consumed at a higher rate in the latter.

An interesting additional step would be to measure the ratio of nicotinamide adenine dinucleotide phosphate (NADP+/NADPH) as a biomarker for redox metabolism in the cells. NADPH not only plays an important role in the anabolic biosynthetic reactions related to cell growth and division, but also in mitigating ROS-related cellular damage (106) . The oxidation of GSH neutralizes excessive ROS in the cell, and its reduced form can be regenerated by NADPH (107). Coupling the changes seen in GSH levels with those of NADPH, would therefore yield further mechanistic insight on the oxidative stress levels in our cell culture. Furthermore, measuring the ratio of the non-phosphorylated molecule of nicotinamide adenine dinucleotide ($NAD^+$/NADH) could provide additional insights on the cell viability analysis. Several studies have suggested that NADH is the main electron donor in the reduction of MTT, not necessarily mitochondria, as has traditionally been thought (108) . Because rapidly diving cells such as PC12 have inherently high rates of MTT reduction, these rates may be influenced by high concentration of NADH in the samples. Thus, we could investigate the correlation between high levels of NADH and high levels of MTT reduction, by comparing to CGNs which have a slower rate of division.

## 4.3 Calcium influx

### 4.3.1 PC12 cells

PC12 cells express the p75 and trk receptors for NGF, and in response differentiate into a sympathetic neuronal phenotype (109). As seen in Figure 3.4, the growth of neurites and change in morphology and proliferation were used as a confirmation of differentiation. Although we were not able to determine this merely with a morphological study, the cells were assumed at this point to have gained electrical excitability as well as the expression of neuronal markers (110). The differentiation of PC12 cells by NGF is accompanied by a large increase in the number of mAChRs. Heterogeneous cell populations may contain several different classes of mAChRs, whose signals are in turn transduced by different mechanisms. PC12 cells on the other hand, comprise a relatively homogenous population, allowing for the signaling processes trigged by mAChRs activation to be less complex and difficult to interpret, and thus allowing the feasibility of this investigation (111).

No significant differences were found between the $Ca^{2+}$ influx levels of the cells exposed to DEP and the control, for the time points measured. However, an interesting response was seen by cells exposed to B20 at 10 µg/ml, as this concentration elicited a stronger calcium influx response than either the lowest concentration (2 µg/ml) or the highest concentration (50 µg/ml) at every time point (Figure 3.5 B). Furthermore, as the exposure time increased, the B20 50 µg/ml exposure elicited an even lower calcium response than the 2 µg/ml exposure. Interestingly, this exposure also had a statistically significant decrease in cell viability at 24 and 48 hours, as well as decrease in GSH. It is therefore reasonable to supposed that the exposure of B20 at 10 µg/ml exerts a negative effect on the cells. A possible explanation for the lack of DEP-induced toxicity in PC12 cells may be their reported lack of expression of functional NMDAR (112). Indeed, PC12 cells have been used to verify lower toxicity of chemicals in cells not expressing NMDAR (97).

Nevertheless, $PM_{10}$ which are represented in DEP, have been associated with increased $Ca^{2+}$ signaling events and oxidants, which in turn are important in the induction of transcription factor activation as well as cytokine gene expression (113). Therefore, it would be useful to explore the effects on $Ca^{2+}$ further, by adding a mAChR antagonist such as atropine, to examine whether the calcium influx changes are mediated by this receptor, and the site of calcium mobilization. Oxidative stress is known to initiate lipid peroxidation, a major contributor cell membrane damage, which leads to the rapid influx of calcium (114). Another possibility would therefore be to study the effect of the addition of $Ca^{2+}$ channel blockers, such as verapamil, to examine whether the influx is due to the voltage-dependent $Ca^{2+}$ channels, or if it is activated by a different transmembrane pathway, and whether any antiperoxidative protection is afforded.

It would be worth investigating other cell signaling pathways, such as cyclic AMP (cAMP), which is another important second messenger, that mediates several physiological CNS events after the activation of GPCRs. There have indeed been reports suggesting that cAMP is also involved in NGF-induced responses of PC12 cells (115).

### 4.3.2 Cerebellar granule neurons

An important difference between our two *in vitro* cell cultures, is that while PC12 cells lack the functional NMDAR, they are prominent in CGNs. These are ionotropic glutamate receptors with high calcium permeability that have an essential role in brain development, neuropathology, and synaptic plasticity (116). However, the overactivation of NMDARs has been shown to promote neuronal death in several neurodegenerative diseases such as AD and PD (117) . As $Ca^{2+}$ influx acts as a primary modulator after NMDAR channel activation, an imbalance in $Ca^{2+}$ homeostasis has also been associated with the synaptic dysfunction and neuronal loss underlying many of the neurodegenerative diseases (116). Extracellular $Mg^{2+}$ has the ability to block NMDAR, leading to a decrease in $Ca^{2+}$ permeability. Therefore, we explored whether the presence of $Mg^{2+}$ would show any significant influence on the $Ca^{2+}$ influx levels compared to an absence of extracellular $Mg^{2+}$. Figure 3.9 shows that while the attenuation of the $Ca^{2+}$ influx response for cells exposed in the presence of $Mg^{2+}$ is evident, this difference was not found to be statistically significant compared to the absence of $Mg^{2+}$. Furthermore, no significant differences were found in the calcium responses of the cells exposed to the three types of DEP compared to the control, at any time point or concentration, in the presence of $Mg^{2+}$. Nevertheless, the cells exposed in the absence of $Mg^{2+}$ did differ significantly from the control at different concentrations and time points. B7 elicited significantly higher levels of $Ca^{2+}$ influx compared to the control, for every exposure concentration (2, 10, 50 µg/ml) at 24 minutes. In addition, B20 was significant at 24 minutes at 50 µg/ml. These significant responses correlate with the previous results of decreased viability, decreased levels of GSH, increased cell death seen by B7 at the exposure highest concentration (50 µg/ml). To investigate the effect of NMDA on calcium permeability, NMDA was added to the cells before the 30-minute measurement. The sharp increase seen in $Ca^{2+}$ influx response confirms the activation of the NMDAR. To elucidate whether DEP toxicity is dependent on NMDA receptor function, we could study the effect of an NMDAR antagonist such as MK-801. If such an antagonist were to block toxicity caused by DEP exposure, it could help direct further studies on the role that NMDAR play in the mechanisms of DEP-induced toxic effects.

The effect of calcium influx on Pyrene and B(a)P was also attenuated by the presence of $Mg^{2+}$ but was not found to be statistically significantly different compared to the presence of $Mg^{2+}$. The effect of NMDA on the calcium channel was evident at its addition at 30 minutes. As with the DEP exposure, no significant differences were found between the amount of $Ca^{2+}$ influx in the PAHs and the control, in the presence of $Mg^{2+}$. However, in the absence of $Mg^{2+}$, B(a)P was significant at both concentrations (0.1µM and 0.5 µM) at 24 and 30 minutes and Pyrene was significant at 0.1 µM also at 24 and 30 minutes, and at the higher concentration of 0.5 µM earlier at 18, 24, and 30 minutes. It is not surprising that pyrene and B(a)P show similar effects, as they share many of the same physicochemical characteristics and have a similar structure which influences their toxicity. The mechanism of toxicity of PAHs is thought to be disturbances to cellular membrane function, as well as with the associated enzyme systems (118). These results may serve as a comparison to compounds that are known to exert negative effects, as well as to highlight the difference between the toxicity of a single compound, to that of a mixture of compounds. The general population is exposed to toxic compounds predominantly as mixtures; however, it is also useful to study these separately in an effort to determine the interactions that occur when they are present in a mixture. Interestingly, DEP from B7 has previously been found to contain the highest total content of PAHs, while SHB20 has the lowest (119).

The AhR inhibitors GNF-351 and CH223191 were used for screening of the involvement of AhR in DEP-induced effects on viability in CGNs. However, based on the literature and the established effects of these inhibitors to attenuate the calcium signaling response, these results were both unexpected and interesting. Previous studies have indeed shown the CH223191 inhibitor to markedly attenuate the pyrene-induced $Ca^{2+}$ influx response (120). On the contrary, our results showed a sharp increase in the levels of intracellular $Ca^{2+}$. This indicated a potential inhibition of the NMDAR, except for cells exposed to B20, in which there was a slight increase in calcium signaling with the addition of NMDA (C). As the inhibitors were tested alone, we were able to see the effect without the addition of DEP or PAHs. A sharp increase in the levels of cytosolic $Ca^{2+}$ was seen, indicating that these inhibitors themselves were causing an effect. A possible explanation is the incorrect dilution of the inhibitors in DMSO, to an extent that was toxic to the cells. Both GNF-351 and CH223191 had an initial concentration of 10mM in DMSO, and were further diluted to 0.25

μM, and 2.5 μM, respectively. DMSO is widely used to dissolve neuroprotective or neurotoxic agents in neuroscience research, but DMSO itself can exert pathological effects on the nervous system (121). Exposures at 1% DMSO have not been shown to significantly affect cell viability, but concentrations of 5% have shown significantly decreased cell viability as well as the induction of apoptosis and severe mitochondrial damage in cells of the nervous system (121). As only one independent experiment was performed, it is not possible to deduce a mechanism for these results. Thus, this assay should be repeated in future studies.

## 4.4 The relevance of *in vitro* studies

A considerable amount of attention is currently being devoted to the use of *in vitro* alternatives in neurotoxicity testing. This is due to many factors including the increasing costs and time requirements of *in vivo* and epidemiological studies, an increasing number of chemicals being developed and commercialized, and animal welfare concerns. There are significant limitations since results from *in vitro* procedures do not take into consideration the route of exposure, the distribution of the toxicant in the body, the metabolism of the compound, and the ability to measure toxicokinetics is more limited compared to *in vivo*. Nonetheless the advantages that *in vitro* testing confers are plentiful: strict control of exposure conditions, ability to choose continuous or intermittent exposure, generally smaller amounts of chemicals required for exposures, increased precision of the response (stemming from less biological variation than with *in vivo* systems). Moreover, *in vitro* tests reduce the amount of animal sacrifice during toxicity screening of various compounds, refine toxicity, and replace *in vivo* studies, conforming to the "3 Rs" of alternative tests (122). And while it may be difficult to extrapolate *in vitro* toxicity data to human toxicity, this data enables the examination of the toxicity of xenobiotics at the fundamental level of the cell, without the physiological effects of the entire organism. Thus, *in vitro* tests may be a powerful tool for identifying the intrinsic mode of action of chemicals, with the caveat that the data are related to the whole organism in some way. This may be used to further the knowledge on the prevention and treatment of neurodegenerative and neurodevelopmental diseases.

## 4.5 *In ovo* exposure

### 4.5.1 Gene expression by qPCR

An increase in ROS and subsequent oxidative stress often activates different cellular pathways and the deregulation of genes that code for regulatory transcription factors, antioxidant defense systems, and structural proteins (123) . We analyzed the effects of the DEP and of the PAHs genes related to oxidative stress (GSR, Gpx1, Gpx2, Prdx6, SOD1) and to the metabolism of xenobiotics (CYP1A1). CYP1A1 belongs to the Cytochrome P450 superfamily of enzymes which are important in the clearance of various compounds. CYP1A1 is involved Phase1 xenobiotic and drug metabolism, including the metabolic activation of PAHs such as those investigated in our current study, pyrene and B(a)P. Therefore, an increase in the production of CYP enzymes would be expected upon exposure of PAHs, to meet the increasing demand for their metabolic activation. This increase is achieved by binding of the PAH molecules to the AHR, and its subsequent activation as a transcription factor (124). However, neither pyrene or B(a)P led to an upregulation of CYP1A1 at 1µM exposure. The activity of P450 enzymes is generally lower in brain tissue than in other major organs such as the liver or lung (125). Perhaps therefore, the CGNs do not produce a high rate of metabolism of PAHs. The sensitivity of this endpoint may therefore be limited.

GSR, a central enzyme of cellular antioxidant defense system, reduces GSSG to GSH. The upregulated expression of GSR is therefore an indicator of antioxidant responses (126). Prdx1 belongs to the peroxiredoxin family of antioxidant enzymes and is involved in cell protection against oxidative stress but its physiological role in oxidization–reduction balance remains unclear because it is highly susceptible to oxidative stress. Gpx1 and Gpx2 belong to the glutathione peroxidase family, members of which catalyze the reduction of organic hydroperoxides and ($H_2O_2$) by glutathione, and thereby protect cells against oxidative damage. SOD1 binds copper and zinc ions and is one of two isozymes responsible for destroying free superoxide radicals in the body. The non-injection control (untreated embryos) was used as the control for our calculations. ACTB and GADPH were tested and found to be stable candidates for use as reference genes. Their average was used to normalize the results. The data were analyzed using the comparative $2^{-\Delta\Delta Cq}$ (Livak) method, which assumes that both target and reference genes are amplified with efficiencies near 100% and within 5% of each other. The result is the ratio of the target gene

in the test sample to the control, normalized to the expression of the reference genes. We normalized the expression of the target gene to that of the reference gene to compensate for any difference in the amount of sample tissue. No significant differences were found between the expression of the genes analyzed and the control. Evidence from autopsy samples of individuals living in air-polluted cities have shown the deposition of DEP within the brain, acknowledging the fact that these particles can cross cell membranes and barrier tissues such as the BBB (127). PAHs have also been shown to cross the BBB, due in part to their lipophilicity (128). Therefore, it is reasonable to assume that these particles did indeed reach the brain. Indeed, a previous study found changes in expression of genes related to oxidative stress, inflammation, and cognitive effects in rat frontal cortex and the hippocampus, after exposure to DEP (129). Perhaps, therefore the exposure concentration was not toxically relevant, or the DEP had a different mode of action in the brains of chicken embryos. To complement the results obtained in this gene expression analysis, the enzymatic activity levels of the analyzed genes could be examined. In addition, chronic exposure to these DEP and other TRAP related compounds is usually experienced by individuals, and therefore should be considered for future studies. In addition, for mixed exposures at low chronic exposures, investigations of the epigenetic mechanisms regulating gene expression may provide valuable insight.

# 5 Conclusion

TRAP has consistently been associated with adverse effects on mental development and behavioral functions and is linked to higher prevalence of both neurodegenerative and neurodevelopmental disorders (130). Diseases whose origins result from, or are exacerbated by, exposure to environmental toxicants are largely preventable by eliminating or reducing exposure to the toxicant. It is therefore a major public health concern to investigate the potential neurotoxic effects of TRAP, including DEP to which the general population are chronically exposed. The results of such investigations may lead to a decrease in the incidence of neurotoxicological disorders.

Our investigations with PC12 cells revealed that B7, especially at the highest concentration tested (50 µg/ml) had the largest effect on cell viability, cell death, and the depletion of intracellular GSH levels. SHB20 on the other hand, showed the least amount of negative effects. In terms of investigating potential cell-signaling disturbances, the $Ca^{2+}$ influx assay revealed no significant differences between the cells exposed to DEP and the control. However, this should be investigated further, as PC12 cells lack functional NMDAR which may have led to a decreased toxicity response. Therefore, studies conducted on muscarinic or nicotinic receptors would be useful.

The CGN cell culture showed similar patterns of effects as the PC12 cells, but these were attenuated in comparison. Nevertheless, B7 at the highest concentration (50 µg/ml) showed the greatest amount of effects as well, for the cell viability, cell death, and depletion of intracellular GSH levels. The $Ca^{2+}$ influx response in the absence of $Mg^{2+}$ revealed B7 had the only statistically significant differences from the control, at every concentration tested (2, 10, 50 µg/ml). While the presence of $Mg^{2+}$ had an inhibitory effect on $Ca^{2+}$ influx, this was not shown to be statistically significant in our analysis. The PAHs found in DEP, pyrene and B(a)P were tested as single compounds and found to elicit a greater $Ca^{2+}$ influx response in the absence of $Mg^{2+}$ where they showed statistically significant responses. In the presence of $Mg^{2+}$ the response was inhibited, albeit not significantly. The gene expression analysis showed no significant changes in the expression of genes related to oxidative stress (GSR, Gpx1, Gpx2, Prdx6, SOD1) nor in the metabolism of xenobiotics (CYP1A).

Overall our results show that neurotoxicity due to DEP exposure were marginal, suggesting that biodiesel fuel may be a suitable alternative to conventional petroleum diesel fuel.

# 6 Further Perspectives

The central purpose of primary prevention in disease handling is to identify toxic hazards *before* humans are exposed. When it comes to neurotoxicological testing, however, secondary prevention is often employed, where the early detection of disease is identified, and then further exposure is prevented and/or limited. An understanding of the specific components of DEP that contribute to risk could be used to create regulatory polices to minimize exposures.

Future studies that could shed light on the risk of DEP exposure for negative CNS outcomes include toxicokinetic and physicochemical property comparison of the different DEP particles found in biodiesel blends currently on the market. Although knowledge of the chemical toxicities of individual compounds is of critical importance, mixtures of compounds may differ significantly in their toxicities from their individual components. This may be due to a variety of factors, including receptor competition, metabolic modulation, or changes in bioavailability, mechanisms which could be further investigated. Additionally, examining the initial triggering mechanisms of the proinflammatory effects of DEP could lead to possible prevention strategies. Lastly, further *in vitro* studies with neuronal cell models, and *in vivo* studies with animal models could help ascertain mechanisms for DEP deposition in the brain.

# References


1. Bourguignon D. EU biofuels policy: Dealing with impacts of indirect land use change. 2015.

2. Manisalidis I, Stavropoulou E, Stavropoulos A, Bezirtzoglou E. Environmental and Health Impacts of Air Pollution: A Review [Internet]. Vol. 8, Frontiers in Public Health. Frontiers Media S.A.; 2020 [cited 2020 Sep 9]. p. 14. Available from: /pmc/articles/PMC7044178/?report=abstract

3. Ambient air pollution: A global assessment of exposure and burden of disease.

4. Genc S, Zadeoglulari Z, Fuss SH, Genc K. The Adverse Effects of Air Pollution on the Nervous System. J Toxicol. 2012;2012.

5. Costa LG, Cole TB, Dao K, Chang YC, Coburn J, Garrick JM. Effects of air pollution on the nervous system and its possible role in neurodevelopmental and neurodegenerative disorders. Vol. 210, Pharmacology and Therapeutics. Elsevier Inc.; 2020. p. 107523.

6. Buettner T. Urban Estimates and Projections at the United Nations: The Strengths, Weaknesses, and Underpinnings of the World Urbanization Prospects. Spat Demogr [Internet]. 2015 Nov 9 [cited 2020 Sep 9];3(2):91–108. Available from: https://link.springer.com/article/10.1007/s40980-015-0004-2

7. Reşitoɬlu IA, Altinişik K, Keskin A. The pollutant emissions from diesel-engine vehicles and exhaust aftertreatment systems [Internet]. Vol. 17, Clean Technologies and Environmental Policy. Springer Verlag; 2015 [cited 2020 Sep 5]. p. 15–27. Available from: https://link.springer.com/article/10.1007/s10098-014-0793-9

8. Transport emissions | Climate Action [Internet]. [cited 2020 Sep 9]. Available from: https://ec.europa.eu/clima/policies/transport_en

9. ( 1 ) ( 2 ) DECISIONS ADOPTED JOINTLY BY THE EUROPEAN PARLIAMENT AND THE COUNCIL OF THE EUROPEAN PARLIAMENT AND OF THE COUNCIL. 2009.

10. González Ortiz A. Air quality in Europe — 2016 report. 2000;

11. Nyström I, Bokinge P. Production of liquid advanced biofuels-global status Per-Åke Franck.

12. Mohr A, Raman S. Lessons from first generation biofuels and implications for the sustainability appraisal of second generation biofuels. Effic Sustain Biofuel Prod Environ Land-Use Res [Internet]. 2015 Jan 1 [cited 2020 Sep 9];63:281–310. Available from: /pmc/articles/PMC4048104/?report=abstract

13. Hombach LE, Cambero C, Sowlati T, Walther G. Optimal design of supply chains for second generation biofuels incorporating European biofuel regulations. J Clean Prod. 2016 Oct 1;133:565–75.

14. Elliott MA, Nebel GJ, Rounds FG. Journal of the Air Pollution Control Association The Composition of Exhaust Gases from Diesel, Gasoline and Propane Powered Motor Coaches. J Air Pollut Control Assoc [Internet]. 2012 [cited 2020 Sep 9];5(2):103–8. Available from: https://www.tandfonline.com/action/journalInformation?journalCode=uawm20

15. Reşitoɨlu IA, Altinişik K, Keskin A. The pollutant emissions from diesel-engine vehicles and exhaust aftertreatment systems [Internet]. Vol. 17, Clean Technologies and Environmental Policy. Springer Verlag; 2015 [cited 2020 Sep 9]. p. 15–27. Available from: https://link.springer.com/article/10.1007/s10098-014-0793-9

16. Hamanaka RB, Mutlu GM. Particulate Matter Air Pollution: Effects on the Cardiovascular System. Front Endocrinol (Lausanne) [Internet]. 2018 Nov 16 [cited 2020 Sep 9];9:680. Available from: www.frontiersin.org

17. Wang X, Michaelis EK. Selective neuronal vulnerability to oxidative stress in the brain [Internet]. Vol. 2, Frontiers in Aging Neuroscience. Frontiers Media SA; 2010 [cited 2020 Sep 9]. p. 12. Available from: www.frontiersin.org

18. Okubo M, Kuwahara T. Principle and design of emission control systems. In: New Technologies for Emission Control in Marine Diesel Engines. Elsevier; 2020. p. 53–143.

19. Ray PD, Huang BW, Tsuji Y. Reactive oxygen species (ROS) homeostasis and redox regulation in cellular signaling [Internet]. Vol. 24, Cellular Signalling. NIH Public Access; 2012 [cited 2020 Sep 9]. p. 981–90. Available from: /pmc/articles/PMC3454471/?report=abstract

20. Øvrevik J, Refsnes M, Låg M, Holme JA, Schwarze PE. Activation of proinflammatory responses in cells of the airway mucosa by particulate matter: Oxidant- and non-oxidant-mediated triggering mechanisms [Internet]. Vol. 5, Biomolecules. MDPI AG; 2015 [cited 2020 Sep 9]. p. 1399–440. Available from: /pmc/articles/PMC4598757/?report=abstract

21. Twigg M V., Phillips PR. Cleaning the air we breathe - controlling diesel particulate emissions from passenger cars. Platin Met Rev. 2009 Jan;53(1):27–34.

22. El Morabet R. Effects of Outdoor Air Pollution on Human Health. In: Reference Module in Earth Systems and Environmental Sciences. Elsevier; 2018.

23. Sturm R. Deposition of diesel exhaust particles in the human lungs: theoretical simulations and experimental data. J Public Heal Emerg [Internet]. 2017 Jul 25 [cited 2020 Sep 9];1:70–70. Available from: http://jphe.amegroups.com/article/view/4064/4908

24. Cassee FR, Héroux ME, Gerlofs-Nijland ME, Kelly FJ. Particulate matter beyond mass: Recent health evidence on the role of fractions, chemical constituents and sources of emission [Internet]. Vol. 25, Inhalation Toxicology. Taylor & Francis; 2013 [cited 2020 Sep 9]. p. 802–12. Available from: /pmc/articles/PMC3886392/?report=abstract

25. Harkema JR, Nikula KJ, Haschek WM. Respiratory System. In: Haschek and Rousseaux's Handbook of Toxicologic Pathology. Elsevier Inc.; 2013. p. 1935–2003.

26. Cattani-Cavalieri I, Valença S dos S, Schmidt M. Nanodomains in cardiopulmonary disorders and the impact of air pollution. Biochem Soc Trans [Internet]. 2020 [cited 2020 Sep 9];48(3):799–811. Available from: /pmc/articles/PMC7329344/?report=abstract

27. Mills NL, Donaldson K, Hadoke PW, Boon NA, MacNee W, Cassee FR, et al. Adverse

cardiovascular effects of air pollution [Internet]. Vol. 6, Nature Clinical Practice Cardiovascular Medicine. Nat Clin Pract Cardiovasc Med; 2009 [cited 2020 Sep 9]. p. 36–44. Available from: https://pubmed.ncbi.nlm.nih.gov/19029991/

28. De Hartog JJ, Hoek G, Peters A, Timonen KL, Ibald-Mulli A, Brunekreef B, et al. Effects of fine and ultrafine particles on cardiorespiratory symptoms in elderly subjects with coronary heart disease: The ULTRA study. Am J Epidemiol [Internet]. 2003 Apr 1 [cited 2020 Sep 9];157(7):613–23. Available from: https://academic.oup.com/aje/article/157/7/613/69740

29. Kim CS, Hu S-C. Total respiratory tract deposition of fine micrometer-sized particles in healthy adults: empirical equations for sex and breathing pattern. J Appl Physiol [Internet]. 2006 [cited 2020 Sep 9];101:401–12. Available from: http://www.jap.org

30. Block ML, Calderón-Garcidueñas L. Air pollution: mechanisms of neuroinflammation and CNS disease [Internet]. Vol. 32, Trends in Neurosciences. NIH Public Access; 2009 [cited 2020 Sep 9]. p. 506–16. Available from: /pmc/articles/PMC2743793/?report=abstract

31. Meador JP. Polycyclic Aromatic Hydrocarbons. In: Encyclopedia of Ecology, Five-Volume Set. Elsevier Inc.; 2008. p. 2881–91.

32. Keyte IJ, Albinet A, Harrison RM. On-road traffic emissions of polycyclic aromatic hydrocarbons and their oxy- and nitro- derivative compounds measured in road tunnel environments. Sci Total Environ. 2016 Oct 1;566–567:1131–42.

33. de Prado Bert P, Mercader EMH, Pujol J, Sunyer J, Mortamais M. The Effects of Air Pollution on the Brain: a Review of Studies Interfacing Environmental Epidemiology and Neuroimaging [Internet]. Vol. 5, Current environmental health reports. Springer; 2018 [cited 2020 Sep 9]. p. 351–64. Available from: https://pubmed.ncbi.nlm.nih.gov/30008171/

34. Power MC, Adar SD, Yanosky JD, Weuve J. Exposure to air pollution as a potential contributor to cognitive function, cognitive decline, brain imaging, and dementia: A systematic review of epidemiologic research. Neurotoxicology [Internet]. 2016 Sep 1 [cited 2020 Sep 9];56:235–53. Available from:

/pmc/articles/PMC5048530/?report=abstract

35. Clifford A, Lang L, Chen R, Anstey KJ, Seaton A. Exposure to air pollution and cognitive functioning across the life course - A systematic literature review [Internet]. Vol. 147, Environmental Research. Academic Press Inc.; 2016 [cited 2020 Sep 9]. p. 383–98. Available from: https://pubmed.ncbi.nlm.nih.gov/26945620/

36. Chen H, Kwong JC, Copes R, Tu K, Villeneuve PJ, van Donkelaar A, et al. Living near major roads and the incidence of dementia, Parkinson's disease, and multiple sclerosis: a population-based cohort study. Lancet [Internet]. 2017 Feb 18 [cited 2020 Sep 9];389(10070):718–26. Available from: https://pubmed.ncbi.nlm.nih.gov/28063597/

37. Block ML, Calderón-Garcidueñas L. Air pollution: mechanisms of neuroinflammation and CNS disease [Internet]. Vol. 32, Trends in Neurosciences. Trends Neurosci; 2009 [cited 2020 Sep 9]. p. 506–16. Available from: https://pubmed.ncbi.nlm.nih.gov/19716187/

38. Calder´on L, Calder´on-Garcidue˜nas C, Garcidue˜nas G, Reed W, Maronpot RR, Henr´iquez C, et al. Brain Inflammation and Alzheimer's-Like Pathology in Individuals Exposed to Severe Air Pollution. Toxicol Pathol. 2004;32:650–8.

39. Calderón-Garcidueñas L, Solt AC, Henríquez-Roldán C, Torres-Jardón R, Nuse B, Herritt L, et al. Long-term air pollution exposure is associated with neuroinflammation, an altered innate immune response, disruption of the blood-brain barrier, ultrafine particulate deposition, and accumulation of amyloid β-42 and α-synuclein in children and young adult. Toxicol Pathol [Internet]. 2008 Feb [cited 2020 Sep 9];36(2):289–310. Available from: https://pubmed.ncbi.nlm.nih.gov/18349428/

40. Suades-González E, Gascon M, Guxens M, Sunyer J. Air pollution and neuropsychological development: A review of the latest evidence [Internet]. Vol. 156, Endocrinology. Endocrine Society; 2015 [cited 2020 Sep 9]. p. 3473–82. Available from: https://pubmed.ncbi.nlm.nih.gov/26241071/

41. Flores-Pajot MC, Ofner M, Do MT, Lavigne E, Villeneuve PJ. Childhood autism spectrum disorders and exposure to nitrogen dioxide, and particulate matter air pollution: A review and meta-analysis [Internet]. Vol. 151, Environmental Research.

Academic Press Inc.; 2016 [cited 2020 Sep 9]. p. 763–76. Available from: https://pubmed.ncbi.nlm.nih.gov/27609410/

42. Xu X, Ha SU, Basnet R. A Review of Epidemiological Research on Adverse Neurological Effects of Exposure to Ambient Air Pollution. Front Public Heal [Internet]. 2016 Aug 5 [cited 2020 Sep 9];4:1. Available from: /pmc/articles/PMC4974252/?report=abstract

43. Genc S, Zadeoglulari Z, Fuss SH, Genc K. The adverse effects of air pollution on the nervous system [Internet]. Vol. 2012, Journal of Toxicology. J Toxicol; 2012 [cited 2020 Sep 9]. Available from: https://pubmed.ncbi.nlm.nih.gov/22523490/

44. Davis DA, Akopian G, Walsh JP, Sioutas C, Morgan TE, Finch CE. Urban air pollutants reduce synaptic function of CA1 neurons via an NMDA/NÈ® pathway in vitro. J Neurochem [Internet]. 2013 Aug 26 [cited 2020 Sep 9];127(4):509–19. Available from: https://europepmc.org/articles/PMC3818296

45. Saunders CR, Das SK, Ramesh A, Shockley DC, Mukherjee S. Benzo(a)pyrene-induced acute neurotoxicity in the F-344 rat: Role of oxidative stress. J Appl Toxicol [Internet]. 2006 Sep [cited 2020 Sep 9];26(5):427–38. Available from: https://pubmed.ncbi.nlm.nih.gov/16858674/

46. Campbell A, Oldham M, Becaria A, Bondy SC, Meacher D, Sioutas C, et al. Particulate matter in polluted air may increase biomarkers of inflammation in mouse brain. Neurotoxicology [Internet]. 2005 Jan [cited 2020 Sep 9];26(1):133–40. Available from: https://pubmed.ncbi.nlm.nih.gov/15527881/

47. Loane C, Pilinis C, Lekkas TD, Politis M. Ambient particulate matter and its potential neurological consequences. Rev Neurosci [Internet]. 2013 Jun 1 [cited 2020 Sep 9];24(3):323–35. Available from: https://www.degruyter.com/view/journals/revneuro/24/3/article-p323.xml

48. Banks WA. Characteristics of compounds that cross the blood-brain barrier. In: BMC Neurology [Internet]. BioMed Central; 2009 [cited 2020 Sep 9]. p. S3. Available from: /pmc/articles/PMC2697631/?report=abstract

49. Elder A, Gelein R, Silva V, Feikert T, Opanashuk L, Carter J, et al. Translocation of

inhaled ultrafine manganese oxide particles to the central nervous system. Environ Health Perspect [Internet]. 2006 Aug [cited 2020 Sep 9];114(8):1172–8. Available from: https://pubmed.ncbi.nlm.nih.gov/16882521/

50. Weil ZM, Norman GJ, DeVries AC, Nelson RJ. The injured nervous system: A Darwinian perspective [Internet]. Vol. 86, Progress in Neurobiology. Prog Neurobiol; 2008 [cited 2020 Sep 9]. p. 48–59. Available from: https://pubmed.ncbi.nlm.nih.gov/18602443/

51. Solleiro-Villavicencio H, Rivas-Arancibia S. Effect of chronic oxidative stress on neuroinflammatory response mediated by CD4+T cells in neurodegenerative diseases [Internet]. Vol. 12, Frontiers in Cellular Neuroscience. Frontiers Media S.A.; 2018 [cited 2020 Sep 9]. p. 114. Available from: /pmc/articles/PMC5934485/?report=abstract

52. Gao HM, Zhou H, Hong JS. Oxidative stress, neuroinflammation, and neurodegeneration. In: Neuroinflammation and Neurodegeneration [Internet]. Springer New York; 2014 [cited 2020 Sep 9]. p. 81–104. Available from: https://link-springer-com.ezproxy.uio.no/chapter/10.1007/978-1-4939-1071-7_5

53. Uttara B, Singh A, Zamboni P, Mahajan R. Oxidative Stress and Neurodegenerative Diseases: A Review of Upstream and Downstream Antioxidant Therapeutic Options. Curr Neuropharmacol [Internet]. 2009 Mar 6 [cited 2020 Sep 9];7(1):65–74. Available from: /pmc/articles/PMC2724665/?report=abstract

54. Kudryavtseva A V., Krasnov GS, Dmitriev AA, Alekseev BY, Kardymon OL, Sadritdinova AF, et al. Mitochondrial dysfunction and oxidative stress in aging and cancer. Oncotarget [Internet]. 2016 [cited 2020 Sep 9];7(29):44879–905. Available from: /pmc/articles/PMC5216692/?report=abstract

55. Ballatori N, Krance SM, Notenboom S, Shi S, Tieu K, Hammond CL. Glutathione dysregulation and the etiology and progression of human diseases [Internet]. Vol. 390, Biological Chemistry. NIH Public Access; 2009 [cited 2020 Sep 9]. p. 191–214. Available from: /pmc/articles/PMC2756154/?report=abstract

56. Cobley JN, Fiorello ML, Bailey DM. 13 reasons why the brain is susceptible to

oxidative stress. Vol. 15, Redox Biology. Elsevier B.V.; 2018. p. 490–503.

57. Fonnum F, Lock EA. Cerebellum as a target for toxic substances. In: Toxicology Letters. Elsevier; 2000. p. 9–16.

58. Chen X, Guo C, Kong J. Oxidative stress in neurodegenerative diseases. Neural Regen Res [Internet]. 2012 [cited 2020 Sep 9];7(5):376. Available from: /pmc/articles/PMC4350122/?report=abstract

59. Wang J, Huang J, Wang L, Chen C, Yang D, Jin M, et al. Urban particulate matter triggers lung inflammation via the ROS-MAPK- NF-κB signaling pathway. J Thorac Dis [Internet]. 2017 Nov 1 [cited 2020 Sep 9];9(11):4398–412. Available from: /pmc/articles/PMC5721041/?report=abstract

60. Øvrevik J, Refsnes M, Låg M, Brinchmann BC, Schwarze PE, Holme JA. Triggering Mechanisms and Inflammatory Effects of Combustion Exhaust Particles with Implication for Carcinogenesis. Basic Clin Pharmacol Toxicol [Internet]. 2017 Sep 1 [cited 2020 Sep 9];121:55–62. Available from: http://doi.wiley.com/10.1111/bcpt.12746

61. Bootman MD. Calcium signaling. Cold Spring Harb Perspect Biol [Internet]. 2012 Jul [cited 2020 Sep 9];4(7):1–3. Available from: /pmc/articles/PMC3385957/?report=abstract

62. Bondy SC. Intracellular calcium and neurotoxic events. Neurotoxicol Teratol. 1989 Nov 1;11(6):527–31.

63. Mattson MP. Excitotoxicity. In: Stress: Physiology, Biochemistry, and Pathology. Elsevier; 2019. p. 125–34.

64. Dong XX, Wang Y, Qin ZH. Molecular mechanisms of excitotoxicity and their relevance to pathogenesis of neurodegenerative diseases [Internet]. Vol. 30, Acta Pharmacologica Sinica. Nature Publishing Group; 2009 [cited 2020 Sep 9]. p. 379–87. Available from: /pmc/articles/PMC4002277/?report=abstract

65. Castañeda AR, Pinkerton KE, Bein KJ, Magaña-Méndez A, Yang HT, Ashwood P, et al. Ambient particulate matter activates the aryl hydrocarbon receptor in dendritic cells

and enhances Th17 polarization. Toxicol Lett [Internet]. 2018 Aug 1 [cited 2020 Sep 9];292:85–96. Available from: https://pubmed.ncbi.nlm.nih.gov/29689377/

66. Juricek L, Coumoul X. The aryl hydrocarbon receptor and the nervous system [Internet]. Vol. 19, International Journal of Molecular Sciences. MDPI AG; 2018 [cited 2020 Sep 9]. Available from: https://pubmed.ncbi.nlm.nih.gov/30149528/

67. Siauciunaite R, Foulkes NS, Calabrò V, Vallone D. Evolution shapes the gene expression response to Oxidative Stress [Internet]. Vol. 20, International Journal of Molecular Sciences. MDPI AG; 2019 [cited 2020 Sep 9]. Available from: /pmc/articles/PMC6627103/?report=abstract

68. HOLLOWAY JW, SAVARIMUTHU FRANCIS S, FONG KM, YANG IA. Genomics and the respiratory effects of air pollution exposure. Respirology [Internet]. 2012 May 1 [cited 2020 Sep 9];17(4):590–600. Available from: http://doi.wiley.com/10.1111/j.1440-1843.2012.02164.x

69. Kunsch C, Medford RM. Oxidative stress as a regulator of gene expression in the vasculature [Internet]. Vol. 85, Circulation Research. Lippincott Williams and Wilkins; 1999 [cited 2020 Sep 9]. p. 753–66. Available from: https://pubmed.ncbi.nlm.nih.gov/10521248/

70. Sunyer J. The neurological effects of air pollution in children.

71. Gluckman PD, Hanson MA, Cooper C, Thornburg KL. Effect of in utero and early-life conditions on adult health and disease [Internet]. Vol. 359, New England Journal of Medicine. Massachussetts Medical Society; 2008 [cited 2020 Sep 9]. p. 61. Available from: https://www.ncbi.nlm.nih.gov/pmc/articles/PMC3923653/

72. Rice D, Barone S. Critical Periods of Vulnerability for the Developing Nervous System: Evidence from Humans and Animal Models. Environ Health Perspect. 2000 Jun;108:511.

73. Perera FP, Li Z, Whyatt R, Hoepner L, Wang S, Camann D, et al. Prenatal airborne polycyclic aromatic hydrocarbon exposure and child IQ at age 5 years. Pediatrics [Internet]. 2009 Aug [cited 2020 Sep 9];124(2):e195. Available from: /pmc/articles/PMC2864932/?report=abstract

74. Kerin T, Volk H, Li W, Lurmann F, Eckel S, McConnell R, et al. Association Between Air Pollution Exposure, Cognitive and Adaptive Function, and ASD Severity Among Children with Autism Spectrum Disorder. J Autism Dev Disord [Internet]. 2018 Jan 1 [cited 2020 Sep 9];48(1):137–50. Available from: /pmc/articles/PMC5764162/?report=abstract

75. Van Den Hazel P, Zuurbier M, Babisch W, Bartonova A, Bistrup ML, Bolte G, et al. Today's epidemics in children: Possible relations to environmental pollution and suggested preventive measures. Acta Paediatr [Internet]. 2006 Oct 1 [cited 2020 Sep 9];95(0):18–25. Available from: http://doi.wiley.com/10.1080/08035320600885846

76. Neurobehavioural effects of developmental toxicity. [cited 2020 Sep 9]; Available from: http://nrs.harvard.edu/urn-3:HUL.InstRepos:33087516

77. Stoodley CJ. Distinct regions of the cerebellum show gray matter decreases in autism, ADHD, and developmental dyslexia. Front Syst Neurosci [Internet]. 2014 May 20 [cited 2020 Sep 9];8(MAY). Available from: /pmc/articles/PMC4033133/?report=abstract

78. von Bartheld CS, Bahney J, Herculano-Houzel S. The search for true numbers of neurons and glial cells in the human brain: A review of 150 years of cell counting [Internet]. Vol. 524, Journal of Comparative Neurology. Wiley-Liss Inc.; 2016 [cited 2020 Sep 9]. p. 3865–95. Available from: /pmc/articles/PMC5063692/?report=abstract

79. Bear M. Neuroscience : exploring the brain. 3rd ed. Philadelphia PA: Lippincott Williams & Wilkins; 2007.

80. Environmental Neurotoxicology. Environmental Neurotoxicology. National Academies Press; 1992.

81. Levesque S, Surace MJ, McDonald J, Block ML. Air pollution and the brain: Subchronic diesel exhaust exposure causes neuroinflammation and elevates early markers of neurodegenerative disease. J Neuroinflammation [Internet]. 2011 Aug 24 [cited 2020 Sep 9];8(1):105. Available from: http://jneuroinflammation.biomedcentral.com/articles/10.1186/1742-2094-8-105

82. Levesque S, Taetzsch T, Lull ME, Kodavanti U, Stadler K, Wagner A, et al. Diesel

exhaust activates and primes microglia: Air pollution, neuroinflammation, and regulation of dopaminergic neurotoxicity. Environ Health Perspect. 2011 Aug;119(8):1149–55.

83. Kritis A, Pourzitaki C, Klagas I, Chourdakis M, Albani M. Proteases Inhibition Assessment on PC12 and NGF Treated Cells after Oxygen and Glucose Deprivation Reveals a Distinct Role for Aspartyl Proteases. Linden R, editor. PLoS One [Internet]. 2011 Oct 18 [cited 2020 Sep 9];6(10):e25950. Available from: https://dx.plos.org/10.1371/journal.pone.0025950

84. Westerink RHS, Ewing AG. The PC12 cell as model for neurosecretion. In: Acta Physiologica [Internet]. NIH Public Access; 2008 [cited 2020 Sep 9]. p. 273–85. Available from: /pmc/articles/PMC2663028/?report=abstract

85. Stern CD. The Chick. Dev Cell. 2005 Jan 1;8(1):9–17.

86. Bjørnstad S, Austdal LPE, Roald B, Glover JC, Paulsen RE. Cracking the egg: Potential of the developing chicken as a model system for nonclinical safety studies of pharmaceuticals [Internet]. Vol. 355, Journal of Pharmacology and Experimental Therapeutics. American Society for Pharmacology and Experimental Therapy; 2015 [cited 2020 Sep 9]. p. 386–96. Available from: https://pubmed.ncbi.nlm.nih.gov/26432906/

87. Hubrecht RC, Carter E. The 3Rs and Humane Experimental Technique: Implementing Change. Anim an open access J from MDPI [Internet]. 2019 Sep 30 [cited 2020 Sep 9];9(10). Available from: http://www.ncbi.nlm.nih.gov/pubmed/31575048

88. Bünger J, Krahl J, Baum K, Schröder O, Müller M, Westphal G, et al. Cytotoxic and mutagenic effects, particle size and concentration analysis of diesel engine emissions using biodiesel and petrol diesel as fuel. Arch Toxicol [Internet]. 2000 [cited 2020 Sep 9];74(8):490–8. Available from: https://pubmed.ncbi.nlm.nih.gov/11097388/

89. (PDF) Comparison of relevant exhaust gas emissions from biodiesel and fossil diesel fuel [Internet]. [cited 2020 Sep 9]. Available from: https://www.researchgate.net/publication/317063811_Comparison_of_relevant_exhaust_gas_emissions_from_biodiesel_and_fossil_diesel_fuel

90. Szybist JP, Kirby SR, Boehman AL. NOx emissions of alternative diesel fuels: A comparative analysis of biodiesel and FT diesel. Energy and Fuels [Internet]. 2005 Jul [cited 2020 Sep 9];19(4):1484–92. Available from: https://pubs.acs.org/doi/abs/10.1021/ef049702q

91. Chapter 9. Biofuels. [cited 2020 Sep 9]; Available from: http://dx.doi.org/10.1787/agr-outl-data-en.

92. Oecd-fao. BIOFUELS. [cited 2020 Sep 9]; Available from: http://dx.doi.org/10.1787/agr_outlook-2016-13-en

93. Steiner S, Czerwinski J, Comte P, Popovicheva O, Kireeva E, Müller L, et al. Comparison of the toxicity of diesel exhaust produced by bio- and fossil diesel combustion in human lung cells invitro. Atmos Environ. 2013 Dec 1;81:380–8.

94. Bakeas E, Karavalakis G, Fontaras G, Stournas S. An experimental study on the impact of biodiesel origin on the regulated and PAH emissions from a Euro 4 light-duty vehicle. Fuel. 2011 Nov 1;90(11):3200–8.

95. Çelik TA. Introductory Chapter: Cytotoxicity. In: Cytotoxicity [Internet]. InTech; 2018 [cited 2020 Sep 9]. Available from: http://dx.doi.org/10.5772/intechopen.77244

96. An L, Li Z, Zhang T. Reversible effects of vitamins C and E combination on oxidative stress-induced apoptosis in melamine-treated PC12 cells. Free Radic Res [Internet]. 2014 Feb [cited 2020 Sep 9];48(2):239–50. Available from: https://www.tandfonline.com/doi/abs/10.3109/10715762.2013.861598

97. Berntsen HF, Bjørklund CG, Strandabø R, Haug TM, Moldes-Anaya A, Fuentes-Lazaro J, et al. PFOS-induced excitotoxicity is dependent on Ca 2+ influx via NMDA receptors in rat cerebellar granule neurons. Toxicol Appl Pharmacol. 2018 Oct 15;357:19–32.

98. Ma K, Yang LM, Chen HZ, Lu Y. Activation of muscarinic receptors inhibits glutamate-induced GSK-3β overactivation in PC12 cells. Acta Pharmacol Sin [Internet]. 2013 Jul [cited 2020 Sep 9];34(7):886–92. Available from: /pmc/articles/PMC4002616/?report=abstract

99. Green DR, Llambi F. Cell death signaling. Cold Spring Harb Perspect Biol [Internet]. 2015 Dec 1 [cited 2020 Sep 9];7(12):a006080. Available from: http://cshperspectives.cshlp.org/

100. Quent VMC, Loessner D, Friis T, Reichert JC, Hutmacher DW. Discrepancies between metabolic activity and DNA content as tool to assess cell proliferation in cancer research. J Cell Mol Med [Internet]. 2010 Apr [cited 2020 Sep 9];14(4):1003–13. Available from: https://pubmed.ncbi.nlm.nih.gov/20082656/

101. Crowley LC, Marfell BJ, Waterhouse NJ. Analyzing cell death by nuclear staining with Hoechst 33342. Cold Spring Harb Protoc [Internet]. 2016 Sep 1 [cited 2020 Sep 9];2016(9):778–81. Available from: https://pubmed.ncbi.nlm.nih.gov/27587774/

102. York JL, Maddox LC, Zimniak P, McHugh TE, Grant DF. Reduction of MTT by glutathione S-transferase. Biotechniques [Internet]. 1998 [cited 2020 Sep 9];25(4):622–8. Available from: https://pubmed.ncbi.nlm.nih.gov/9793644/

103. Jiang B, Liu JH, Bao YM, An LJ. Hydrogen peroxide-induced apoptosis in pc12 cells and the protective effect of puerarin. Cell Biol Int [Internet]. 2003 [cited 2020 Sep 9];27(12):1025–31. Available from: https://pubmed.ncbi.nlm.nih.gov/14642535/

104. Kilian J, Kitazawa M. The emerging risk of exposure to air pollution on cognitive decline and Alzheimer's disease – Evidence from epidemiological and animal studies [Internet]. Vol. 41, Biomedical Journal. Elsevier B.V.; 2018 [cited 2020 Sep 9]. p. 141–62. Available from: /pmc/articles/PMC6138768/?report=abstract

105. Chen S, Ren Q, Zhang J, Ye Y, Zhang Z, Xu Y, et al. N-acetyl-L-cysteine protects against cadmium-induced neuronal apoptosis by inhibiting ROS-dependent activation of Akt/mTOR pathway in mouse brain. Neuropathol Appl Neurobiol [Internet]. 2014 Oct 1 [cited 2020 Sep 9];40(6):759–77. Available from: /pmc/articles/PMC4043941/?report=abstract

106. Veskoukis AS, Margaritelis N V., Kyparos A, Paschalis V, Nikolaidis MG. Spectrophotometric assays for measuring redox biomarkers in blood and tissues: the NADPH network. Redox Rep [Internet]. 2018 Jan 1 [cited 2020 Sep 9];23(1):47–56. Available from:

https://www.tandfonline.com/doi/full/10.1080/13510002.2017.1392695

107. Circu ML, Aw TY. Reactive oxygen species, cellular redox systems, and apoptosis [Internet]. Vol. 48, Free Radical Biology and Medicine. NIH Public Access; 2010 [cited 2020 Sep 9]. p. 749–62. Available from: /pmc/articles/PMC2823977/?report=abstract

108. Berridge M V., Tan AS. Characterization of the Cellular Reduction of 3-(4,5-dimethylthiazol-2- yl)-2,5-diphenyltetrazolium bromide (MTT): Subcellular Localization, Substrate Dependence, and Involvement of Mitochondrial Electron Transport in MTT Reduction. Arch Biochem Biophys [Internet]. 1993 [cited 2020 Aug 26];303(2):474–82. Available from: https://pubmed.ncbi.nlm.nih.gov/8390225/

109. Fanger GR, Brennan C, Henderson LP, Gardner PD, Maue RA. Membrane Biology Differential Expression of Sodium Channels and Nicotinic Acetylcholine Receptor Channels in nnr Variants of the PC12 Pheochromocytoma Cell Line. Vol. 144, J. Membrane Biol. 1995.

110. Wiatrak B, Kubis-Kubiak A, Piwowar A, Barg E. PC12 Cell Line: Cell Types, Coating of Culture Vessels, Differentiation and Other Culture Conditions. Cells [Internet]. 2020 Apr 14 [cited 2020 Sep 9];9(4). Available from: /pmc/articles/PMC7227003/?report=abstract

111. Bradykinin B, Ransom JT, CherwinskiS HM, Delmendoy RE, Sharifl NA, Eglenll R. THE JOURNAL OF BIOLOGICAL CHEMISTRY Characterization of the m4 Muscarinic Receptor Ca2+ Response in a Subclone of PC-12 Cells by Single Cell Flow Cytometry INHIBITION OF THE RESPONSE. Vol. 266. 1991.

112. Edwards MA, Loxley RA, Williams AJ, Connor M, Phillips JK. Lack of functional expression of NMDA receptors in PC12 cells. Neurotoxicology [Internet]. 2007 Jul [cited 2020 Sep 9];28(4):876–85. Available from: https://pubmed.ncbi.nlm.nih.gov/17572500/

113. Brown DM, Hutchison L, Donaldson K, Stone V. The effects of PM $_{10}$ particles and oxidative stress on macrophages and lung epithelial cells: modulating effects of calcium-signaling antagonists. Am J Physiol Cell Mol Physiol [Internet]. 2007 Jun

[cited 2020 Sep 9];292(6):L1444–51. Available from: https://www.physiology.org/doi/10.1152/ajplung.00162.2006

114. Burton GJ, Jauniaux E. Oxidative stress [Internet]. Vol. 25, Best Practice and Research: Clinical Obstetrics and Gynaecology. Elsevier; 2011 [cited 2020 Sep 9]. p. 287–99. Available from: /pmc/articles/PMC3101336/?report=abstract

115. Fujita K, Lazarovici P, Guroff G. Regulation of the Differentiation of PC12 Pheochromocytoma Cells. Vol. 80, Environmental Health Perspectives. 1989.

116. Carvajal FJ, Mattison HA, Cerpa W. Role of NMDA Receptor-Mediated Glutamatergic Signaling in Chronic and Acute Neuropathologies [Internet]. Vol. 2016, Neural Plasticity. Hindawi Limited; 2016 [cited 2020 Sep 9]. Available from: /pmc/articles/PMC5007376/?report=abstract

117. Olivares D, K. Deshpande V, Shi Y, K. Lahiri D, H. Greig N, T. Rogers J, et al. N-Methyl D-Aspartate (NMDA) Receptor Antagonists and Memantine Treatment for Alzheimer's Disease, Vascular Dementia and Parkinson's Disease. Curr Alzheimer Res [Internet]. 2013 Jul 25 [cited 2020 Sep 9];9(6):746–58. Available from: http://www.molgen.ua.ac.be/ADMutations].

118. Rengarajan T, Rajendran P, Nandakumar N, Lokeshkumar B, Rajendran P, Nishigaki I. Exposure to polycyclic aromatic hydrocarbons with special focus on cancer. Vol. 5, Asian Pacific Journal of Tropical Biomedicine. Asian Pacific Tropical Biomedicine Press; 2015. p. 182–9.

119. Lankoff A, Brzoska K, Czarnocka J, Kowalska M, Lisowska H, Mruk R, et al. A comparative analysis of in vitro toxicity of diesel exhaust particles from combustion of 1st- and 2nd-generation biodiesel fuels in relation to their physicochemical properties—the FuelHealth project. Environ Sci Pollut Res [Internet]. 2017 Aug 1 [cited 2020 Sep 9];24(23):19357–74. Available from: https://link.springer.com/article/10.1007/s11356-017-9561-9

120. Brinchmann BC, Ferrec E Le, Bisson WH, Podechard N, Huitfeldt HS, Gallais I, et al. Evidence of selective activation of aryl hydrocarbon receptor nongenomic calcium signaling by pyrene. Biochem Pharmacol [Internet]. 2018 Dec 1 [cited 2020 Sep

9];158:1–12. Available from: https://pubmed.ncbi.nlm.nih.gov/30248327/

121. Yuan C, Gao J, Guo J, Bai L, Marshall C, Cai Z, et al. Dimethyl Sulfoxide Damages Mitochondrial Integrity and Membrane Potential in Cultured Astrocytes. Buch SJ, editor. PLoS One [Internet]. 2014 Sep 19 [cited 2020 Sep 9];9(9):e107447. Available from: https://dx.plos.org/10.1371/journal.pone.0107447

122. Fenwick N, Griffin G, Gauthier C. Le bien-être des animaux utilisés en science : Comment l'éthique des « Trois R » oriente les améliorations. Can Vet J [Internet]. 2009 [cited 2020 Sep 9];50(5):523–30. Available from: https://www.ncbi.nlm.nih.gov/pmc/articles/PMC2671878/

123. Birben E, Sahiner UM, Sackesen C, Erzurum S, Kalayci O. Oxidative stress and antioxidant defense [Internet]. Vol. 5, World Allergy Organization Journal. BioMed Central Ltd.; 2012 [cited 2020 Sep 9]. p. 9–19. Available from: /pmc/articles/PMC3488923/?report=abstract

124. Nebert DW, Dalton TP, Okey AB, Gonzalez FJ. Role of aryl hydrocarbon receptor-mediated induction of the CYP1 enzymes in environmental toxicity and cancer [Internet]. Vol. 279, Journal of Biological Chemistry. J Biol Chem; 2004 [cited 2020 Sep 9]. p. 23847–50. Available from: https://pubmed.ncbi.nlm.nih.gov/15028720/

125. Ferguson CS, Tyndale RF. Cytochrome P450 enzymes in the brain: Emerging evidence of biological significance [Internet]. Vol. 32, Trends in Pharmacological Sciences. NIH Public Access; 2011 [cited 2020 Sep 9]. p. 708–14. Available from: /pmc/articles/PMC3223320/?report=abstract

126. Drozd E, Krzysztoń-Russjan J, Marczewska J, Drozd J, Bubko I, Bielak M, et al. Up-regulation of glutathione-related genes, enzyme activities and transport proteins in human cervical cancer cells treated with doxorubicin. Biomed Pharmacother. 2016 Oct 1;83:397–406.

127. Hartz AMS, Bauer B, Block ML, Hong J-S, Miller DS. Diesel exhaust particles induce oxidative stress, proinflammatory signaling, and P-glycoprotein up-regulation at the blood-brain barrier. FASEB J [Internet]. 2008 Aug [cited 2020 Sep 9];22(8):2723–33. Available from: /pmc/articles/PMC2493447/?report=abstract

128. Mortamais M, Pujol J, van Drooge BL, Macià D, Martínez-Vilavella G, Reynes C, et al. Effect of exposure to polycyclic aromatic hydrocarbons on basal ganglia and attention-deficit hyperactivity disorder symptoms in primary school children. Environ Int. 2017 Aug 1;105:12–9.

129. Valand R, Magnusson P, Dziendzikowska K, Gajewska M, Wilczak J, Oczkowski M, et al. Gene expression changes in rat brain regions after 7- and 28 days inhalation exposure to exhaust emissions from 1st and 2nd generation biodiesel fuels - The FuelHealth project. Inhal Toxicol [Internet]. 2018 Jul 3 [cited 2020 Sep 9];30(7–8):299–312. Available from: https://www.tandfonline.com/doi/abs/10.1080/08958378.2018.1520370

130. Beckwith T, Cecil K, Altaye M, Severs R, Wolfe C, Percy Z, et al. Reduced gray matter volume and cortical thickness associated with traffic-related air pollution in a longitudinally studied pediatric cohort. PLoS One [Internet]. 2020 Jan 1 [cited 2020 Sep 9];15(1):e0228092. Available from: https://doi.org/10.1371/journal.pone.0228092

# Appendices

## Appendix A: Chemicals, biological products, and equipment

| **Chemicals and biological products** | |
|---|---|
| **Product:** | **Supplier:** |
| B-mercaptoethanol | |
| BioWhittaker's® DMEM (Dulbecco's Modified Eagle's Medium) | Lonza, Verviers, Belgium |
| Calcium chloride ($CaCl_2$) | MERCK KGaA, Darmstadt, Germany |
| Dimethyl sulfoxide (DMSO) | Sigma-Aldrich, St. Louis, USA |
| Ethanol | Arcus ASA, Gjelleråsen, Norway |
| Hoechst 33342 | Invitrogen Molecular Probes™, Oregon, USA |
| L-glutamine | Sigma-Aldrich, St. Louis, USA |
| Magnesium Sulfate ($MgSO_4$) | Sigma-Aldrich, St. Louis, USA |
| MTT (3-(4,5-dimethylthiazol-2-yl)-2,5-diphenyltetrazolium bromide) | Thermo Fisher Scientific, Waltham, MA, USA |
| Penicillin-Streptomycin | Invitrogen Company, California, USA |
| Pepstatin A | Sigma-Aldrich, St. Louis, USA |
| Poly-L-lysine hydrobromide (PLL) | Sigma-Aldrich, St. Louis, USA |
| Sodium dodecyl sulfate (SDS) | Sigma-Aldrich, St. Louis, USA |

| **Equipment** | |
|---|---|
| **Product** | **Producer** |
| 96-well transparent cell culture plate Nunc™ | ThermoFisher Scientific |
| Cell culture flask Nunc™, 75 $cm^2$ | ThermoFisher Scientific |
| CLARIOstar® | BMG Labtech, Germany |
| CFX384 Touch real-time PCR detection system | Bio-Rad |
| CO2- incubator (ThermForma SteriCycle) | Thermo Scientific,Waltham, MA, USA |
| CryotubeTM NuncTM Vials | Thermo Scientific, Rockford, USA |
| Disposable syringe | Terumo Europe, Leuven, Belgium |

| | |
|---|---|
| Eppendorf tubes (0.5mL/1.5mL/2mL) | Eppendorf, Hamburg, Germany |
| Holten LaminAir, model 1.2 LAF bench | Eco Holten AS, Danmark |
| MQ-watertank (MilliQ 5) | Merck, Darmstadt, Germany |
| Multichannel pipette | Thermo Scientific, Rockford, USA |
| Multitube vortexer (VX-2500) | VWR International Ltr., Randor, PA, USA |
| Neumann Haemocytometer | VWR International LLC |
| Ova Easy Advance II series incubator | Brinsea®, USA |
| Pellet pestle® | Kimble Chase, USA |
| Sub Aqua 12 Waterbath | Grant, England |

# Appendix B: Detailed protocols

## B.1 RNA isolation

All work was conducted at room temperature in a sterile LAF fume hood in the cell lab at NIPH.

1. Transfer 1 ml of lysis buffer (Buffer RLT) into a15-ml tube and then add 10 µl of ß-mercaptoethanol.
2. Transfer 30 µl of the homogenate to an Eppendorf tube and add 350 µl of lysis buffer.
3. Vortex the samples thoroughly and spin to remove any lysate from the cap.
4. Add 70% ethanol to the lysate at a1:1 ratio and mix well by pipetting.
5. Transfer up to 700 µl of the sample to the RNeasy spin column and place in the 2 ml collection tube. Centrifuge at 8000 – 12000 x g for 1 minute. Discard the flow-through.
6. Add 350 µl Buffer RW1 to the spin column and centrifuge for 1 minute.
7. Remove the DNase I stock solution aliquots from the freezer and add 70 µl Buffer RDD to each tube containing 10 µl DNase. Centrifuge briefly.
8. Discard the flow- through and add 80 µl Add DNase I incubation mix directly to RNeasy column membrane, and place on benchtop (20–30°C) for 15 min.
9. Add 350 µl Buffer RW1 to spin column and centrifuge for 1 minute.
10. Discard the flow- through and add 500 µl Buffer RPE, centrifuge for 1 minute.
11. Discard the flow- through and add 500 µl Buffer RPE, centrifuge for 2 minutes
12. Place the spin column in a new 2 ml collection tube, centrifuge for 1 min to dry the membrane.
13. Discard the 2 ml collection tube and place the spin column in a new 1.5 ml collection tube.
14. Add 50 µl RNase-free water directly to the spin column membrane, centrifuge 1 minute to elute the RNA.
15. Discard the spin column and transfer 5 µl RNA into small tubes for nanodrop measurements and quality control.
16. Freeze the remaining RNA samples.

## B.2 cDNA synthesis

Applied biosystems High-Capacity RNA-to-cDNA™ Kit:

1. Use up to 2 μg of total RNA per 20-μL reaction.
2. Allow the kit components to thaw on ice.
3. Referring to the table below, calculate the volume of components needed to prepare the required number of reactions
4. Aliquot the RT reaction mix into a plate or tubes.
5. Seal the plates or tubes with the appropriate seal or caps.
6. Briefly centrifuge the plate or tubes to spin down the contents and to eliminate any air bubbles.
7. Place the plate or tubes on ice until you are ready to start the reverse transcription reaction.
8. Incubate the reaction for 37°C for 60 minutes. Stop the reaction by heating to 95°C for 5 minutes and hold at 4°C.
9. The cDNA is ready for use in real-time PCR applications or long-term storage in a freezer (−25°C to −15°C).

## B.3 Procedure for PC12 splitting

1. Wipe the bench
2. Get pipettes, glass pipettes, a new bottle and waste container
3. See if the cells are confluent under the microscope
4. Empty the old medium in waste container on the latest bottle (oldest reserve)
5. Pour in 10 ml of fresh PC12 medium using pipette
6. Tighten cork, Dislodge cells by hitting the sides of the flask against the bench
7. Forcefuly triturate the cell suspension using pipette (Pipette up and down with 10 ml pipette) reduce cell clumping (press the pipette opening against the bottom side of the bottle)
8. Check under the microscope; the homogenate need to be free of cell clumps. Repeat step 7 until the homogenate is free of cell aggregates.

9. Take out all cell suspension using a pipette, pour 1.5 ml into a new bottle and another 1.5 ml in to the old bottle from which the cell suspension was taken out. Discard the remaining cell suspension.
10. Add 20 ml of fresh medium in each of the bottles
11. Put the bottles into the 37 degrees incubator with 5% CO2

NB: Don't forget to tighten the corks and openings during procedures that might result in spillage. Spray disinfectant ethanol to everything that gets its way into the hood including gloves.

**B.3.1 Splitting into dishes**

Follow the same procedure as above until you get homogeneous cell suspension (Step 8).

9. Prepare a clean Neubauer Haemocytometer and place the coverslip over it
10. Pipette out 20 µl of cell suspension and put a drop on both sides of the slip so the cell suspension reaches the counting area by capillary action.
11. Count three 4x4 fields under the microscope, count cells on two of the boarder lines of each the 16 square areas, and not at the other two (Count the cells on top of the left and lower lines)
12. Calculate the average of the three readings and the cell density is calculated as the average multiplied by $10^4$
13. Calculate the volume of cell suspension required to make a cell suspension of your interest. Eg. To make a $10*10^4$ cells/ml in a small dish (1 ml or 2 ml), use the following equation (if you intend to prepare $10*10^4$ cells in 2ml of the small dishesdon't increae the number of cells and only "2000 µL media" is used instead of the yellow shaded volume in the following formula

$$Volume\ in\ \mu L = \frac{10 * 10^4\ cells/ml * 1000\ \mu L\ media}{Calculated\ Average * \ 10^4\ cells/ml} = \frac{10^4}{Calculated\ Average}\mu L$$

For a 96 plate, each well holds a volume of 0.1 ml and the cell suspension is proportionally reduced to $10*10^3$ cells/well. But in the calculation, it is only necessary to change the volume of the media (in yellow) to 100 µL.

14. A new suspension of cells is then prepared taking into consideration the number of dishes/wells
15. Once prepared, the dishes are placed in incubator with 37 degrees and 5% $CO_2$.

### B.3.2 Counting of cells using Neubauer Haemocytometer

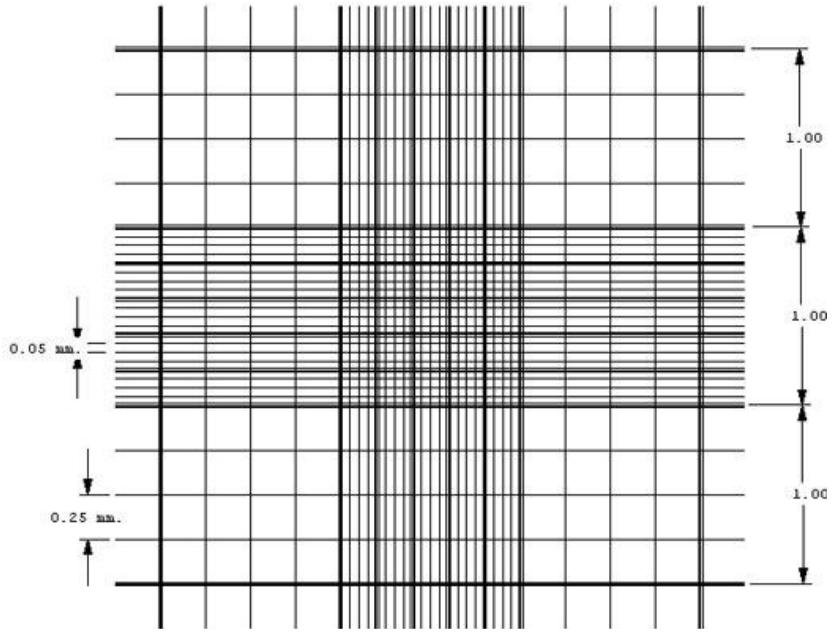


- Prepare a clean Neubauer Haemocytometer and place the coverslip over it
- Pipette out 20 µl of cell suspension and put a drop on both sides of the slip so the cell suspension reaches the counting area by capillary action.
- Count three 4x4 fields under the microscope, count cells on two of the boarder lines of each the 16 square areas, and not at the other two (Count the cells on top of the left and lower lines)
- Count the cells on 3 of the four 4x4 squares and then take the average of the three.
- The number of cells is then the average reading X 104 cells/ml
- This factor is a result of the following calculation

- The volume of one 4x4 square on the corners is 1mm x 1mm x 0,1mm = 0,1mm$^3$
  - 0,1mm$^3$ = 0,1 x $10^{-3}$ cm$^3$ = $10^{-4}$ ml.
  - Hence the number of cells per a 4x4 field is average number of cells / $10^{-4}$ ml = The average x $10^4$ / ml

## B.4 Preparation of chicken cerebellum granule cell culture

The following equipment must be autoclaved prior to use:

- Scissors, tweezers, spatula, for dissection of brain and isolation of cerebellum
- Pasteur pipette, trypsinizing flask and four glass bottles with cork
- Take note that a day ahead or on Friday, Solutions 1-5 need to be prepared, check availability of the media (two types) and preplate the dishes and plate wells with poly-L-lysine

**Procedure:**

1. 17 days old chicken eggs are taken out of the incubator and transferred to the cell lab
2. The eggs are submerged in a pool of ice for 7 min (stuns the chicken embryos)
3. Taking 6 eggs at a time seems manageable
4. Sink eggs in a 70% alcohol to sterilize the surface of the egg before the egg shell is crushed (use 14 cm sterile petri dishes)
5. Uses a sterile scalpel to cut across the neck, take the heads of the embryo to the hood, where the cerebellum is isolated using scissors and tweezers
6. Cerebellum is then placed in a bowl of solution 1
7. Meninges removed using tweezers and the cerebellum put in a new bowl of solution 1
8. Solution 1 is then pipetted out, the cerebellum piled in the middle of the bowl and cut into small pieces with a scalpel in two directions perpendicular to each other.
9. 10 ml of solution 1 is added to the bowl and the cerebellar tissue suspension is transferred to a sterile 50 ml tube with 10 ml of solution 1 and the tube is centrifuged at 1000 rpm for 1 minute
10. Supernatant removed
11. 8 ml of solution 2 is added and pipetted up and down carefully to disperse the pellet

12. Cell suspension is transferred to a sterile trypsinizing flask, which is then placed in a water bath at 37 degrees for 15 minutes. The bottle is shaken periodically. The corks of the trypsinizing flask should remain loose and should not be turned to fasten.
13. Cell suspension is transferred from the trypsinizing flask to a sterile 50 ml tube with 15 ml of solution 4. Then fill the tube with the solution 4.
14. The tube is centrifuged at 1000 rpm for 2 minutes. If the supernatant is not clear, a small amount of solution 3 are added and the centrifugation repeated (Equal amount of the supernatanat should be removed before an amount of solution 3 can be added)
15. Supernatant removed
16. Add 3 ml of solution 3 to the pellet, pipetting up and down 15-20 times using sterile Pasteur pippete. Allow the suspension to stand and for lumps of tissue to settle. Transferred the top lump free part of the suspension to a sterile 50 ml tube with 15 ml of solution 5
17. 2 ml solution 3 are added to the tube with cell suspension. Repeat as above, until clumps are no longer visibly present. Transfer the remaining solution to the tube with solution 5
18. Centrifuge at 900 rpm for 7 minutes
19. Remove the supernatant
20. 10 ml of cell culture medium with chicken serum and without KCl is added. After mixing the cell suspension well, 10 µL of the cell suspension is taken for cell counting and diluted to 100 µL with the medium containing chicken serum and no KCl (10 times dilution).
21. The cells counted in a counting chamber. The cell suspension is diluted with cell medium so that the cells are plated at a density of 1.7-1.9 x $10^6$ cells / ml of medium

$$Volume\ of\ cell\ suspension\ in\ ml = \frac{17\ (\text{min})\ \text{or}\ 19\ (\text{max})\quad)}{Average\ Reading} X\ Total\ volume\ in\ ml$$

The formula considers the 10x dilution

22. The calculated volume of the cell suspension is then transferred to a sterile conical flask with the same medium (containing half the amount of medium which is calculated from the number of prepared dishes). The volume is then made up using the same medium.
23. The plates have in advance been coated with poly-L-lysine.
24. The plates are incubated in the incubator cabinet at 37 degrees and 5% $CO_2$

## B.5 Parameters to consider for calculating the amount of cell suspension and number of eggs

| Type analysis | Number | Type of plate | medium in ml/plate (each well) | Cell density in cells/ml |
|---|---|---|---|---|
| Neurite outgrowth | | 96 well-plate | 10 (0,1) | 1,7-1,9 x $10^6$ |
| MTT | | 96 well-plate | 10 (0,1) | 1,7-1,9 x $10^6$ |
| Microscopy | | 6 well-plate | 12 (2) | 1,7-1,9 x $10^6$ |
| Western | | Large dishes | 10 | 1,7-1,9 x $10^6$ |
| Transfection | | Small dishes | 1 | 1,7-1,9 x $10^6$ |
| | | | | |
| Consideration for number of eggs calculation | | | | |
| 1,5 eggs is sufficient to prepare cell suspension of about 20 ml and hence, $The\ number\ of\ eggs\ = \frac{1,5}{20} X\ Total\ volume\ of\ cell\ suspension\ required$ | | | | |

### B5.1. Plating and Feeding medium preparation, Chicken neuronal cell culture

**Plating medium for long term free medium in chicken (DIV 0)**

| Storage | Reagents | Final Conc | Mol Wt | Quantity |
|---|---|---|---|---|
| Cold room | BME (GIBCO) | | | 500 ml |
| Cell lab freezer | Chicken serum | 7,5% | | 37,5 ml |
| Weigh room | KCl | 22 mM | | 825 |
| Rom 164 | Glutamine Sigma G-8540 | 2 mM | | 146 mg |
| Cell lab freezer | Pen.Strep | 1% | | 5 ml |
| Freezer room 164 | Insulin Sigma 16634 | 100 nM | | 50 µL from 1 mM stock (5,7335 mg |

| | | | | |
|---|---|---|---|---|
| | | | | dissolved in 1 ml dis. Water pH 2,0 |

**Feeding medium for long term serum free medium in chicken (DIV 1)**

| **Storage** | **Reagents** | **Final Conc** | **Mol Wt** | **Quantity** |
|---|---|---|---|---|
| Cold rom | BME (GIBCO) | | | 500 ml |
| Weigh rom | KCl | 22 mM | | 825 |
| Room 164 | Glutamine Sigma G-8540 | 2 mM | | 146 mg |
| Cell lab freezer | Pen.Strep | 1% | | 5 ml |
| K1 fridge room 166 | h-transferrin T-0665 (Sigma) | 100 µg/ml | | 50 mg |
| Room 164 | Putrescine P-5780 (Sigma) | 60 µM | | 4,8 mg |
| Room 164 | Insulin 16634 (Sigma) | 25 µg/ml | | 12,5 mg insulin dissolved in 6,25 ml ist. Water pH 2,0 and sterifiltered |
| Stock in cell lab freezer, dried material in freezer room 166 | T3 | 1 nM | | 17 µL from 20 µg/ml stock solution |
| Stock in cell lab freezer | $Na_2SeO_3$<br>(Highly toxic)<br>Fume hood | 30 nM | 172,94 | 150 µL from 100 µM stock marked NaSel. |

## B.6 Pre-coating of plates with poly-L-lysine

To enhance adhesion of cells to plates, dishes need to be pre-plated with poly-L-lysin.

1. 10 ml MQ-water is added to 5 mg poly-L-lysine to make a 0,5 mg/ml solution. If you have not used everything, then note the amount remaining on the bottle
2. The solution is transferred to a sterile Erlenmeyer flask where it is further diluted to a concentration of 0,01 mg/ml
    a. 1 ml of poly-L-lysin solution is added to small dishes, which is moved to cover the entire surface
    b. 5 ml of poly-L-lysin solution is added to large dishes and made to cover the entire surface
    c. 100 µL of the solution is added to wells of 96 well plates and made to cover the entire surface.
3. After 30-60 minutes, pipette out poly-L-lysin solution off all the dishes and leave the dishes in the hood with air speed at maximum strength (if you have to seed the dishes the next day, it might be necessary to leave the dishes open but if they have been plated on Friday, then leave them closed and they will be dried by monday)

NB: To give a 0,01 mg/ml solution, the 10 ml poly-L-lysine solution will have to be diluted to 500 ml with MQ-water. To prepare a less than 500 ml volume, one needs to calculate based on the 10 ml poly-L-lysine/500 ml MQ-Water = 0,02.

## B.7 Preparation of solutions used in preparing chicken neuronal cell culture

| Solution | Ingredients | Amount |
|---|---|---|
| Solution 1 | Bovine Serum Albumin | 1,5 g |
| | Krebs Ringer Solution 10x | 50 ml |
| | $MgSO_4$ (38,2 mg/ml distilled water) | 4 ml |
| | Distilled water | ad 500 ml |
| Solution 2 | Trypsin | 25 mg |
| | Solution 1 | 100 ml |
| Solution 3 | Trypsin inhibitor | 26 mg |
| | DNAse 1 | 6,2 mg |
| | MgSO4 (38,2 mg/ml distilled water) | 0,5 ml |
| | Solution 1 | ad 50 ml |
| Solution 4 | Solution 1 | 100 ml |
| | Solution 3 | 16 ml |
| Solution 5 | Solution 1 | 40 ml |
| | $MgSO_4$ (38,2 mg/ml distilled water) | 320 µL |
| | $CaCl_2$ (12,0 mg/ml distilled water | 320 µL |
| | | |
| 4. Make the solutions right before use | | |
| 5. Solution 1 is made in an erlenmeyer flask with a magnetic stirrer | | |
| 6. Solutions 1-5 has to be sterile filtered using 0,2 µm filters | | |
| 7. The volumes are for cell culture with up to 80 chicken embryo cerebellum | | |

### B.7.1 Preparation of chicken cerebellum granule cell culture

The following equipment must be autoclaved prior to use:

- Scissors, tweezers, spatula, for dissection of brain and isolation of cerebellum
- Pasteur pipette, trypsinizing flask and four glass bottles with cork
- Take note that a day ahead or on Friday, Solutions 1-5 need to be prepared, check availability of the media (two types) and preplate the dishes and plate wells with poly-L-lysine

**Procedure:**

1. 17 days old chicken eggs are taken out of the incubator and transferred to the cell lab
2. The eggs are submerged in a pool of ice for 7 min (stuns the chicken embryos)
3. Taking 6 eggs at a time seems manageable
4. Sink eggs in a 70% alcohol to sterilize the surface of the egg before the egg shell is crushed (use 14 cm sterile petri dishes)
5. Uses a sterile scalpel to cut across the neck, take the heads of the embryo to the hood, where the cerebellum is isolated using scissors and tweezers
6. Cerebellum is then placed in a bowl of solution 1
7. Meninges removed using tweezers and the cerebellum put in a new bowl of solution 1
8. Solution 1 is then pipetted out, the cerebellum piled in the middle of the bowl and cut into small pieces with a scalpel in two directions perpendicular to each other.
9. 10 ml of solution 1 is added to the bowl and the cerebellar tissue suspension is transferred to a sterile 50 ml tube with 10 ml of solution 1 and the tube is centrifuged at 1000 rpm for 1 minute
10. Supernatant removed
11. 8 ml of solution 2 is added and pipetted up and down carefully to disperse the pellet
12. Cell suspension is transferred to a sterile trypsinizing flask, which is then placed in a water bath at 37 degrees for 15 minutes. The bottle is shaken periodically. The corks of the trypsinizing flask should remain loose and should not be turned to fasten.
13. Cell suspension is transferred from the trypsinizing flask to a sterile 50 ml tube with 15 ml of solution 4. Then fill the tube with the solution 4.

14. The tube is centrifuged at 1000 rpm for 2 minutes. If the supernatant is not clear, a small amount of solution 3 are added and the centrifugation repeated (Equal amount of the supernatanat should be removed before an amount of solution 3 can be added)
15. Supernatant removed
16. Add 3 ml of solution 3 to the pellet, pipetting up and down 15-20 times using sterile Pasteur pippete. Allow the suspension to stand and for lumps of tissue to settle. Transferred the top lump free part of the suspension to a sterile 50 ml tube with 15 ml of solution 5
17. 2 ml solution 3 are added to the tube with cell suspension. Repeat as above, until clumps are no longer visibly present. Transfer the remaining solution to the tube with solution 5
18. Centrifuge at 900 rpm for 7 minutes
19. Remove the supernatant
20. 10 ml of cell culture medium with chicken serum and without KCl is added. After mixing the cell suspension well, 10 µL of the cell suspension is taken for cell counting and diluted to 100 µL with the medium containing chicken serum and no KCl (10 times dilution).
21. The cells counted in a counting chamber. The cell suspension is diluted with cell medium so that the cells are plated at a density of 1.7-1.9 x $10^6$ cells / ml of medium

$$Volume\ of\ cell\ suspension\ in\ ml = \frac{17\ (\text{min})\ \text{or}\ 19\ (\text{max})\quad)}{Average\ Reading} X\ Total\ volume\ in\ ml$$

The formula considers the 10x dilution

22. The calculated volume of the cell suspension is then transferred to a sterile conical flask with the same medium (containing half the amount of medium which is calculated from the number of prepared dishes). The volume is then made up using the same medium.
23. The plates have in advance been coated with poly-L-lysine.
24. The plates are incubated in the incubator cabinet at 37 degrees and 5% $CO_2$.

## B.8 Preparation of PC12 medium

| Ingredient | Amount in ml | Location |
|---|---|---|
| 1. DMEM | 500 | Take the bottle from the cold room |
| 2. Fetal Bovine Serum (FBS) | 50 (10%) | Freezer in Cell lab, 50 ml aliquots |
| 3. Horse serum (HS) | 25 (5%) | Freezer in Cell lab, 50 ml aliquots |
| 4. Pyruvate (P) | 5 | Freezer in cell lab, 10 ml aliquots |
| 5. Pen-strep (PS) | 5 | Freezer in cell lab, 10 ml aliquots |
| 6. L-Glutamine (G) | 10 | Freezer in cell lab, 10 ml aliquots, or fridge the whole bottle |

Comment:

Take the DMEM and thaw all the ingredients and add the ingredients to the DMEM bottle and the DMEM bottle becomes the medium bottle.

## B.9 MTT assay

1. Collect cells from a flask.
2. Calculate cell density with Neubauer Chamber.
3. Calculate the volume of original cell suspension needed to reach a final density of $3.5 \cdot 10^4$ cells/mL (in our case).
4. Add 100 µL/well of the cell suspension in a transparent 96-well plate.
5. Incubate the plate at 37°C and 5% $CO_2$ for 24 hours.
6. Add the desired treatment.
7. Incubate the plate at 37°C and 5% $CO_2$ for 24 hours.
8. Prepare the MTT solution: 5 mg MTT/mL PBS. You must use the mask when preparing this solution. Sterilize the solution with a filter.
9. Add 10 µL of MTT solution in each well of the plate (except in the last row).
10. Incubate the plate at 37°C and 5% $CO_2$ for 3-4 hours.
11. Remove the entire contents of the wells and add 100 µL of DMSO.
12. Incubate the plate at 37°C and 5% $CO_2$ for 30 minutes.
13. Read the absorbance at 570 nm in a plate reader.

## B.10 Glutathione measurements with mBCL

1. Seed cells in **black** 96-well plates
2. On DIV 1, treat cells with desired concentrations
3. After 24hr exposure load with 40 uM mBCL in medium
4. Incubate for 30 min
5. Remove, wash and replace with N-buf
6. Fluorescence was recorded using a CLARIOstar® plate reader at excitation and emission wavelengths of 380 nm (15 nm bandwidths) and 478 nm (21 nm bandwidths), respectively (Program mBCl kylling)
7. After measuring, replace with 0,4ug/ml Hoechst (dissolved in N-buf) and incubate for 1 minute
8. Again replace with new N-buffer

9. Hoechst was measured at excitation and emission wavelengths of 350 nm (22 nm bandwidths) and 461 nm (36 nm bandwidths), respectively.
10. Program Hoechst 33342 on the plate reader

## B.11 PC12 calcium influx measurement

1. Seed out PC12 in Corning® CellBIND® 96-well Flat Clear Bottom Black Polystyrene Microplates (black with clear bottom) precoated with poly-L-lysine
2. After 24h change the medium to blank serum-free medium + NGF, incubate 2 days
3. After 2 days load with Fura 2 (take out 55 µl of medium from each well using multi-pipete (except first column - leave the first column as a control), gather in a plastic container, add 50 µl of Fura 2 and put back 45 µl in each well (except first column - leave the first column as a control)
4. Incubate 20 minutes in 37°C and 5% of CO2 (cell incubator)
5. Take off all media carefully and add 100 µl Wash Buffer to each well x 2 z (I observed that double washing step results in decreased SD) Incubate 10-15 minutes. (15 minutes is the maximum time after then I observed leaking of Fura 2)
6. Measure the baseline Ca2+ level in the cells
7. Remove wash buffer. Add 100 µl of N-buffer with treatment. Use Calcium Ionophore A23187 (final concentration 1mM) as a positive control.
8. Measure response in the plate reader immediately after treatment and 15, 30, 45, 60 and 75 minutes after treatment.

### B.11.1 N-buffer (50 ml):

- 1.4 ml of 5M NaCl
- 175 µl of 1M KCl
- 750 µl of 1M Tris buffer, pH 7.0
- 600 µl of 0,1M $NaPO_4$ buffer
- 250 µl of 1M Glucose
- 100 µl of 1M $CaCl_2$
- Fill up to 50 ml with distilled weather

### B.11.2 Wash buffer:

- 20 ml of N-buffer
- 20 µl of 1M $MgSO_4$

## B.13 CGNC Calcium measurement

**Procedure:**

1. Seed out chicken cerebellar granular neurons in Corning Cell-bind plates, black with clear bottom, pre-poly-L-coated.
2. On DIV1 load with Fura-2 (fluorescent calcium indicator): Take out 55 uL medium from each well using a multi-pipette, gather in a plastic container. Add 50 uL of Fura-2 (in the freezer, regular lab, aliquoted), and put back 45 ul in each well. Leave the first row unloaded as control.
3. Incubate for 45 minutes in 37*C and 5% $CO_2$.
4. Bring the plates to the regular lab, take off all media carefully and add 100 ul of washbuffer to each well. Put in drawer to de-esterify (Fura-2 is cleaved and trapped inside the cells).
5. Measure the baseline intracellular $Ca^{2+}$ level in the cells. While you do this, prepare for the next step if you haven't already.
6. Remove the washbuffer. Add 100 uL of N-buf with treatment if applicable. Treatment can be dose-response of channel inhibitors (Ro 04-5595, ifenprodil, MK-801 +++), potentiators (spermine, spermidine), drugs (morphine/paracetamole/methadone ++) or other chemicals (PFOS ++).
7. Add 25 uL of stimulating buffer to each well.
8. Measure response in the plate reader.